Digital Self-Interference Cancellation in Full-Duplex Wireless Systems

by

Muhammad Sohaib Amjad

Submitted to the Graduate School of Engineering and Natural Sciences
in partial fulfillment of
the requirements for the degree of
Master of Science

Sabancı University
August 2016

Digital Self-Interference Cancellation in Full-Duplex Wireless Systems

APPROVED BY:

Assoc. Prof. Dr. Özgür Gürbüz   ....
(Thesis Supervisor)

Prof. Dr. Ibrahim Tekin   ....
(Thesis Co-supervisor)

Prof. Dr. Özgür Erçetin   ....

Assoc. Prof. Dr. Husnu Yenigun   ....

Asst. Prof. Dr. Ali Özer Ercan   ....
(Özyeğın University)

DATE OF APPROVAL: 05/08/2016

to my family

Acknowledgments

First and foremost, I would like to express my deepest gratitude to my supervisors Dr. Özgür Gürbüz and Dr. Ibrahim Tekin. I am grateful for their guidance, knowledge, motivation and kind advisory services. I would also like to thank Kerem Ozsoy for all his help and guidance.

I am thankful to my thesis jury, Dr. Özgür Erçetin, Dr. Husnu Yenigun and Dr. Ali Özer Ercan for accepting to be part of thesis jury and their valuable feedback.

I would like to thank Muhammad Usman Ghani for his help and support. Completion of this research would not have been possible without the valuable support from my friends, and therefore I would take this opportunity to thank them all.

I would like to express my heart-felt gratitude to my family, they have been a constant source of love, support and strength all these years.

Digital Self-Interference Cancellation in Full-Duplex Wireless Systems

Muhammad Sohaib Amjad

EE, M.Sc. Thesis, 2016

Thesis Supervisors: Özgür Gürbüz and Ibrahim Tekin

Abstract

Present half-duplex (HD) wireless technologies are currently striving to meet the growing demand of high speed wireless connectivity. Recent works have demonstrated the feasibility and potential of full-duplex (FD) wireless systems to double the spectral efficiency of HD systems, which makes FD communication an attractive solution to address the present wireless spectral congestion. Self-interference (SI) cancellation is the key to FD communication and the residual SI is the major factor determining the performance of an FD radio. At the receiver of an FD system, SI suppression is achieved in two stages, first in analog domain at RF level, and then in digital domain at baseband level. Digital SI cancellation, being the last stage, plays a crucial role, as it primarily quantifies the signal-to-noise ratio (SNR) of the desired signal. In this thesis, we present a novel frequency domain approach for the reconstruction of SI signal in digital domain. For the realization and performance evaluation of the proposed and the existing time domain reconstruction approaches with different SI channel estimation algorithms, we have considered the baseband model of FD implemented on an OFDM system under time dispersive fading channel. We have evaluated the performance of digital SI cancellation techniques for such an FD system via detailed simulations and extensive tests with WARP Software Defined Radio (SDR), also analyzing computational complexity. Through the simulation and test results, it is shown that, for the AWGN channel, the amount of digital cancellation increases with increasing SNR of

the received SI signal, and a maximum cancellation of $\sim$36 dB is achieved. Under fading, the SI suppression capability of all digital techniques degrades, especially with increasing delay spread. However, since the frequency domain estimation is resilient to large delay spreads, better performance is observed as compared to the time domain estimation based techniques, which are more prone to frequency selectivity. Additionally, it is demonstrated that with least square frequency domain estimate, the cancellation obtained by the proposed frequency domain reconstruction, outperforms the existing time domain approach by 5 - 10 dB, while the computational complexity is reduced to one-fourth of that required by the time domain reconstruction. Furthermore, it is observed that the SI suppression capability of the digital cancellation techniques can be improved up to 1 dB, by increasing the number of training sequence symbols, which can be achieved by slight modifications in the preamble structure. Lastly, FD operation is demonstrated on the WARP SDR set up, by applying the frequency and time domain reconstruction approaches, showing simultaneous transmission and reception of a tone.

Tam Çift Yönlü Kablosuz Haberleşme Sistemleri için Sayısal Özgirişim Giderimi

Muhammad Sohaib Amjad

EE, Yüksek Lisans Tezi, 2016

Tez Danışmanları: Özgür Gürbüz ve Ibrahim Tekin

Anahtar Kelimeler: Tam Çift Yönlü Haberleşme, Özgirişim, Sayısal Giderim, Zamanda Dağıtıcı Sönümleme, Zaman Düzleminde Yeniden Yapılanma, Frekans Düzleminde Yeniden Yapılanma

Özet

Günümüzdeki yarı çift yönlü kablosuz haberleşme teknolojileri ile gün geçtikçe artan veri trafiğinin karşılanması zorlaşmaktadır. Son zamanlarda yapılan çalışmalarda gösterilen tam çift yönlü (ÇY) haberleşme ile, spektral verimliliğin yarı çift yönlü sistemlere göre iki katına çıkarılması ve günümüzün kablosuz haberleşme ihtiyaçlarına etkin bir çözüm oluşturulması mümkün olabilecektir. Öz-girişim giderimi tam çift yönlü haberleşme için büyük önem arz etmektedir; zira, tam ÇY haberleşmenin başarımını öz-girişim gideriminden sonra kalan artık girişim belirlemektedir. ÇY sistemlerin alıcılarında öz-girişim giderimi iki aşamada gerçeklenir. Bunlardan ilki analog düzlemde ve RF devre seviyesinde, ikincisi de sayısal düzlemde temel bant üzerinde giderimi sağlamaktadır. Son aşamada yapılan sayısal giderim alıcı girişindeki işaretin gürültüye oranını belirlemektedir. Bu tezde, ÇY radyolarda sayısal öz-girişim için özgün, frekans düzleminde çalışan yeniden yapılanma teknikleri önerilmektedir. Literatürde var olan ve burada önerilen yeniden yapılandırma teknikleri farklı öz-girişim kestirimi algoritmaları ile birleştirilerek başarımları, WiFi, LTE gibi güncel sistemlerde olduğu gibi, OFDM'e dayalı bir hava ara yüzü için ve gürültülü ve sönümlemeli kablosuz kanal modelleri ile incelenmiştir. Sayısal öz-girişim giderim tekniklerinin başarım analizleri, detaylı benzetimlerin yanında, WARP Yazılım Tabanlı Radyo (YTR) sistemi üzerinde kapsamlı testler ile yapılmış, ayrıca algoritmaların hesaplama karmaşıklıkları da analiz edilmiştir. Benze-

tim ve test sonuçları doğrultusunda, toplanan beyaz gauss gürültüsü (AWGN) altında sayısal öz-girişim giderimi, alınan işaretin gürültüye oranı ile doğru orantılı olarak artmakta olup, yapılan çalışmada en yüksek ∼36dB giderim elde edilmiştir. Sönümlemeli kanal altında bütün sayısal giderim tekniklerinin yetkinlikleri zayıflamakta, özellikle, artan kanal gecikme yayılımı ile başarım daha da düşmektedir. Ayrıca, frekans düzleminde yapılan kestirimler büyük gecikme yayılımlarına daha dirençlidir ve zaman düzleminde yapılan kestirimlere göre daha iyi performans göstermektedir. Buna ek olarak, en küçük kare frekans düzlemi kestirimi ile yapılan öz-girişim giderimi ile zaman düzleminde yapılan giderime göre 5 − 10 dB iyileşme görülürken hesaplama karmaşıklığı da dörtte bir oranında azalmaktadır. Bunlara ek olarak, benzetim ve testler ile öz-girişim giderim yetkinliğinin eğitim dizisinin uzunluğu ile 1 dB kadar daha artırılabildiği gözlemlenmiştir. Eğitim dizisi preamble yapısını değiştirerek yapılmaktadır. Son olarak, tam ÇY haberleşme WARP YTR düzeneği üzerinde, hem zaman hem frekans düzleminde yeniden yapılandırma teknikleri kullanılarak gösterilmiş, aynı zamanda gönderim ve ton işaretinin başarı ile alımı gerçeklenmiştir.

Table of Contents

List of Figures

List of Tables

Chapter 1

Introduction

In this chapter, we start with the main challenges in full-duplex wireless communication and the role of digital self-interference cancellation while enabling it. Further, we provide an overview of the contributions of this thesis, and then present the structure of this thesis.

1.1   Problem Definition

Present wireless systems require separate resources in time or frequency for transmission and reception for reliable communication. As a result, all current wireless devices operate in half-duplex (HD) mode, where separate resources are allocated for transmission and reception. In recent years, a huge number of wireless network users are recorded to switch to the trending smart phones and similar devices, due to which the wireless data traffic has increased dramatically. To address this growing demand of wireless traffic, the researchers in both industry and academia are investigating new areas and technologies, to curb the need. Full-duplex (FD) is an emerging wireless technology with a capacity and potential to overcome the present wireless spectral congestion. An FD radio, which can transmit and receive simultaneously using a single channel, ideally cuts the spectrum need by half, i.e. it doubles the spectral efficiency of an HD system, and it has the capacity to accommodate twice the number of users in the same cell zone.
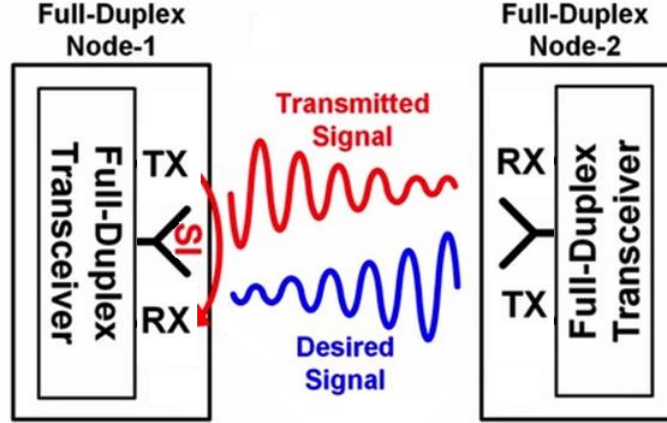
Figure 1.1: Illustration of full-duplex and SI relation.

The key challenge in realizing FD wireless communications is the huge power difference between the self-interference (SI) generated by a radio's own wireless transmissions and the desired received signal arriving from a distant transmitting antenna. This large power difference is due to the reason that the SI signal travels much shorter distances compared to the desired signal, as illustrated in Figure 1.1. The received SI signal more or less occupies the whole dynamic range of the analog to digital converter (ADC) in the received signal processing path, making the processing of the desired signal impossible. Thus, in order to enable an FD communication at maximum capacity, a radio is required to fully suppress the SI signal to the receiver's noise floor. To prevent the saturation of ADC at the receiver due to the high power SI signal, a considerable amount of SI suppression is required first in the analog domain, i.e. at the RF stage. The remaining SI signal, including multi path components, is then suppressed in digital domain. Any residual SI after digital domain cancellation ultimately acts as (additive) noise, and decreases the signal-to-noise ratio (SNR) of the desired signal, which eventually reduces the system throughput.

Recent works [1, 3, 9–19] have presented different system architecture and SI cancellation techniques to suppress SI signal, for enabling FD transmission. Apart from SI suppression techniques employed in analog/RF stage through antenna isolation [10, 11, 18, 19], single antenna with circulator [3, 13] or through orthogonal polarization, implementation of an FD transmission on an existing HD system, such as,

IEEE 802.11a/g standard for WiFi, requires some major structural modification of the design flow in the digital domain. This primarily includes the reconstruction of an approximate SI signal in baseband with the aid of an additional channel estimation block prior to receiver processing for the desired signal. To reconstruct SI signal in digital domain, the knowledge of channel effects (from transmitter to receiver) on the SI signal is crucial, thus the need for an additional channel estimate is essential.

Digital self-interference cancellation plays a key role in deciding the performance of an FD system, as it primarily quantifies the SNR levels after the suppression of SI. To achieve digital cancellation, previous designs have used time domain approach for SI signal reconstruction, as given in [3, 9, 10] with least square channel estimates. However, the performance of time domain reconstruction approach suffers significantly in channels with prolonged impulse response, i.e. large number of channel taps, because of the limited length of the cyclic prefix (CP). Besides time domain approach requires convolution operation, whose computationally complexity can grows as $O(N^2)$, where N represents the number of samples under channel filtering process, having N coefficients.

This thesis proposes a novel frequency domain approach for the reconstruction of SI signal. The proposed approach uses FFT processing, which is computationally less demanding than convolution, and uses channel estimate acquired for each sub-carrier, to perform equalization procedure. We have evaluated the proposed approach in terms of computational requirement for implementation perspective. Additionally, we have conducted a detailed performance analysis and comparison of the proposed frequency domain approach with the existing time domain approach, first through MATLAB with the help of a baseband system model for an FD OFDM system, while considering the widespread IEEE 802.11a/g standard, and then, on WARP software-defined radio (SDR) along with different analog domain SI suppression structures. We have also studied the effect of varying the number of long training sequence (LTS) symbols (in the preamble structure) on digital cancellation with different estimation and reconstruction schemes. Moreover, we have tested reception under FD communication with both proposed and existing SI reconstruction approaches.

1.2   Contributions

The contributions of this thesis can be summarized as follows:

- In this work, we have proposed a new frequency domain based SI signal reconstruction approach to achieve digital cancellation for FD communications. Unlike the existing time domain approach that requires convolution operation for the reconstruction of SI signal, the proposed technique requires FFT processing, and uses only multiplication operation to equalize the known transmitted data with channel effects for SI signal reconstruction.

- We have evaluated the proposed frequency domain approach in-terms of computational complexity for implementation perspective, and compared its computational requirement with the existing time domain reconstruction approach. It has been shown that the least expensive implementation structure for time domain reconstruction approach used in [3, 9, 10], is nearly three times more computationally demanding as compared to the proposed frequency domain approach.

- In order to do the performance analysis and comparison of the proposed approach with the existing time domain approach in terms of achieved digital cancellation we first developed a baseband model of FD implemented on an OFDM based air-interface, similar to IEEE 802.11a/g standard with variable length preamble structures, in MATLAB environment, while considering simple AWGN channel and 802.11 indoor channel model proposed in [20], which incorporates time dispersive, slowly fading multi path channel effects on the transmitted OFDM packet. In this model, we implemented both proposed and time domain reconstruction approaches, along with different channel estimation schemes, presented in the literature for the reconstruction of SI signal.

- Our simulation results have shown that, for the AWGN channel, the amount of digital cancellation increases with increasing SNR of the received SI signal, and a maximum cancellation of ~36 dB is achieved, with 40 dB received SNR. Also, under fading, the SI suppression capability of all digital techniques degrades,

especially with increasing delay spread. However, since the frequency domain estimation is resilient to large delay spreads, better performance is observed as compared to the time domain estimation based techniques, which are by design more prone to frequency selectivity.

- Our performance comparison of the two approaches, via simulations, stipulates that, for frequency domain channel estimates, the proposed frequency domain reconstruction approach is more practical, as it offers 5-10 dB more digital cancellation for a medium to high SNR under selective channel, and it reduces the computational requirements to 3488 flops from 7376 flops required to reconstruct the approximate SI signal when using time domain approach [10]. Similarly, with time domain channel estimates, the performance of both reconstruction approaches is similar, a roughly 1 dB difference is observed in the cancellation amount of the two approaches under all channel conditions, with a flop count requirement of 12912 and 10592 for time domain reconstruction used in [3] and proposed frequency domain reconstruction, respectively.

- We have used variable number of LTS symbols, which are enclosed within preamble structure, to investigate their effect on the digital cancellation for various SI suppression techniques. By mean of simulations, it has been demonstrated that the preamble with more LTS symbols offers approximately 1 dB more digital cancellation over the preamble with standard IEEE 802.11a/g LTS length of 2 symbols.

- To critically assess the performance of the digital cancellation approaches on a real setup, we tested the channel estimates and the reconstruction approaches that showed superior cancellation results, on WARP SDR [21], which also includes a channel emulator developed in MATLAB environment. These tests are conducted with different analog suppression structures, including RF antenuators, antenna separation and patch antenna, as provided in the literature [10, 11, 18, 19]. It is shown that the tested digital SI cancellation techniques, offers similar performance as that shown in MATLAB simulation, but with a slight degradation in

the cancellation amounts because of the non-linearities introduced by the transmit and receive chains, of the WARP radio. Also, with more analog suppression less digital cancellation is observed, which basically agrees with the simulations results of lower digital cancellation with decreasing SNR. Additionally, degradation in digital cancellation is seen in highly selective fading conditions.

- Finally, we tested the reception under FD communication on WARP radio, while using a single patch antenna for providing analog domain suppression, and both frequency domain and time domain SI signal reconstruction approaches, for digital domain suppression. With simultaneous transmission of an OFDM packet and reception of a tone at 2.414 GHz, it is demonstrated that the self-interfering OFDM packet is suppressed to the noise floor of the WARP radio, while receiving a spectrally clean tone of $\sim$40 dB SNR at 2.414 GHz.

1.3   Organization

Outline of this thesis is as follows: In chapter 2, we provide a detailed background on FD radios. It also covers the basics of 802.11a/g physical layer (PHY) and wireless fading channel. Chapter 3 first presents the FD OFDM system model and the SI channel estimation techniques used in the literature, and then explains the two SI signal reconstruction approaches. Chapter 4 covers the channel model employed to validate the performance of digital cancellation in fading conditions, the simulations under different scenarios and the computational complexities of estimation and reconstruction techniques. The performance test and reception under FD with WARP SDR are discussed in chapter 5, and chapter 6 concludes the main findings of this thesis.

Chapter 2

Background

This chapter begins with a background on FD radios, their implementation requirement and bottlenecks. Later on, we present the background on 802.11a/g PHY and wireless channel effects.

2.1 Full-Duplex Radios

A radio that can achieve a bidirectional communication over a same temporal and spectral resource is classified as full-duplex radio.

2.1.1 The Problem

Until recently, the very idea of FD wireless transmission was considered impossible. Consequently, all the radios were designed to operate in HD mode, which uses separate resources in time or frequency. The major problem, that was impeding FD implementation, is the large SI signal that appears at the receiver of an FD radio because of its own transmission as illustrated in Figure 1.1. This SI signal, which can be a million times stronger compared to the desired signal, saturates the ADC at the receiver, and makes the processing of the desired signal impossible. However, the implication of FD transmission, e.g. the possibility to cut the spectrum requirement to half, due to the utilization of just one resource for both transmission and reception, were quite alluring and kept the scientists and researchers to explore different ideas for suppressing this

huge SI signal.

In order to enable FD communication, a radio is required to completely suppress the large SI signal to the noise floor. To understand the extent of SI suppression requirement, consider the WiFi systems, in which the signal are transmitted at 20 dBm average power [3], and the noise floor of these systems is typically around -90 dBm. Therefore, to achieve FD the transmitted signal must be suppressed to the noise floor, i.e. 20dBm - (-90dBm) = 110 dB. Thus, a total of 110 dB suppression is required to enable the FD WiFi transmission at maximum throughput. If the FD system fails to meet this requirement of 110 dB SI suppression, let's say by 20 dB, then this 20 dB residual SI will raise the noise floor for the desired signal by 20 dB, i.e. 70 dBm noise floor for the desired signal. Therefore, if the strength of the desired signal is -60 dBm, with an SNR of 30 dB without residual SI, then with residual SI signal, the SNR of the desired signal will be dropped down from 30 db to 10 dB. This example clearly states the effect of residual SI signal of increased noise floor, which eventually reduces the system throughput.

2.1.2 Self-Interference Suppression

Recent works [1, 3, 9–12, 14, 16–19] have presented different techniques and system architectures to mitigate the SI signal, while performing FD transmissions. These SI suppression techniques can be categorized into: passive suppression and active cancellation. A combination of both is typically employed to achieve maximum SI suppression.

Passive Suppression

In passive suppression [1, 12, 19] the SI is suppressed in propagation domain, i.e. before the processing at the receiver. The techniques to achieve passive suppression includes: electromagnetic isolation of transmit and receive antenna by orthogonal polarization or cross polarization, transmit and receive antenna separation with RF absorbers, adjusting the antenna position and directivity, using a circulator providing isolation between the transmit and receive port, etc. Figure 2.1 presents the different mechanisms to achieve passive suppression of SI signal.
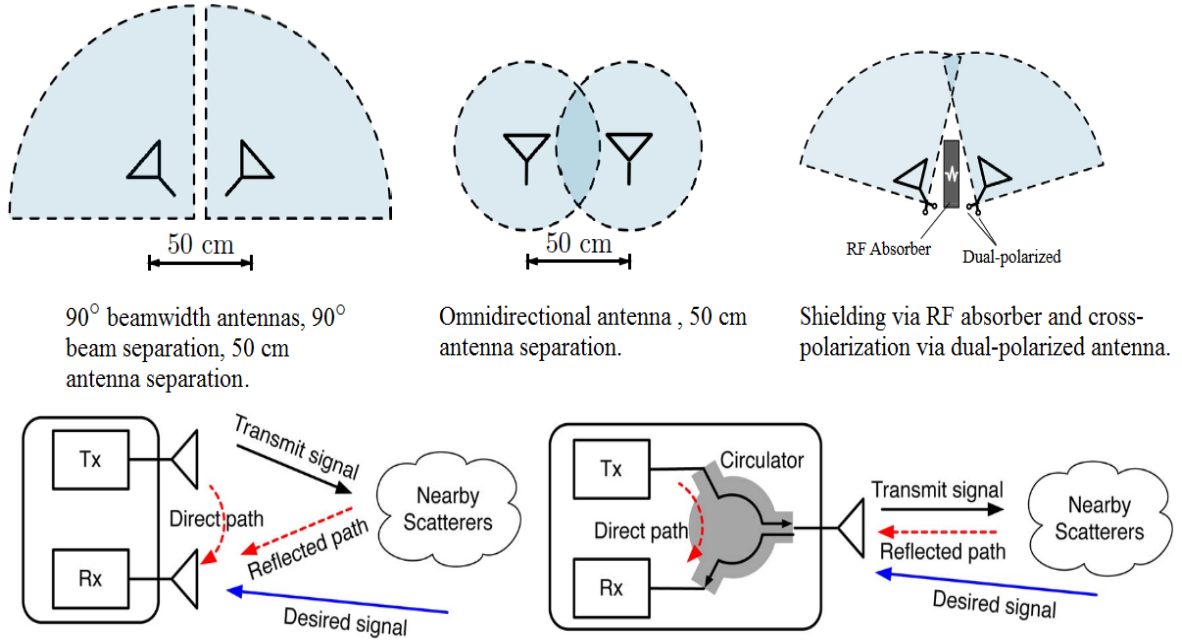
Figure 2.1: Different structures and antenna settings providing passive suppression [1, 2].

Active Cancellation

In active cancellation [3, 9–11, 13] the SI signal is suppressed by the subtraction of a processed copy of the transmitted signal from the received signal. This is usually done by the injection of the processed transmitted waveform into the received signal path that nullifies the SI signal. Active cancellation is typically achieved into two steps: analog cancellation stage and digital cancellation stage. The analog cancellation stage is required to suppress the SI signal to an extent, that the combined received signal (SI + desired) does not saturates the ADC of the receiver chain. The residual SI signal, which also includes the multi path SI components, is then cleaned out via digital cancellation.

The analog cancellation is the suppression of SI signal in analog domain. It is usually obtained via analog cancellation boards [3], in which the transmitted chain is tapped to obtain a small copy of the transmitted signal just before the RF front end. The benefit of using such tapped signal is that it also includes the transmitter noise introduced by the transmit chain, which helps towards better SI suppression. A typical analog

cancellation board contains parallel lines of fixed length, where each line introduces a variable delay. The delayed copies of the tx signal from each line are then added up to generated the processed tx signal, which is then subtracted from the signal on the receive path.

The digital cancellation of the SI signal on the other hand is achieved in digital domain, i.e. at baseband level. In order to learn the channel effects on the SI signal [3, 10, 15, 17], the digital domain processing utilizes the received SI signal's preamble (obtained after analog cancellation) to estimate the SI channel. With the knowledge of the SI channel, acquired via channel estimation procedure, and the known transmitted data, an approximate SI signal is first reconstructed, and then, subtracted from the residual signal, to obtain digital cancellation. Some other approaches of digital cancellation uses an additional RF chain [17, 22] to generate an antidote signal for the suppression of SI.

Figure 2.2 presents the employment of both passive suppression and active cancellation to achieve maximum SI suppression, while enabling FD communication. In the figure, the circulator is used to provide passive suppression, whereas the cancellation board and the digital cancellation is used to provide active cancellation.

2.1.3 Bottlenecks and Trade-offs Between Different Stages

To further explore the bottlenecks and trade-offs between different passive suppression and active cancellation methods, consider the FD schematic presented with Figure 2.2, that has a single shared antenna connected using a circulator. Notice that, a separate antenna FD terminal would look similar, except that the circulator with single antenna will be replaced with two separate antennas.

As can be seen in Figure 2.2, the digital samples T_b in the transmit path are first converted into analog form using a digital to analog converter (DAC), up-converted to a high carrier frequency, amplified with a power amplifier, and then radiated using an RF front end [2]. With actual hardware, this process will include several non-linearities starting from the DAC, which is the first source of adding quantization noise, ahead of the DAC is the local oscillator, which introduces phase noise, and then power amplifier

10
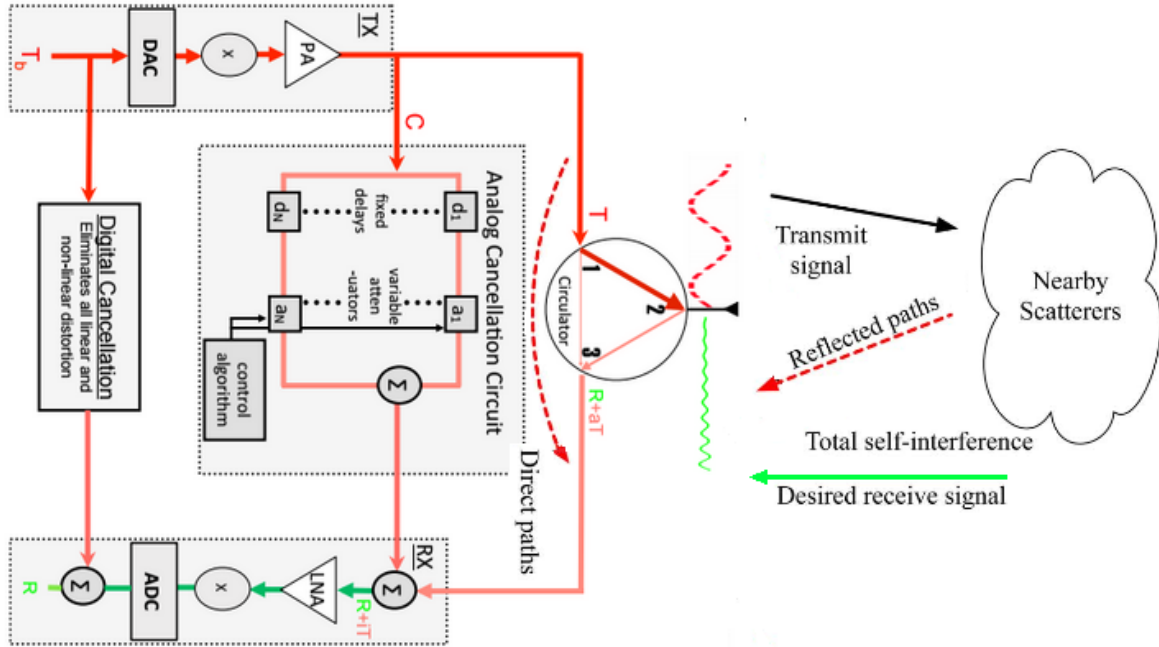
Figure 2.2: Employment of passive suppression and active cancellation for FD transmission [2, 3].

(PA), which empowers non-linear frequency components and therefore, creating distortions in the radiated signal. All these noise sources reshape the actual transmitted signal, which makes the apparently simple looking suppression process more complex. Now, since the same channel is used for both transmission and reception in FD, so the received signal can be decomposed into three components: the desired signal (shown as green in Figure 2.2), the leaked SI signal, through circulator or any other kind of passive suppression technique, due to limited in RF isolation (labeled as direct path), and the reflected multi path SI signal.

To clean out the received SI signal, the first line of action is the passive suppression or the propagation domain isolation. The major benefit of having considerable propagation domain isolation is that the receiver no longer requires to process the received signal with huge dynamic range. The different passive suppression schemes are illustrated using Figure 2.1, however the major bottleneck with these passive suppression methods is that they can suppress the direct path/leaked SI signal very well, but cannot discriminate between the reflected SI components and the desired signal. To address the reflected

SI signal suppression problem, channel aware passive suppression methods that can respond to channel effects are required, e.g. transmit beamforming, that electronically steers the multi-antenna transmit array. Nevertheless, for effective beamforming more transmit antennas are required, besides there is a possibility that it might suppress the desired signal as well. Hence, passive suppression of the reflected SI components is too risky.

The advantage of analog domain cancellation (shown in Figure 2.2 with tapped delay line circuit) is that it captures the non-linearities like oscillator phase noise, and the distortions because of power amplifier. Therefore, it can offer better and further SI suppression on top of passive suppression, which may results in further lowering of the received signal dynamic range. Because of the ability to adjust the delay lines in the cancellation board, it has the ability to achieve channel aware active suppression of reflected SI components, by adjusting the tapped delay lines according to reflected components. However, this process can get quite challenging and needs to be done after every transmission, besides channel aware SI suppression can be performed more easily in digital domain. The other major bottleneck linked with analog cancellation board is the size of the additional circuitry, which may limits the applicability of this method.

The digital domain cancellation is the last line of defense, and any residual SI after digital cancellation, ultimately raises the noise floor for the desired signal, i.e. decrease in the SNR, leading to poor overall performance. Since, digital domain cancellation is performed at baseband level; the sophisticated digital signal processing techniques can be used to handle the reflected SI components, which is quite easy as compared to channel aware techniques needed to be employed in analog domain and propagation domain suppression methods. For digital domain cancellation a discrete time system, that captures everything between the DAC at the transmitter side and the ADC on the receiver side including the propagation domain and analog domain SI suppression, is required to be modeled within the processor, as shown in Figure 2.2 with digital cancellation block. To model such system, the received preamble and the transmitted preamble per packet is used to perform the estimation process (SI channel estimation). The disadvantage of digital domain cancellation is that it cannot be achieved, unless

12

there is a significant SI suppression after analog/propagation domains, because of the ADC's dynamic range limitations. Also, if the analog/propagation domain suppression is too large, then the SNR of the received SI signal will be smaller, which results in poor SI channel estimation, thus a lower digital SI cancellation.

The different SI suppression stages as discussed above, have their own benefits and at the same time performance limitations. In any case, all three of them contribute towards the suppression of SI signal and their combine application has shown the best results. Figure 2.3, illustrates the frequency domain representation of SI suppression at different stages using WARP SDR, leading to complete suppression of SI signal to the noise floor.
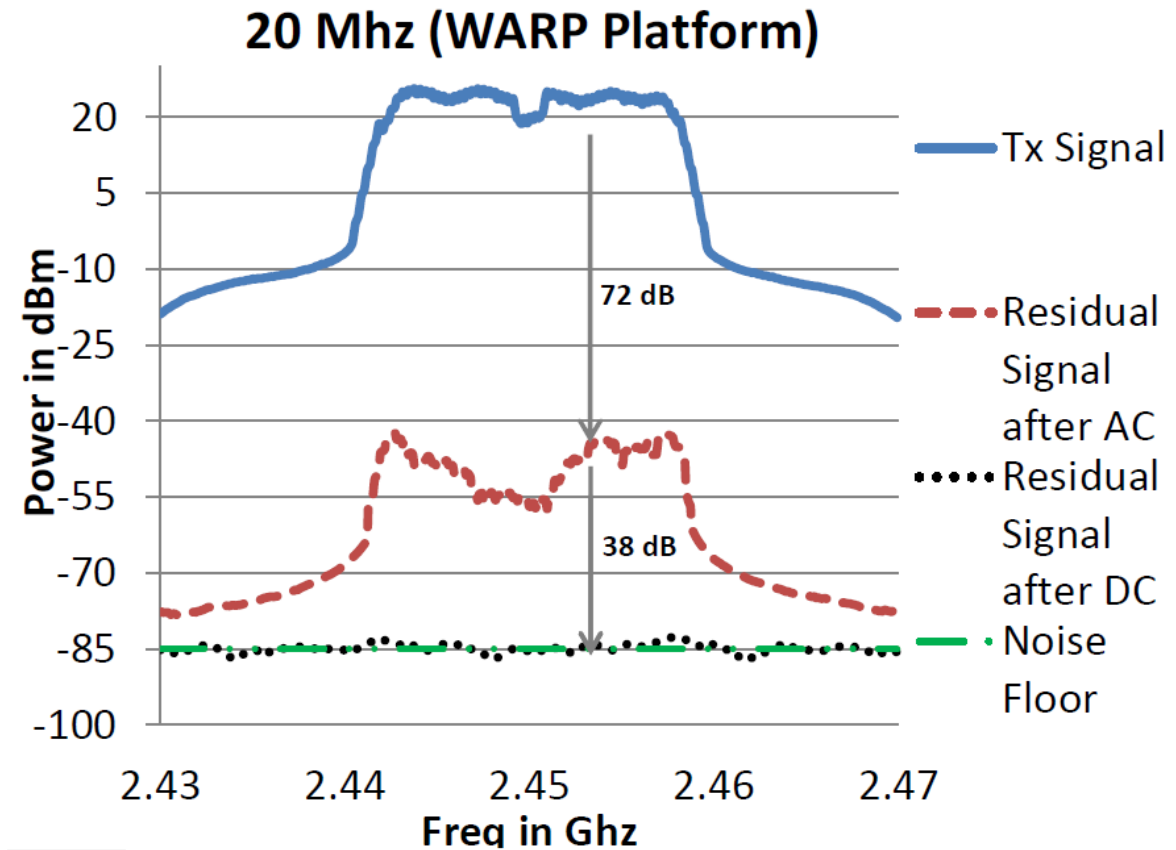
Figure 2.3: SI cancellation at different stages [3].

13

2.2 802.11 Physical Layer

802.11 is a set of physical layer (PHY) specifications created and maintained by the Institute of Electrical and Electronics Engineers (IEEE), for the implementation of wireless local area network (WLAN), more commonly known as WiFi, in the frequency bands of 900 MHz and 2.4, 3.6, 5, and 60 GHz. The first version of the standard was launched in 1997. The 802.11 standards define the air interface between a wireless client and a base station. The initial 802.11 standards (802.11-1997, 802.11a, 802.11b) have used three types of spread spectrum modulation: direct sequence spread spectrum (DSSS), frequency hopping spread spectrum (FHSS) and orthogonal frequency division multiplexing (OFDM). However, due to the capability of OFDM to maintain high data rates in harsh wireless conditions, the later standards of 802.11 are based on OFDM modulation.

2.2.1 IEEE 802.11a/g PHY

The IEEE 802.11a/g standard specifies an OFDM based physical layer (PHY) with a bandwidth of 20 MHz, supporting different data rates of 6, 9, 12, 18, 24, 36, 48, or 54 Mbps depending on the wireless link capacity, and has operational frequency bands of 2.4 GHz and 5 GHz.

OFDM is a promising technique that offers high data rates, and it has the ability to combat multi path fading in wireless channel. The input data stream in 802.11a/g standard is first processed through the stages of scrambling, convolutional coding and interleaving. The encoded stream is then divided into pairs of one, two, four or six bits, to perform the task of bit mapping on the BPSK, QPSK, 16-QAM or 64-QAM modulation scheme, respectively. The mapped symbols are further divided into 48 parallel symbols streams, where four pilot symbols and 12 null symbols are further added in each parallel streams of data symbols to make a total of 64 symbols per block, i.e. 48 data symbols, 4 pilots and 12 nulls, thus a total of 312.5 kHz (20 MHz / 64) carrier spacing. 802.11a/g uses pilot symbols as a reference to disregard frequency or phase shifts of the signal during transmission, whereas the nulls are added to mitigate the ef-

fect of inter-channel interference due variable channel conditions. The 64 symbols block is then converted into time domain through Inverse Fast Fourier Transform (IFFT) process with FFT size equal to 64, therefore generating one OFDM symbol containing 64 time domain samples; where the sampling time is 50 nsec (1 / 20 MHz) making the OFDM symbol duration 3.2 µsec. After the process of IFFT, a cyclic prefix of duration equal to one fourth of the OFDM symbol duration, i.e. 800 nsec containing 16 samples (800 nsec / 50 µsec), is attached at the beginning of the time domain samples, as guard interval. The samples attached as the guard interval, are the last 16 samples of the OFDM symbol, added to avoid inter-symbol-interference (ISI). After the IFFT process and the CP attachment, a fixed preamble containing 10 short training sequence (STS) symbols, used for packet detection and timing synchronization, and 2 long training sequence (LTS) symbols, used for channel estimation and fine symbol synchronization, is added ahead of the OFDM packet. The structure of STS is as follows:

$STS = \sqrt{13/6}$. $[0, 0, 1 + j, 0, 0, 0, -1 - j, 0, 0, 0, 1 + j, 0, 0, 0, -1 - j, 0, 0, 0, -1 - j, 0, 0, 0, 1 + j, 0, 0, 0, 0, 0, 0, 0, -1 - j, 0, 0, 0, -1 - j, 0, 0, 0, 1 + j, 0, 0, 0, 1 + j, 0, 0, 0, 1 + j, 0, 0, 0, 1 + j, 0, 0]$,

where $\sqrt{13/6}$ is the normalization factor of 12 out of 52 symbols. Likewise, the structure of the LTS is given as:

$LTS = [0, 1, -1, -1, 1, 1, -1, 1, -1, 1, 1, 1, 1, 1, 1, -1, -1, 1, 1, -1, 1, -1, 1, 1, 1, 1, 0, 0, 0, 0, 0, 0, 0, 0, 0, 0, -1, -1, -1, -1, 1, 1, -1, -1, 1, -1, 1, -1, 1, 1, 1, 1]$.

Where the zeros in the middle and on the first location represent the null points. After the preamble attachment the digital samples are converted into analog form using DAC, up-converted, amplified and transmitted as shown in Figure 2.4. The operational band of 2.4 GHz in IEEE 802.11g contains 11 overlapping channels in the band of 2.4102 - 2.4172 GHz, whereas, the operational band of 5 GHz in IEEE 802.11a contains 23 non-overlapping channels each with 20 MHz bandwidth.

A list of key 802.11a/g parameters are presented in Table 2.1. The 802.11a/g standard requires receivers to have a minimum sensitivity ranging from -82 to -65 dBm, depending on the chosen data rate [4]. At the receiver, as shown in Figure 2.5, once the frame testing module senses a data packet, receiver activates the automatic-gain control
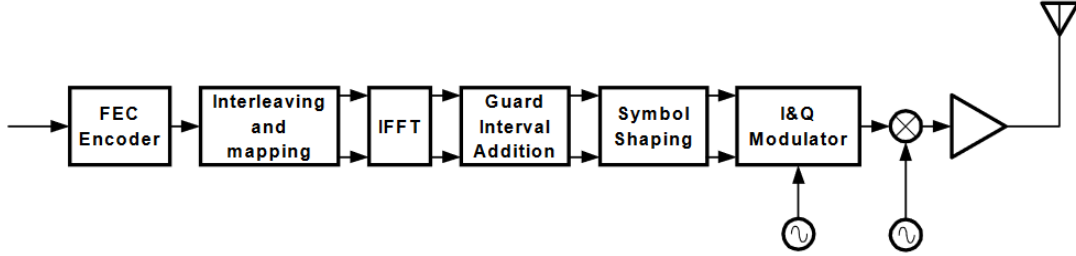
Figure 2.4: 802.11a/g transmitter [4].
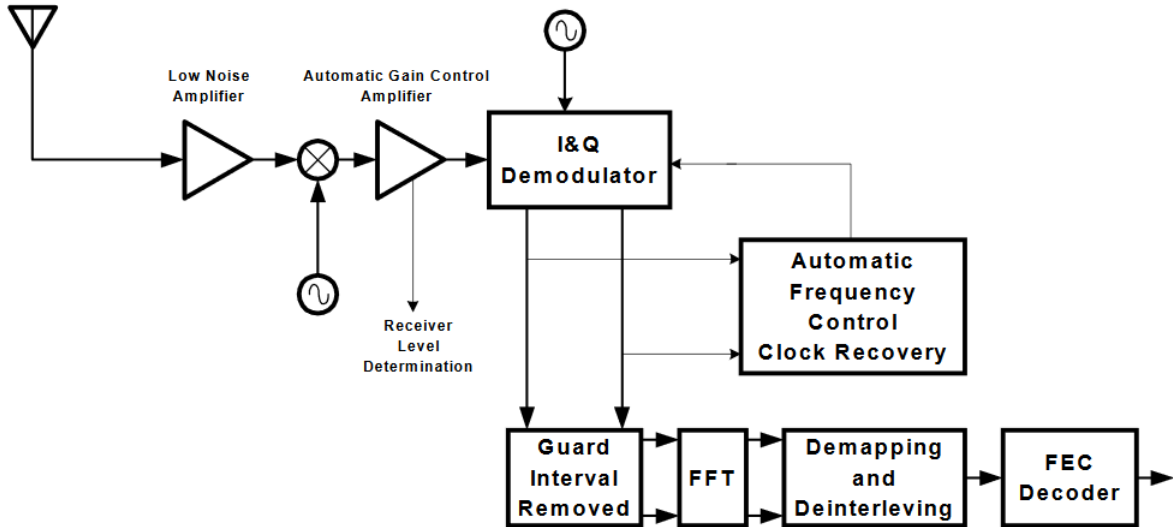
Figure 2.5: 802.11a/g receiver [4].

(AGC) module that control and maintain a fixed signal power to the A/D converter, which prevent the signal from saturation or clipping at the output of the A/D converter [23]. Then, coarse estimation of the carrier's frequency offset and timing recovery is done using STS, following that fine symbol synchronization and channel estimation is realized using LTS. Afterwards, receiver equalizes the received OFDM symbols, and uses the pilots to compensate the residual frequency offset caused by phase rotation. In the final phase, the equalized data is de-mapped, de-interleaved, and decoded.

2.3   Wireless Channel

In wireless communications, the radio signals that propagates through the wireless channel, are primarily affected by three separate modes of physical phenomena [7, 24]

16

Table 2.1: Key Parameters of the IEEE 802.11a/g Standard

Data Rates	6, 9, 12, 18, 24, 36, 48, 54 Mbps
Modulation	BPSK, QPSK, 16-QAM, 64-QAM
Coding Rates	1/2, 2/3, 3/4
No of Subcarriers	52
No of Pilots	4
OFDM Symbol duration + CP	4 μs
Guard Interval	800 ns
Signal Bandwidth	16.66 MHz
Subcarrier Spacing	312.5 kHz
FFT Size	64
Operational Band IEEE 802.11a	5 GHz with 23 Non-overlapping Channels
Operational Band IEEE 802.11g	2.4 GHz with 11 Overlapping Channels

namely: *reflection, diffraction, and scattering.* Reflection occurs when an electromagnetic wave strikes an object with dimensions larger than its wavelength, e.g. surface of the buildings. It makes the transmit signal to reflected back its power to its origin rather than propagating to the receiver. Diffraction is the bending of the waves around the obstacles, it usually occurs when the wireless path between the transmitter and receiver is obstructed by an object with sharp irregularities or slight openings. Scattering is the physical phenomenon in which obstacles having small dimensions compared to the wavelength, deviates an electromagnetic wave from a straight path. The obstacles that induce scattering are referred to as the scatters.

2.3.1 Fading Phenomenon

Fading is a characteristic of wireless channel that originates due to the physical phenomenon discussed in the previous section. It causes variation in the amplitude and phase of a propagating radio signal over time and frequency. In contrast to the additive white Gaussian noise (AWGN) as the most common source of signal degradation, fading

is an additional cause of signal degradation, which appears in wireless channels and characterized as non-additive signal degrading entity. Fading can be broadly classified into two types: large scale fading and small scale fading shown in Figure 2.6. Large
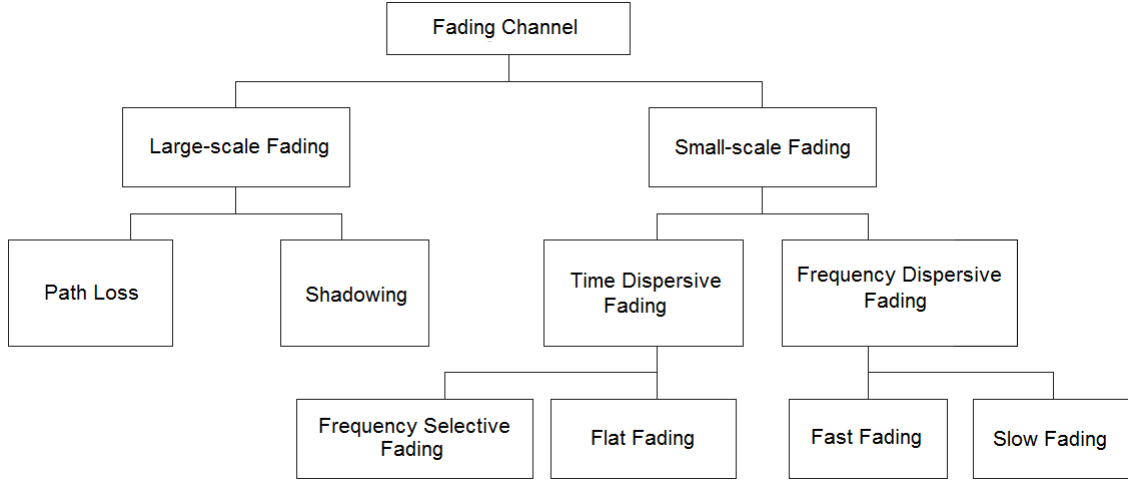
Figure 2.6: Classification of fading phenomenon [5].

scale fading is further characterized by two phenomenon: *path loss* and *shadowing*. Path loss is the signal degradation due to propagation through the wireless channel over large distances. Shadowing on the other hand is caused by large obstacles that appear in the signal propagation path, such as building and intervening terrains. Like large scale fading, small scale fading is also divided into two further classes: *time dispersive fading* and *frequency dispersive fading*. Time dispersive fading [7] is caused by the multi path effect, which creates rapid variation in signal amplitude due to constructive and destructive interference of the multiple copies of the same signal that arrives at the receiver from different path with same or different delays (usually referred as multi path channel, Figure 2.7 is used to illustrate). Frequency dispersive fading [7] on the other hand, originates due to Doppler spread, which is characterized by the time variation in a channel due to receiver speed. Figure 2.8 illustrate the effects of large and small scale fading with distance d.
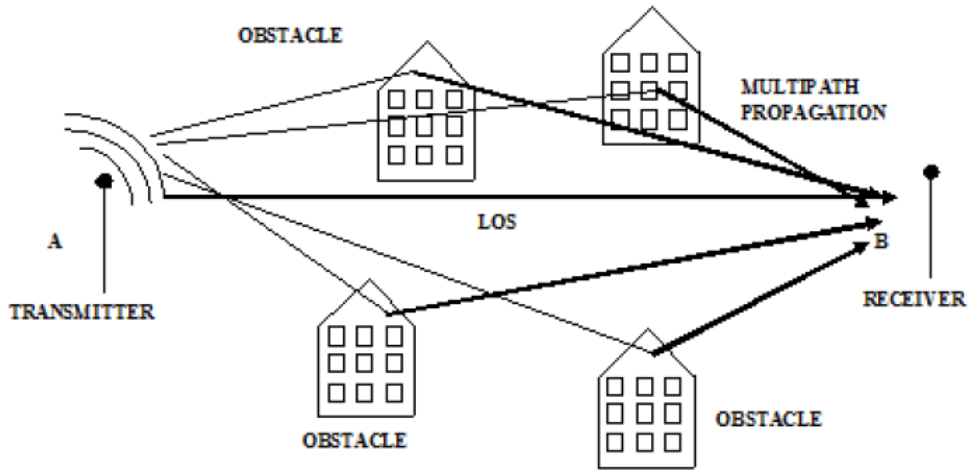
Figure 2.7: Illustration of multi path effect [6].
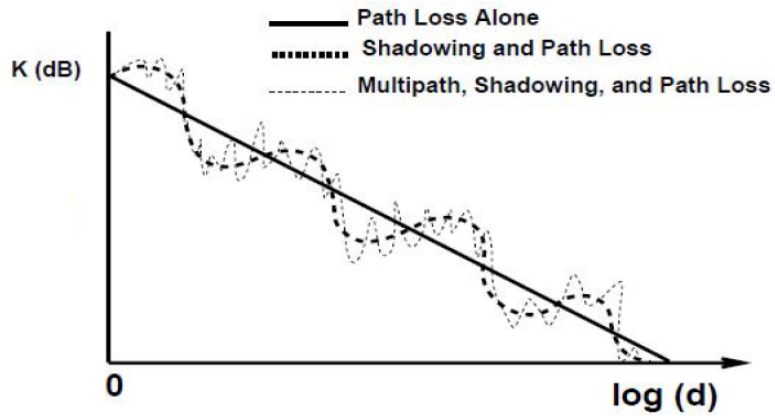
Figure 2.8: Large-scale fading and Small-scale fading effects with transmitted power K dB and distance d, [7].

Parameters for Small-scale Fading

To avoid confusion between large-scale fading and small-scale fading, the word fading from now on will only be referred for small-scale fading, as small scale fading is of more interest and will be studied in great detail, to build a sound foundation for the channel modeling, which is discussed in later chapters. Multi path time dispersive channel is often characterized by: *power delay profile, maximum excess delay spread, mean excess delay, RMS delay spread and coherence bandwidth.*

The power delay profile (PDP) provides the strength of a signal received through

a multi path channel as a function of time delay, where time delay is the difference in travel time between multi path arrivals. The PDP specified by ITU-R [25] for pedestrian channel model with four channel taps in Table 2.2, is presented here as an example. The maximum excess delay is the time difference between the first path and the last

Table 2.2: Power delay profile example defined by ITU-R

Taps	Relative Delay [ns]	Average Power [dB]
1	0	0.0
2	10	-9.7
3	190	-19.2
4	410	-22.8

path with non-negligible power. Similarly, the mean excess delay and the RMS delay spread are the first and second central moments of PDP as a function of channel delay $P(\tau_k)$, respectively. Figure 2.9 illustrates the channel impulse response with time delay parameters of fading, the mathematical expressions to compute these parameters are given as

$$mean\ excess\ delay \quad = \quad \overline{\tau} = \frac{\sum\limits_{k} \tau_k P(\tau_k)}{\sum\limits_{k} P(\tau_k)},$$

$$RMS\ delay\ spread \quad = \quad \sigma_\tau \quad = \quad \sqrt{\overline{\tau^2} - (\overline{\tau})^2}, \qquad where \quad \overline{\tau^2} \quad = \quad \frac{\sum\limits_{k} \tau_k^2 P(\tau_k)}{\sum\limits_{k} P(\tau_k)}.$$

Coherence bandwidth is the statistical measurement of the group of frequencies over which the channel can be considered flat. In general, it is denoted as B_c and it is inversely proportional to RMS delay spread, i.e.

$$B_c \quad \approx \quad \frac{1}{\sigma_\tau} \tag{2.1}$$

The relation given in (2.1) can vary with the exact definition of the coherence bandwidth, e.g. in case, when the approximate bandwidth or frequency range over which two
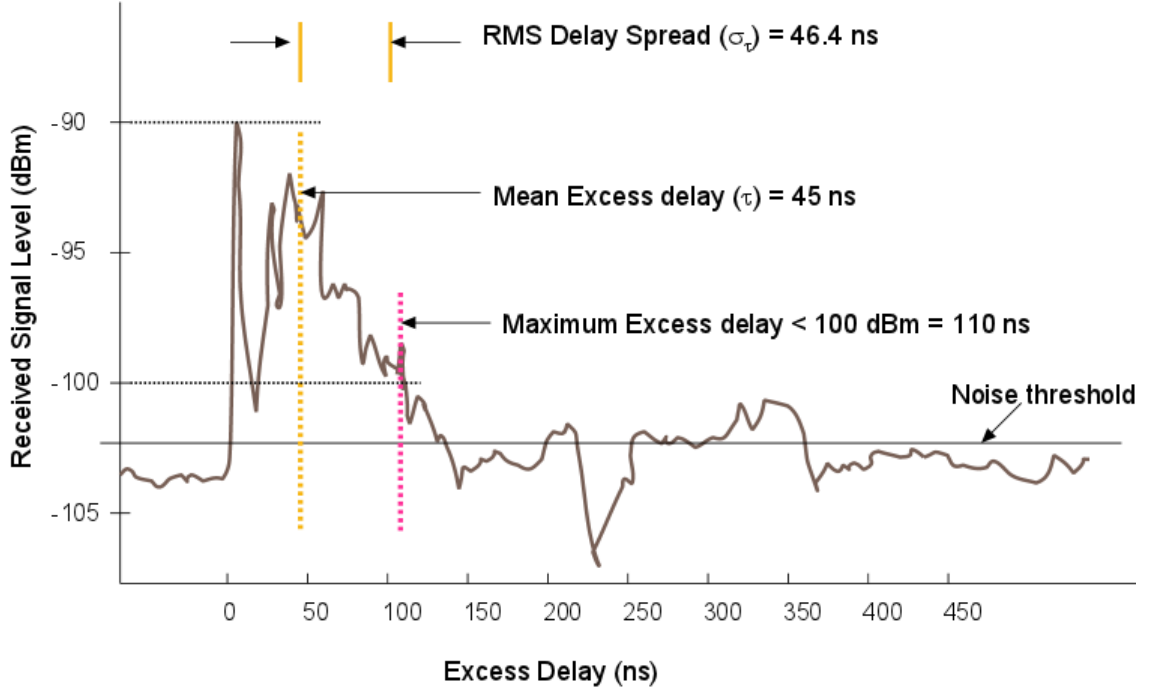
Figure 2.9: Channel impulse response with time delay parameters of fading effects [8].

frequencies of a signal are expected to experience amplitude fading with a correlation of 0.9 or above, then B_c and σ_τ are related as

$$B_c \approx \frac{1}{50\sigma_\tau}$$

In case, when B_c is defined as a bandwidth with correlation of 0.5 or above, it is given as

$$B_c \approx \frac{1}{5\sigma_\tau}$$

Time Dispersive Fading Channel

Time dispersive fading channels are usually characterized by the multi path delay spread that basically causes time dispersion. In time dispersive channels a transmit signal experiences fading in frequency domain, which is classified either as a *flat* or *frequency selective fading*. The magnitude of time dispersion primarily decides the extent of frequency selectivity induced within the transmitted signal.

Flat fading occurs, when the bandwidth of the channel is larger than the band-width of the signal, in such scenarios the transmitted signal experiences a fixed phase

21

shift and amplitude attenuation as it propagates. Whereas, frequency selective fading occurs, when the bandwidth of the channel is smaller compared to signal bandwidth, in such conditions the different frequency components of the transmitted signal may experience different phases shifts and amplitude attenuation as they propagate through the channel. Figure 2.10a and 2.10b illustrates the how a signal is affected under a time dispersive channel by presenting both flat and frequency selective fading conditions. To summarize, a signal with bandwidth B_s and symbol duration T_s, when transmitted

(a)   Flat Fading Channel   (b) Frequency Selective Fading Channel
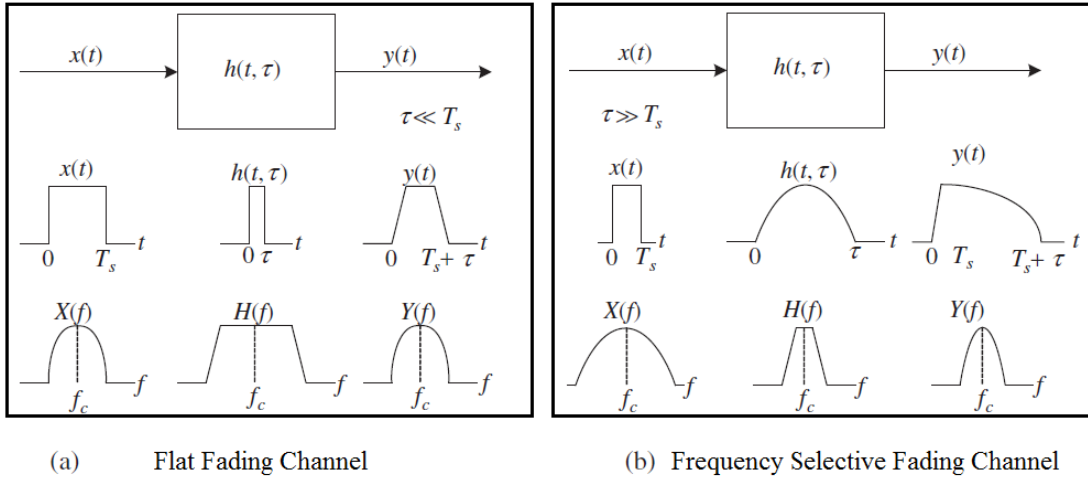
Figure 2.10: Time dispersive fading Characteristics in multi path channel [7].

through a channel with coherence bandwidth B_c and RMS delay spread σ_τ experiences flat fading if,

$$B_s \ll B_c \quad \text{i.e.} \quad T_s \gg \sigma_\tau$$

On the other hand, if the signal bandwidth is greater than the channel coherence bandwidth, i.e. the channel delay spread is large compared to symbol duration, given as

$$B_s > B_c \quad \text{and} \quad T_s < \sigma_\tau,$$

then the transmitted signal will suffer from frequency selective fading. With a shorter symbol duration compared to the multi path delay spread, the delayed copies of a transmitted symbol, overlaps with the subsequent symbols, causing inter-symbol interference (ISI), as illustrated in Figure 2.10b.

22

Frequency Dispersive Fading Channel

Frequency dispersive fading channels are characterized by the Doppler spread, and depending upon the magnitude of the spread, the received signal experiences *fast or slow fading*. In a fast fading channel the channel impulse response quickly varies within the symbol duration T_s. The duration over which a channel impulse response remains the same is called as coherence time T_c. In other words, when coherence time T_c is less than symbol duration T_s, then the signal undergoes fast fading. This rapid variation of channel impulse response is directly related to the movement of the transmitter or receiver, which incurs Doppler shift f_d and $B_d = 2f_d$ is the Doppler spectrum. The coherence time is inversely proportional to Doppler shift, i.e.

$$T_c \approx \frac{1}{f_d},$$

Therefore, $T_s > T_c$ implies $B_s < B_d$, thus all the frequencies in the transmitted signal will undergo a frequency drift due to fast fading conditions.

On the other hand, in slow fading conditions the coherence time T_c is greater than the symbol duration T_s, thus the channel does not change over one or more symbol duration. Such channels are also referred as static channels, with very small Doppler spectrum compared to signal bandwidth, i.e.

$$B_d \ll B_s \qquad \text{and} \qquad T_c \gg T_s$$

2.3.2 Statistical Characterization of Wireless Channel

In the previous sections a detailed study of the phenomenon that basically induces degradation in wireless transmission is presented. We have seen that in wireless communications the transmitted signals are subjected to distortions and degradation caused by reflection, diffraction and scattering. These distortions include delay spread, attenuation in signal strength and spectrum broadening. Based on these degradation, the statistical characterization of wireless channel as in time-varying channel impulse response [23, 26] is as follows

$$C(\tau_n, t) = \sum_n \alpha_n(\tau_n(t)) \exp^{-j2\pi f_{Dn}\tau_n(t)} \delta[t - \tau_n(t)], \tag{2.2}$$

where

- $C(\tau_n, t)$ is the time-varying channel impulse response

- $\alpha_n(t)$ is the complex attenuation factor for each multi path component

- $\tau_n(t)$ is the propagation delay associated with the nth multi path component

- f_{D_n} is the Doppler shift in the received n^{th} component

In (2.2) for considerably large number of signal reflections arriving at the receiver, the central limit theorem can be invoked to model the distortions as complex-valued Gaussian random process, which follows a Rayleigh distribution. Thus the fading process is referred as Rayleigh fading. However, in case of a strong line-of-sight (LOS) component the fading process no longer follows Rayleigh distribution, in-fact due to strong LOS the process follows Rician distribution and thus, this fading process is referred as Rician fading.

Chapter 3

Digital Self-Interference Cancellation Techniques for Full-Duplex Communication

Self-interference cancellation is the key to achieve FD communications and the residual amount of SI is the major factor determining the performance of the FD radio. The digital domain cancellation plays a concluding rule while enabling FD transmission, as it quantifies the SNR and therefore, the throughput of the system. To achieve digital domain cancellation, an approximate SI signal is needed to be reconstructed at the receiver. The reconstruction of the SI signal requires an estimate of the SI channel and the known transmitted data. The quality of the reconstructed signal, in terms of proximity with the actual SI signal, primarily depends on the SI channel estimate, thus making SI channel estimation a crucial stage for obtaining digital domain SI cancellation in FD systems.

Several techniques have been presented in the literature for the estimation of SI channel; this chapter introduces these estimation techniques. We start by presenting our baseband system model for FD implementation, and then discuss each SI channel estimation technique, used in this thesis for the testing of FD system. The concluding part of this chapter, explains the two approaches for the reconstruction of the SI signal. The two approaches include the existing time domain reconstruction approach and the

proposed frequency domain approach.

3.1 System Model

Figure 3.1 shows the structure of our baseband FD node, with the capacity to support both time and frequency domain reconstruction approaches. The model is based on IEEE 802.11a standard HD OFDM system. A list of key parameters of IEEE 802.11a standard that are included in our model is presented in Table 3.1. Besides the systematic OFDM blocks, as described in section 2.2, the noteworthy units in our FD model are the additional blocks of channel estimation and reconstruction, which are required prior to receiver's processing. The obvious reason behind that is the need for the reconstruction (an estimate) of self-interfering signal, and carrying out the subtraction, to mitigate the SI signal as much as possible first, so that clean receiver processing of the desired signal can be done. In this model, the channel estimate of
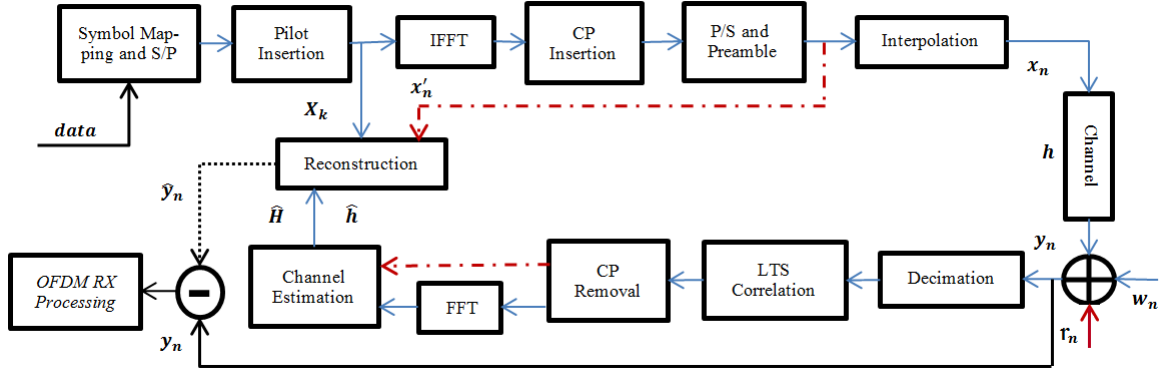
Figure 3.1: Baseband model of FD OFDM system

the first stage is acquired by using the received preamble information of the known SI signal. The reconstruction of the SI signal is completed using the known transmitted data and the obtained channel estimate either in time or frequency domain, as shown in Figure 3.1 with different color dashed lines. In any case the final reconstructed signal $\hat{y}_n$ is a time domain signal. The received signal y_n can be expressed as

$$y_n = h * x_n + r_n + w_n, \tag{3.1}$$

Table 3.1: Key Parameters of the IEEE 802.11a/g OFDM Standard used in our FD system model

Modulation	BPSK, QPSK, 16-QAM
No of Subcarriers	52
No of Pilots	4
OFDM Symbol duration	4 μs
Guard Interval	800 ns
Signal Bandwidth	16.66 MHz
Subcarrier Spacing	312.5 kHz
FFT Size	64

where h is the channel impulse response corrupting x_n the SI signal, r_n is the desired signal and w_n is AWGN noise. It is assumed that during the channel estimation process, no signal other than SI signal being received, is at hand (for best possible estimation of the SI channel, h) i.e. $r_n = 0$, thus reduces (3.1) to

$$y_n = h * x_n + w_n. \tag{3.2}$$

After performing the SI suppression the RX processing (shown as a single block here) is performed in the standard fashion, i.e. first, coarse estimation of the carrier's frequency offset and timing recovery is done using STS, following that fine symbol synchronization and channel estimation is realized using LTS. Afterwards, receiver equalizes the received OFDM symbols, and uses the pilots to compensate the residual frequency offset caused by phase rotation. In the final phase, the equalized data is de-mapped, de-interleaved, and decoded.

This work considers an OFDM based air interface, similar to the standard IEEE 802.11a, which has a preamble length of 12 symbols with the first 10 belong to the short training sequence (STS), required for synchronization, packet detection and carrier offset correction, and the remaining two belong to the long training sequence (LTS), used to compute channel state information and symbol synchronization, where each LTS

symbol contains identical training sequence as described in section 2.2. The number of LTS symbols are kept variable in our system (e.g. 2, 4 symbols etc.) in order to investigate its effect on SI cancellation. Figure 3.2 shows an example preamble structure, with an LTS of four symbols.
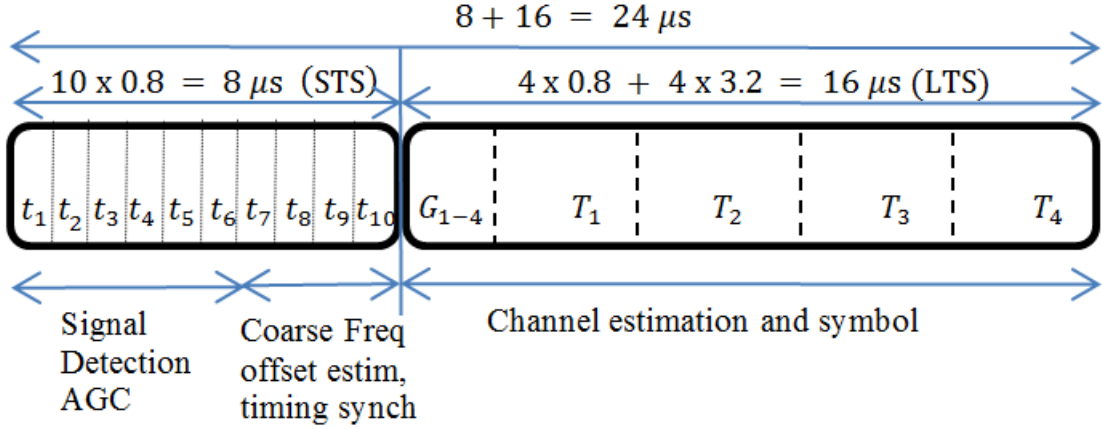
Figure 3.2: Modified preamble structure of IEEE 802.11a/g

3.2 Estimation of Self-Interference Channel

Channel estimation is the task of estimating the wireless channel gain that essentially disrupts the transmitted signal before it actually reaches the receiver. To efficiently complete this task in wireless systems training sequence (transmitted on each sub-carrier) and/or pilots (transmitted on subset of carriers) are used, as they are fixed, known and typically carry the same channel effects as the actual data symbols. Different structures for pilots and training sequence symbols have been proposed and realized for real time implementation.

In our FD system, a preamble structure similar to 802.11a/g is used for the estimation of SI channel. The standard 802.11a/g preamble packs two LTS symbols each with identical training sequence per carrier, so averaging of the two received LTS symbols is used to enhance the quality of the channel estimate. The considered preamble structure in this work, given as an example in Figure 3.2, facilitates an easy and efficient estimation of the channel frequency response for all the sub-carriers. The rational

for increasing the number of LTS symbols is to compare and investigate its effect on channel estimation and later on SI cancellation.

3.2.1 Least Square Frequency Domain Estimation (LS-FDE)

Least square frequency domain estimation (LS-FDE) in a wireless system is usually obtained with the help of training sequence (LTS) transmitted on each sub-carrier, ahead of the data symbols. The estimation process starts with averaging of the received LTS symbols and since FFT is a linear operation, it can be done before the FFT operation i.e. in time domain. Henceforth, only one FFT operation is required to calculate the channel estimate. After the FFT processing, the received LTS symbols are obtained as the product of the training sequence symbols matrix $\mathbf{X_{k_{LTS}}}$ and the channel frequency response H_k plus additive noise $W_{l,k}$ as

$$Y_{l,k} = H_k \mathbf{X_{k_{LTS}}} + W_{l,k}.$$

Where l represents the number of LTS symbols, k represents the FFT size, $Y_{l,k}$ is the average of l received LTS symbols, H_k is the channel frequency response, $\mathbf{X_{k_{LTS}}}$ is a diagonal matrix with LTS symbols for each subcarrier in the diagonals and $W_{l,k}$ is the additive noise per l symbols. Our aim here is to find a maximum likelihood estimate of H and for that we need to minimize the argument, i.e.

$$minimize\|Y_{l,k} - H_k \mathbf{X_{k_{LTS}}}\|_2^2 = \text{MSE}. \tag{3.3}$$

Thus, the channel vector estimate $\hat{H}_k$ is computed as given in [23];

$$\hat{H}_k = Y_{l,k}/\mathbf{X_{k_{LTS}}}, \tag{3.4}$$

$$\hat{H}_k = H_k + Y_{l,k}/\mathbf{X_{k_{LTS}}}. \tag{3.5}$$

Here (3.5) shows that the estimated channel is the sum of actual channel response H_k and the imprecision in the estimate caused by the AWGN noise, and this estimation scheme is used in [10] to obtain digital cancellation.

The sequence in the LTS symbol of our preamble structure incorporates "ones" (maximum power) on the indices of data and pilot symbols and "zeros" (no power) on

the indices of null symbols. With this distribution the multiplication with $\mathbf{X}_{k_{LTS}}^{-1}$ in (3.4) is not required because pseudo inverse of $\mathbf{X}_{k_{LTS}}^{-1} = \mathbf{X}_{k_{LTS}}$, where $\mathbf{X}_{k_{LTS}}$ contains "ones" and "zeros" depending of the index location, thus this reduces (3.4) to

$$\hat{H}_k = Y_{l,k}, \tag{3.6}$$

i.e. one FFT operation to compute the channel estimate.

3.2.2 Least Square Time Domain Estimation (LS-TDE)

Least square time domain estimation (LS-TDE) approach achieves the channel estimation before FFT processing of the training sequence (LTS) and has been used in [3, 9, 11] for SI channel estimation in FD systems. In this scenario, channel impulse response, instead of the channel frequency response, is acquired. From (3.2) the received time domain signal for the l LTS symbols having n samples per symbol is given as

$$y_{l,n} = h * x_{n_{LTS}} + w_{l,n}.$$

The time domain convolution can be expressed as a matrix vector multiplication, specifically for preamble. Thus the above channel equation can be written as

$$y_{l,n} = \mathbf{X_{LTS}} h + w_{l,n},$$

where h is channel impulse response vector and $\mathbf{X_{LTS}}$ is the Toeplitz matrix formed using the known LTS as shown below:

$$\mathbf{X_{LTS}} = \begin{bmatrix} x_1 & x_n & x_{n-1} & \cdots & x_{n-L+2} \\ x_2 & x_1 & x_n & \cdots & x_{n-L+3} \\ \vdots & \vdots & \vdots & \ddots & \vdots \\ x_{n-1} & x_{n-2} & x_{n-3} & \cdots & x_{n-L} \\ x_n & x_{n-1} & x_{n-2} & \cdots & x_{n-L+1} \end{bmatrix} \quad h = \begin{bmatrix} h_1 \\ h_2 \\ \vdots \\ h_{L-1} \\ h_L \end{bmatrix}.$$

Here, the parameter L states the maximum length of the channel impulse response that can be estimated and $\mathbf{X_{LTS}}$ is a circular matrix of order nxL. In our system the length of the channel is defined by the length of CP, which is specified as 800 ns, i.e. 16

samples. Also, the matrix $\mathbf{X_{LTS}}$ can be pre-computed since we know the values of LTS symbols in advance. The aim here is the same like in LS-FDE, i.e. error minimization as given by (3.3) but now for time domain. The channel impulse response estimate and MSE is thus calculated as given in [23]

$$\hat{h} = \mathbf{X_{LTS}}^{\dagger} y_{l,n} \tag{3.7}$$

$$\mathrm{MSE} = \|\hat{h} - h\|_2^2 = \mathbf{X_{LTS}}^{\dagger} w_{l,n}.$$

Where $\mathbf{X_{LTS}}^{\dagger}$ denotes Moore-Penrose (pseudo) inverse of $\mathbf{X_{LTS}}$ (with order Lxn) and $y_{l,n}$ is the average of l LTS symbols (each with order $nx1$). The channel frequency response estimate can then be obtained by performing the FFT of the acquired impulse response as follows

$$\hat{H}_{\mathrm{LS\text{-}T}} = \mathrm{FFT}_k \left\{ \hat{h}_n \right\} \tag{3.8}$$

where the subscript in $\hat{H}_{\mathrm{LS\text{-}T}}$ represents that the estimate is obtained by taking the k point FFT of the time domain estimate acquired using LS-TDE process.

3.2.3 FFT based Frequency Domain Estimation (FFT-FDE)

FFT based channel estimation uses the LS-FDE as a starting point and it is essentially based on the fact that the energy in the time domain channel impulse response is usually concentrated in limited path (taps) with considerable delays, as described in [27, 28]. Therefore, the estimate acquired with LS-FDE is first transformed into time domain through IFFT process to obtain time domain channel impulse response and then, the taps (paths) with significant energy are kept while only noise exist in the remaining paths, thus forced to zero. After the altered channel impulse response acquisition, it is transformed back to frequency domain through FFT process as follows

$$\hat{h}_n = \mathrm{IFFT}_k \left\{ \hat{H}_k \right\}$$

where $\hat{H}_k$ is the channel estimate obtained using (3.6) and $\hat{h}_n$ is channel impulse response obtained by taking k point IFFT,

$$\hat{h}' = \begin{cases} \hat{h}_n & 0 \leq n \leq L_a \\ 0 & \text{otherwise} \end{cases} \tag{3.9}$$

31

Here in (3.9) $\hat{h}'$ is the modified channel impulse response and L_a represent the significant energy taps. In our case L_a is kept equal to CP with length equal of 16 samples, which corresponds to the duration of guard interval presented in Table 3.1. This approach for obtaining time domain channel impulse response estimate is used in [15] for achieving digital cancellation in FD systems. The frequency domain channel estimate $\hat{H}_{\text{FFT}}$ can then be acquired by taking the k point FFT of $\hat{h}'$ as follows

$$\hat{H}_{\text{FFT}} = \text{FFT}_k \left\{ \hat{h}' \right\} \tag{3.10}$$

The FFT based estimate is used in [12, 15] for digital cancellation, which does not requires the reconstruction of SI signal as the digital suppression is performed in frequency domain. However, this method of digital cancellation removes the CP of the SI signal before the SI suppression, which can contain valuable samples of the desired signal as well, thus making it the least efficient method of digital cancellation. That's why, this digital cancellation technique is not investigated in this work.

3.2.4 Least Minimum Mean Square Error Frequency Domain Estimation (LMMSE-FDE)

The LMMSE estimator uses the second-order statistics of the channel conditions i.e. channel correlation matrix and the least square estimate to further minimize the MSE. The LMMSE estimate can be presented as

$$\hat{H}_{\text{LMMSE}} = \mathbf{W}_X \hat{H}_k,$$

$$\mathbf{W}_X = \mathbf{R}_{HH}(\mathbf{R}_{HH} + \sigma_n^2 (X_{LTS} X_{LTS}^H)^{-1})^{-1}. \tag{3.11}$$

Where $\mathbf{W}_X$ is the smoothing matrix that uses correlation properties of the channel to further improve $\hat{H}_k$ the LS-FDE obtained through (3.4). In (3.11) R_{HH} is the auto-covariance matrix of the channel vector H, σ_n^2 is the AWGN noise variance, X_{LTS} are the known transmitted training symbols and the superscript $(.)^H$ indicates Hermitian transpose. According to [29, 30] the LMMSE estimate is given as

$$\hat{H}_{\text{LMMSE}} = \mathbf{R}_{HH}(\mathbf{R}_{HH} + \sigma_n^2 (X_{LTS} X_{LTS}^H)^{-1})^{-1} \hat{H}_k. \tag{3.12}$$

To obtain the estimate using (3.12) the knowledge of R_{HH} channel covariance matrix and σ_n^2 noise variance is a major requirement, which makes LMMSE applications very limited in real-time communication systems as both of these parameters are mostly unknown and are assumed to be known.

3.3   Reconstruction of Self-Interference Signal

The procedure of SI signal reconstruction is similar to that of equalization, in-fact it is kind of reverse equalization. In order to apply the channel effects on the reconstructed SI signal the obtained channel estimate is processed with the known transmit data, so that the reconstructed signal innate the same channel properties as that imposed on the received SI signal. Figure 3.3 shows an example plot of signal reconstruction done
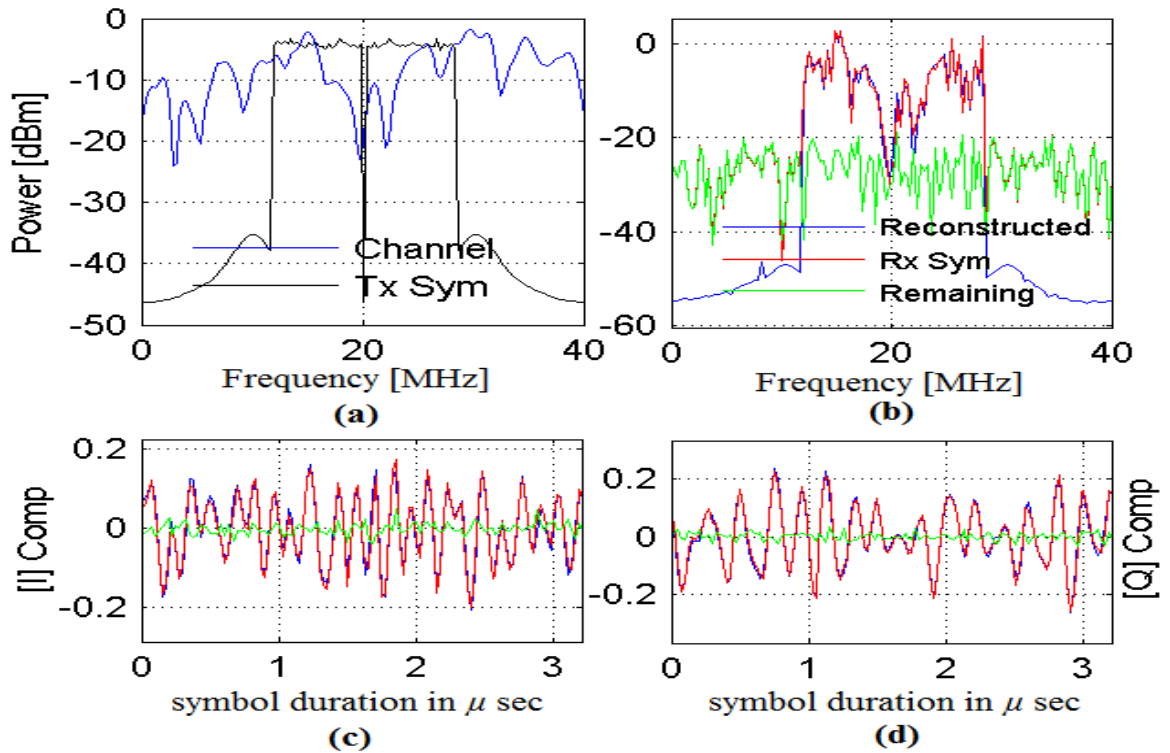
Figure 3.3: Example plot showing signal reconstruction with channel effects.

using proposed frequency domain approach, under frequency selective fading channel with 35 dB received SNR. Figure 3.3a, shows the transmitted OFDM symbol and the simulated channel in frequency domain. Likewise, Figure 3.3b gives the received OFDM

symbol (in red), the reconstructed OFDM symbol (in blue) and the remaining signal after the subtraction of the two (in green) all in frequency domain. In Figure 3.3c and 3.3d, time domain I and Q components are presented respectively, with received OFDM symbol (in red), the reconstructed OFDM symbol (in blue) and the remaining signal (in green).

3.3.1 Time Domain Reconstruction (TD-R)

Time domain reconstruction employed in [3, 10, 15], simply applies the convolution operation on x'_n (the time domain TX samples prior to interpolation filter as shown in Fig.1) and $\hat{h}$ (the channel impulse response estimate) obtained with (3.7) as used in [3, 10] or from (3.9) employed in [15] with the resultant signal given as

$$y'_n = \hat{h} * x'_n$$

Following the convolution operation the output y'_n is interpolated to obtain the reconstructed signal y_n as presented in Figure 3.4.
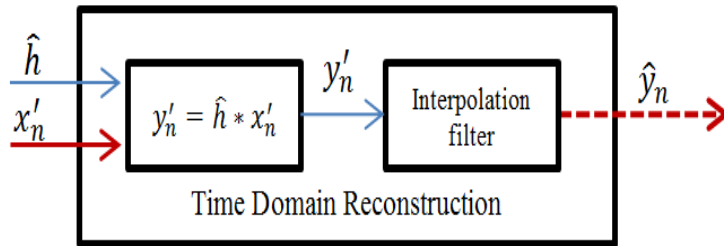
Figure 3.4: Structure presenting the time domain approach for the reconstruction of self-interference signal in digital domain.

3.3.2 Frequency Domain Reconstruction (FD-R)

The proposed frequency domain reconstruction technique takes in the baseband symbols X_k (obtained after pilot insertion) and the frequency domain channel estimate $\hat{H}_k$ obtained using (3.4), (3.8), (3.3.2) or (3.12). The numbers of symbols are kept same as the FFT size, e.g. in 802.11a standard the FFT size is 64, with 52 sub-carriers (data

+ pilots) per ODFM symbol, and the remaining 12 are null symbols, which are added
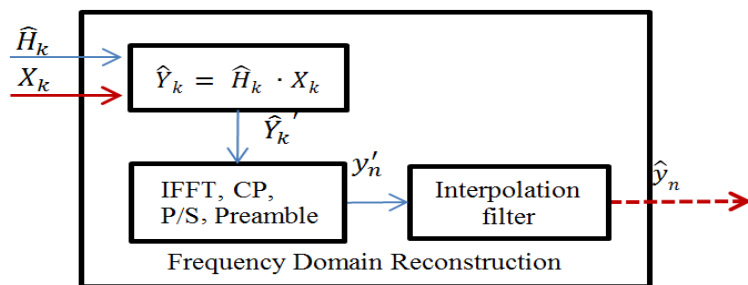
Figure 3.5: Structure presenting the frequency domain approach for the reconstruction of self-interference signal in digital domain.

to mitigate the effect of inter-channel interference due to variable channel conditions. The reconstructed signal is obtained as follows:

$$\hat{Y}_{l,k} = \hat{H}_{l,k}.X_{l,k},$$

$$y'_n = \text{IFFT}_k \left\{ \hat{Y}_{l,k} \right\}$$

where l represents the number of symbols transmitted, k is the FFT size and $\hat{Y}_{l,k}$ are the reconstructed l OFDM symbols. Note that, the same channel estimate $\hat{H}$ needs to be repeated l times so that each transmitted symbol X_k can be equalized. Once the symbols are equalized, they go through the same process of IFFT, CP insertion, parallel to serial conversion, preamble attachment and finally through interpolation filter to obtain time domain reconstructed SI signal $\hat{y}_n$ as shown in Figure 3.5.

3.3.3   Summary of Estimation and Reconstruction Techniques

Table 3.2 presents the summary of all the estimation techniques with the proposed frequency domain and existing time domain reconstruction approaches. Here, the subscript in the representation indicates the type of reconstruction approach, i.e. 'T' for time domain reconstruction and 'F' for frequency domain reconstruction. It is worthwhile to note that in evaluating all these techniques we considered variable number

Table 3.2: Summary of digital SI cancellation techniques for FD implementation.

Sr. no	Estimation	Reconstruction	
		Time Domain	Frequency Domain
1	LS-TDE	Represented as LS-TDE$_T$, used in [3, 9] and re-evaluated in this thesis	Represented as LS-TDE$_F$, proposed and evaluated in this thesis
2	LS-FDE	Represented as LS-FDE$_T$, used in [10] and re-evaluated in this thesis	Represented as LS-FDE$_F$, proposed and evaluated in this thesis
3	FFT-FDE	Performed poorly in even AWGN channel, so it is not evaluated in this thesis	Represented as FFT-FDE$_F$, proposed and evaluated in this thesis
4	LMMSE-FDE	Performed poorly in even AWGN channel, so it is not evaluated in this thesis	Represented as LMMSE-FDE$_F$, proposed and evaluated in this thesis

of LTS symbols in the preamble structure, while investigating the performance under wireless fading channel model as presented in the next two chapters.

Chapter 4

Performance Simulations and Computational Complexity Analysis

To test the performance of SI channel estimation techniques with the proposed frequency domain SI signal reconstruction approach, an indoor wireless channel model has been simulated for the incorporation of wireless fading characteristics on our FD system. This chapter introduces this channel model along with the fading effects characterized using it, and then presents the performance comparison results of the proposed approach and the time domain reconstruction approach under different fading conditions. The last part of this chapter, first explains the computational complexities/requirements of each estimation and reconstruction technique, and then presents a comparison of performance vs complexity.

4.1   Channel Model

The performance of a wireless communication system primarily depends on the wireless channel environs. In contrast to the typically static with known characteristic wired channels, the wireless channels are relatively dynamic and random, which makes a precise analysis of a wireless system often challenging. A detail literature review on wireless channel is presented in section 2.3, where the fading effect that essentially degrades a radio signal are discussed thoroughly and a fundamental channel model that

characterizes all sorts of fading effect is presented at the end of the section.

4.1.1   IEEE 802.11 Indoor Channel Model

In this thesis, to analyze the performance of our FD system and to test and compare our proposed frequency domain reconstruction approach in terms of achieved digital cancellation, we have simulated a time dispersive slowly fading channel, to incorporate the wireless fading effect on our FD system. The complex baseband representation of a time dispersive (multi path) slowly fading (stationary or quasi stationary) channel impulse response is characterized by

$$h(\tau) = \sum_{p=0}^{p_{\max}-1} \alpha_p \delta(\tau - \tau_p), \tag{4.1}$$

where α_p is zero-mean complex Gaussian random variable, τ_p are the time delays of different multipath and $p_{\max}$ is the number of multi path components.

To apply the effects of multi path fading channel on the transmitted OFDM signal in our system, IEEE 802.11 indoor channel model proposed in [20], which adopts the exponential model for generating the power delay profile (PDP) is used. In the exponential model, the channel power decreases exponentially with delayed taps as follows:

$$P(k) = \frac{1}{\sigma_\tau} \exp^{-pT_s/\sigma_\tau}, \qquad p = 0, 1, 2, ..., p_{max}$$

where σ_τ is the root mean square (RMS) delay spread, p is the discrete path index (taps) with p_{max} as the index of the last path (with smallest non-negligible power) and T_s is the sampling time. In contrast to the exponential model in which the maximum excess delay is calculated by a path of the least non-negligible power level, the maximum excess delay in [20] is fixed to 10 times the RMS delay spread. In other words, the maximum number of paths is determined by the RMS delay spread σ_τ and T_s as

$$p_{max} = [10\sigma_\tau/T_s].$$

The sampling time T_s is kept shorter than one symbol duration by at least a factor of four (usually it is a sub-multiple of the symbol duration). Assuming that the power of the pth channel tap has zero mean and variance of $\sigma_p^2/2$, the coefficients of the impulse response in (4.1) are given as:

$$h_p = \gamma_p + j\beta_p, \qquad p = 0, 1, 2, ..., p_{max}$$

where γ_p and β_p are statistically independent and identical Gaussian random variable each with $N(0, \sigma_p^2/2)$, characterizing a multi path channel with $p_{\max}$ components. Figure 4.1 presents a typical response of time dispersive channel with a delay spread of 100 ns.
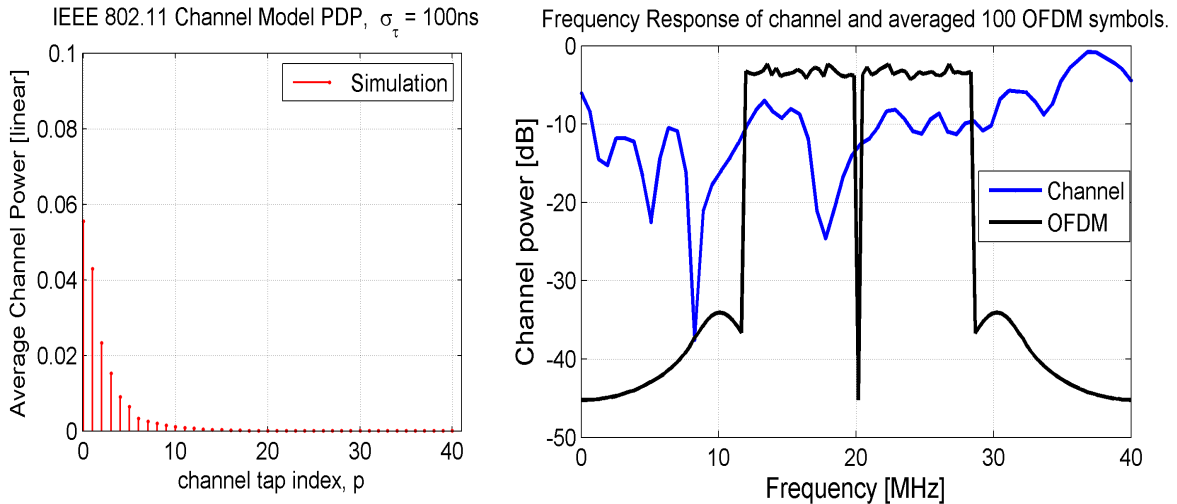
Figure 4.1: Channel PDP and frequency response for $\sigma_\tau = 100ns$ simulated using the IEEE 802.11 indoor channel model.

4.2 Digital Self-Interference Cancellation Performance

To compare the performance of our proposed frequency domain approach, with the existing time domain reconstruction approach presented in [3, 9, 10], we implemented our system and channel models, and simulated the SI channel estimation schemes presented in section 3.2, with the two reconstruction approaches on MATLAB. Via simulations, we investigated the averaged SI cancellation performance of different estimation and reconstruction techniques combinations for different noise figure and multi path delay spreads.

A List of parameters of an OFDM symbol in our simulation settings is shown in Table 3.1. One transmitted OFDM packet carries 100 OFDM symbols. The channel model is simulated with 1000 random realizations. The number of LTS symbols in the

preamble structure is varied between two and eight symbols to demonstrate its effect on the performance of digital SI cancellation. The four channel estimation schemes LS-FDE, LS-TDE, FFT-FDE and LMMSE-FDE are used with time [3, 9, 10] and frequency domain SI reconstruction approaches to compare, and to demonstrate the average digital self-interference cancellation of an OFDM packet with 100 symbols in 1000 random realization of a channel, simulated using the PDP quantified for a certain RMS delay for fading channel. In all the figures, in the legend, the channel estimation technique is specified with the subscript representing the reconstruction approach used for SI cancellation (F for frequency and T for time), the numeric enclosed within the brackets represents LTS length.

4.2.1 Performance of Self-Interference Channel Estimation Techniques

In the first simulation setup, we observed the cancellation performance of all the discussed channel estimation schemes against SNR, for AWGN and fading channels. Figures 4.2 and 4.3 depict the amount of average digital cancellation achieved in pure AWGN channels for different preamble lengths, with no channel gain, i.e. $h = 1$, zero dB channel power. Whereas, Figures 4.4 and 4.5 present the   digital cancellation performance under flat fading channels with $\sigma_\tau = 10 \ ns$, and a coherence bandwidth B_c of 20 MHz for different preamble lengths. As expected, the amount of digital cancellation, except for LMMSE estimator, under flat fading is roughly 2-3 dB lesser as compared to AWGN channels, which is due to the uniform degradation, that is imposed on the whole bandwidth of interest in flat fading, that lowers the SNR of the received signal, thus resulting in poor estimation, and therefore, a lower digital cancellation is seen. Notice that the amount of digital cancellation with LMMSE-FDE has a sharp drop in flat channel, compared to rest of the estimation techniques. This drastic degradation is because of the smoothing matrix, which instead of further improving the LS-FDE, distorted the estimate, leading to poor performance. Due to such poor performance even in flat fading conditions the results for LMMSE-FDE are skipped for the cases of
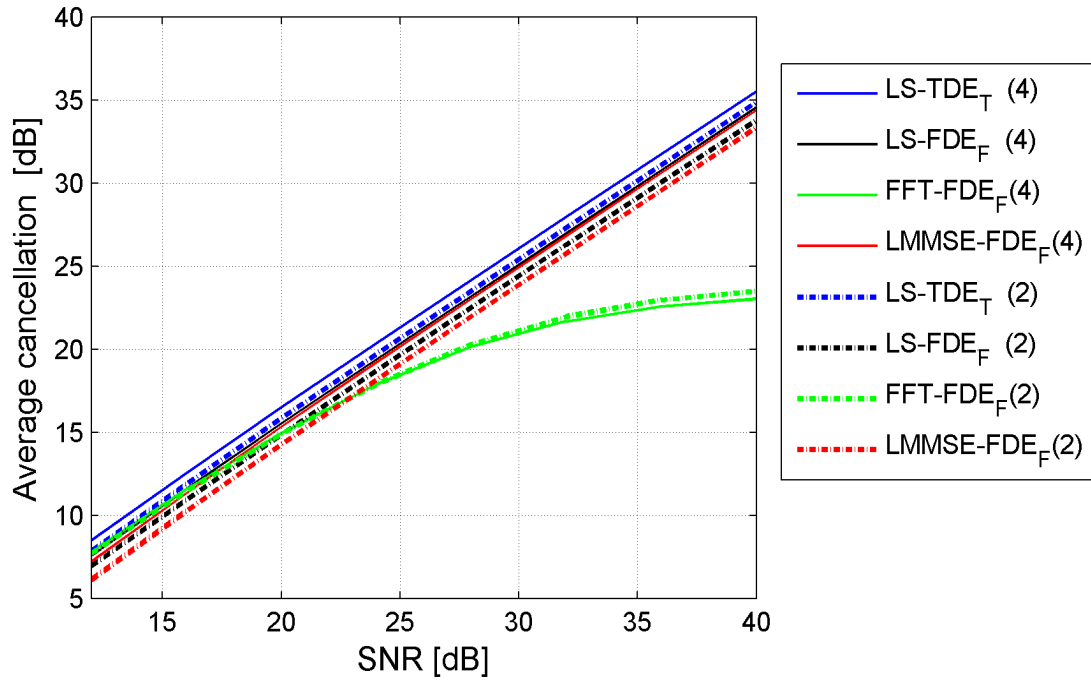
Figure 4.2: Performance of LS-TDE$_T$ [3, 9] and proposed algorithms in AWGN channel.
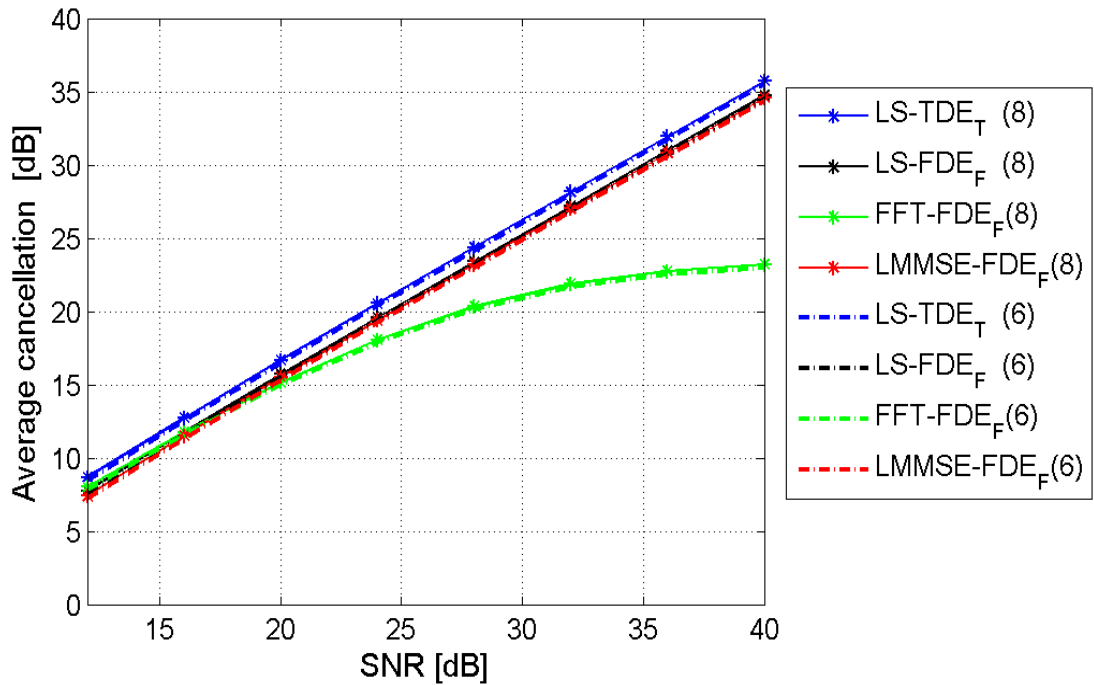
Figure 4.3: Performance of LS-TDE$_T$ [3, 9] and proposed algorithms in AWGN channel.
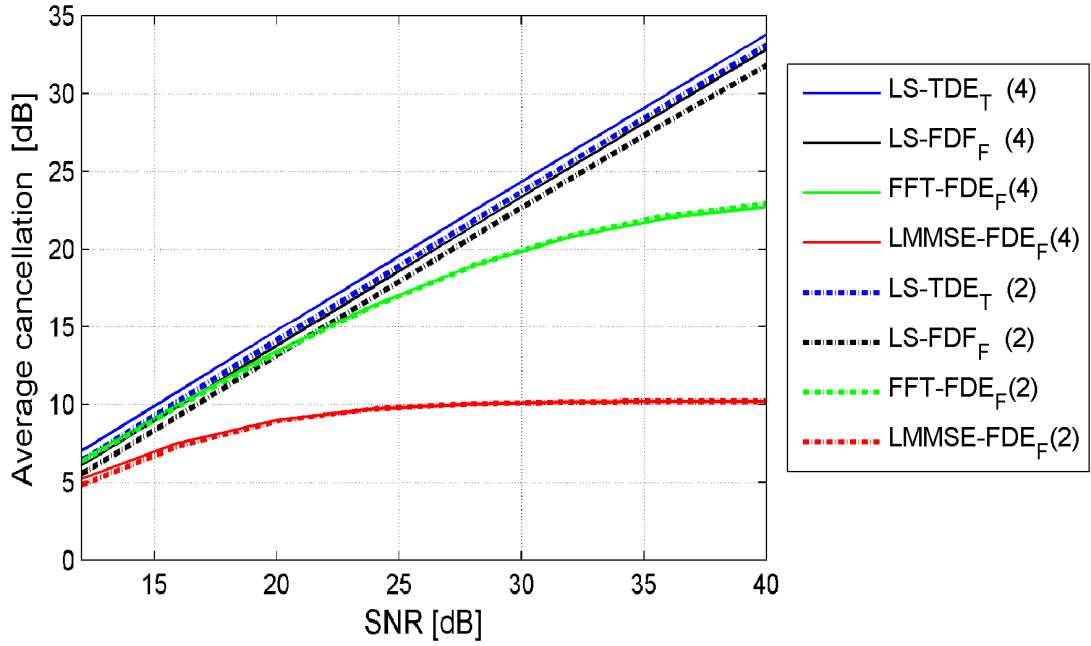
Figure 4.4: Performance of LS-TDE$_T$ [3, 9] and proposed algorithms under fading with $\sigma_\tau = 10$ ns.
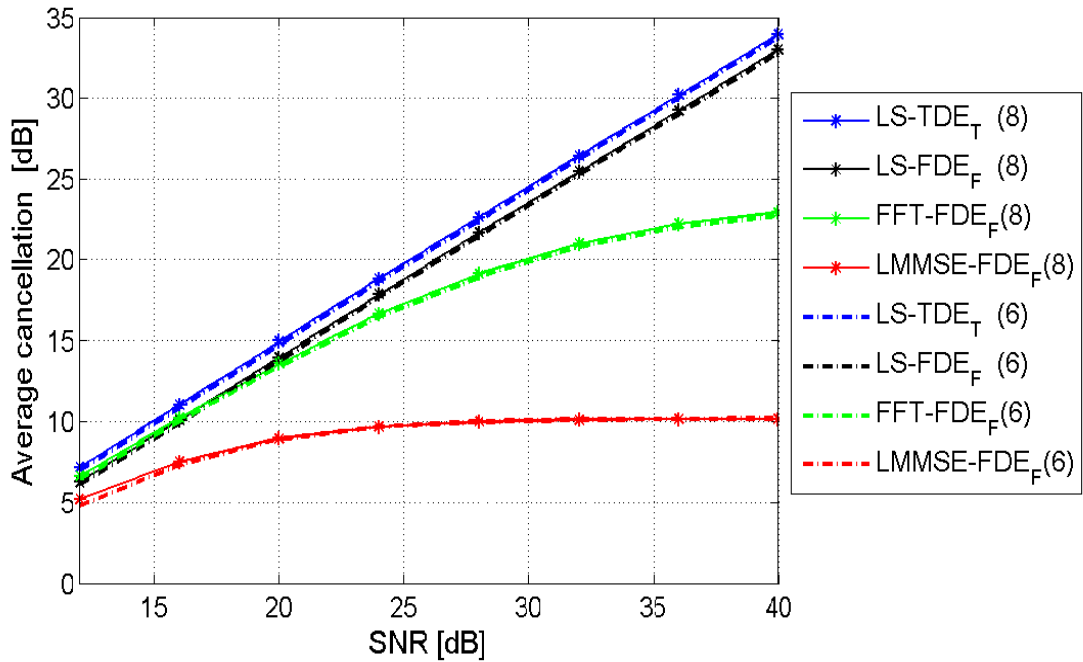
Figure 4.5: Performance of LS-TDE$_T$ [3, 9] and proposed algorithms under fading with $\sigma_\tau = 10$ ns.
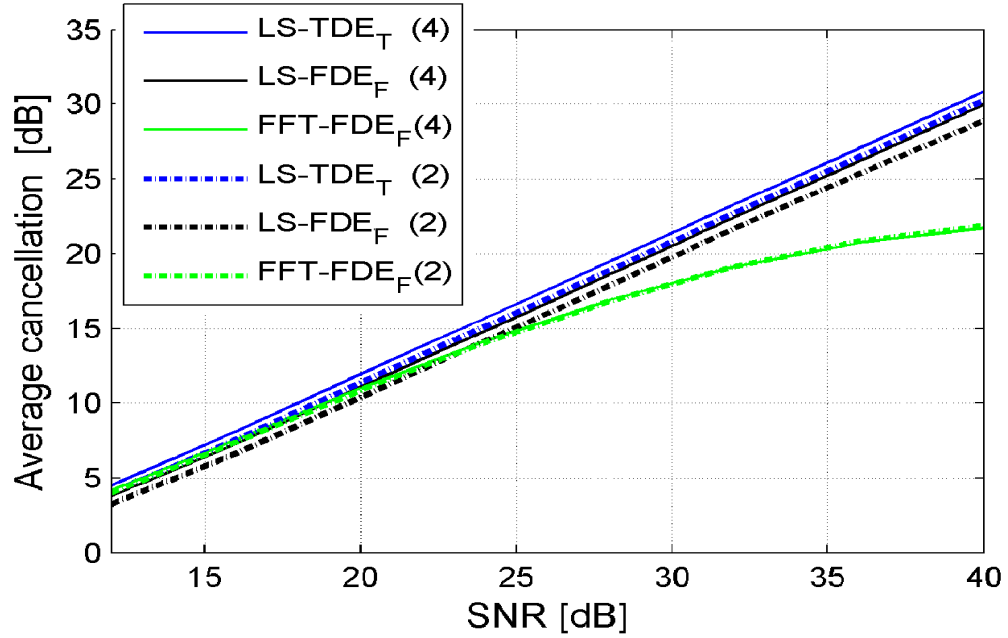
Figure 4.6: Performance of LS-TDE$_T$ [3, 9] and proposed algorithms under fading with $\sigma_\tau = 30$ ns.
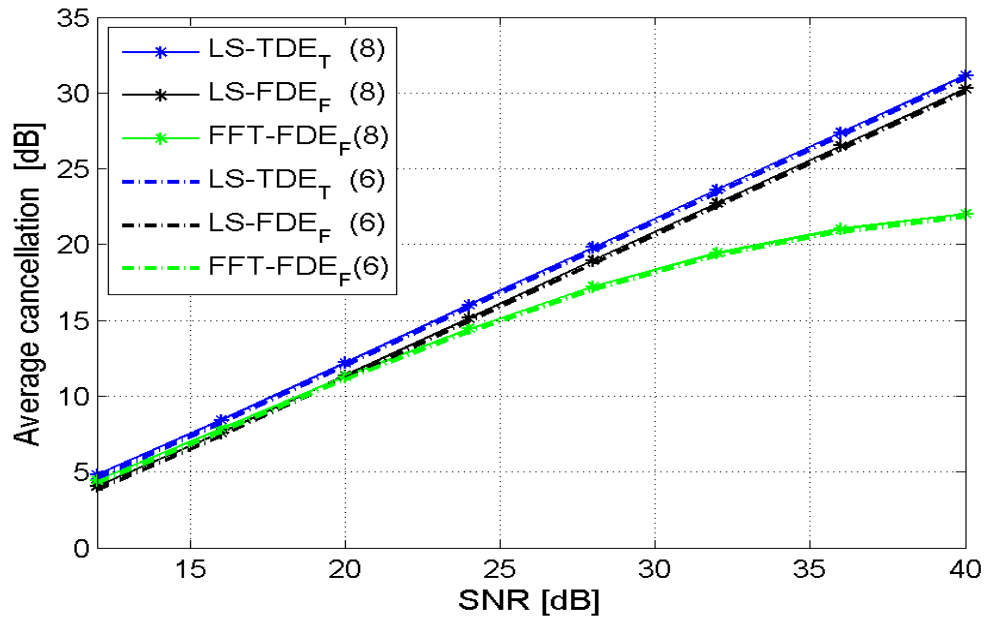
Figure 4.7: Performance of LS-TDE$_T$ [3, 9] and proposed algorithms under fading with $\sigma_\tau = 30$ ns.
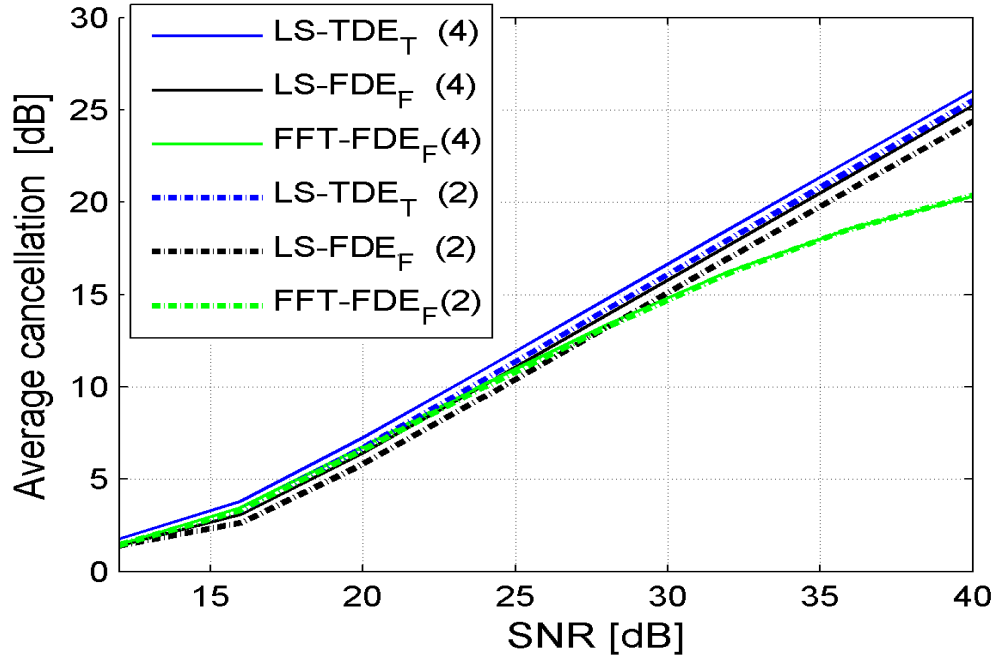
Figure 4.8: Performance of LS-TDE$_T$ [3, 9] and proposed algorithms under fading with $\sigma_\tau = 80$ ns.
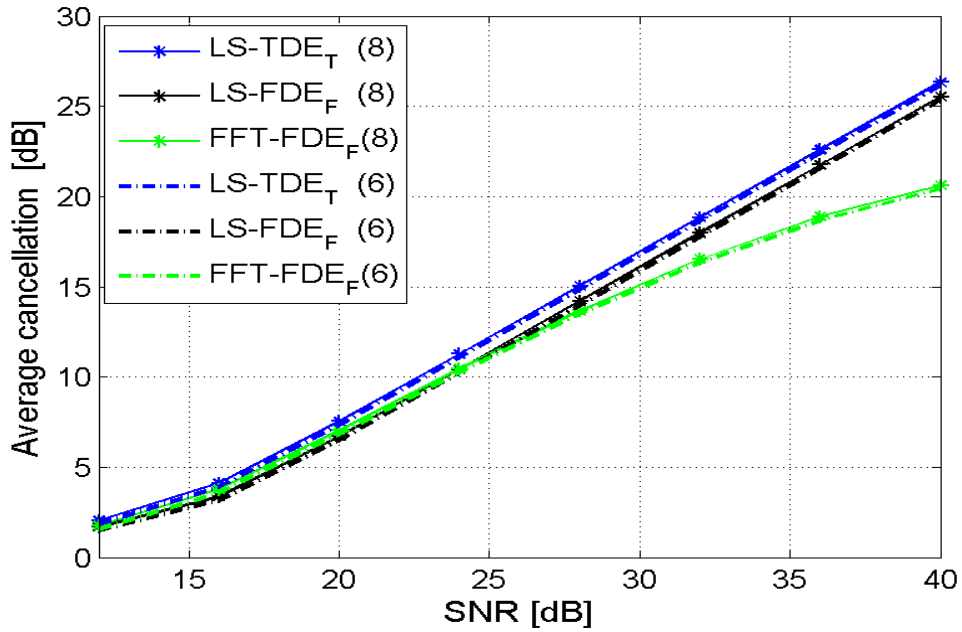
Figure 4.9: Performance of LS-TDE$_T$ [3, 9] and proposed algorithms under fading with $\sigma_\tau = 30$ ns.

sever fading conditions.

Figures 4.6, 4.7, 4.8 and 4.9 shows the SI cancellation in frequency selective channels with coherence bandwidth of roughly 6-7 MHz and 2.5 MHz (a correlation of 0.5 and above is considered) for different preamble lengths, respectively. As anticipated, a larger delay spread degrades the performance of all the employed self-interference cancellation techniques because of the channel's increased selective nature. Also, the LS-TDE$_\text{T}$ used in [3] is leading with highest digital cancellation and FFT-FDE employed in [12] is the least productive in all types of channels. This absolutely signifies the importance of an effective channel estimate for digital cancellation. Notice that, there is a difference of only 0.5-1 dB in the amount of digital cancellation obtained using LS-FDE with frequency domain reconstruction, when compared with LS-TDE$_\text{T}$. Moreover, it can be seen that the longer preamble with 4 LTS symbols provides $\sim 0.8 - 1$ dB more digital cancellation in *averaged cancellation* plots for all and no fading conditions. However, there is no considerable improvement in digital cancellation with lengths over four LTS symbol, besides an undesirable contribution towards the overhead, so the results with these lengths are not included for the next simulations.

One common trend that can be observed in all the digital cancellation techniques, regardless of the channel condition is that the amount of digital cancellation increases with the increasing SNR, because with more SNR a better estimate is acquired, which leads to a finer reconstructed signal and as a result superior cancellation is seen.

4.2.2   Performance with Increasing Delay Spread

In the second simulation setup, we investigated the cancellation performance of the two most effective estimation schemes with increasing RMS delay spread, i.e. severity in frequency selectivity. The plots shown in Figure 4.10 and Figure 4.11 present the performance of the LS-TDE and LS-FDE schemes with time and frequency domain reconstruction approaches in channels with fix SNR but varying RMS delay spread. In this setup, the average achieved cancellation for both SNR levels is getting worse with increasing delay spread, i.e. higher frequency selectivity. The digital cancellation achieved with 4 LTS symbols is consistent with its superior performance over 2 LTS
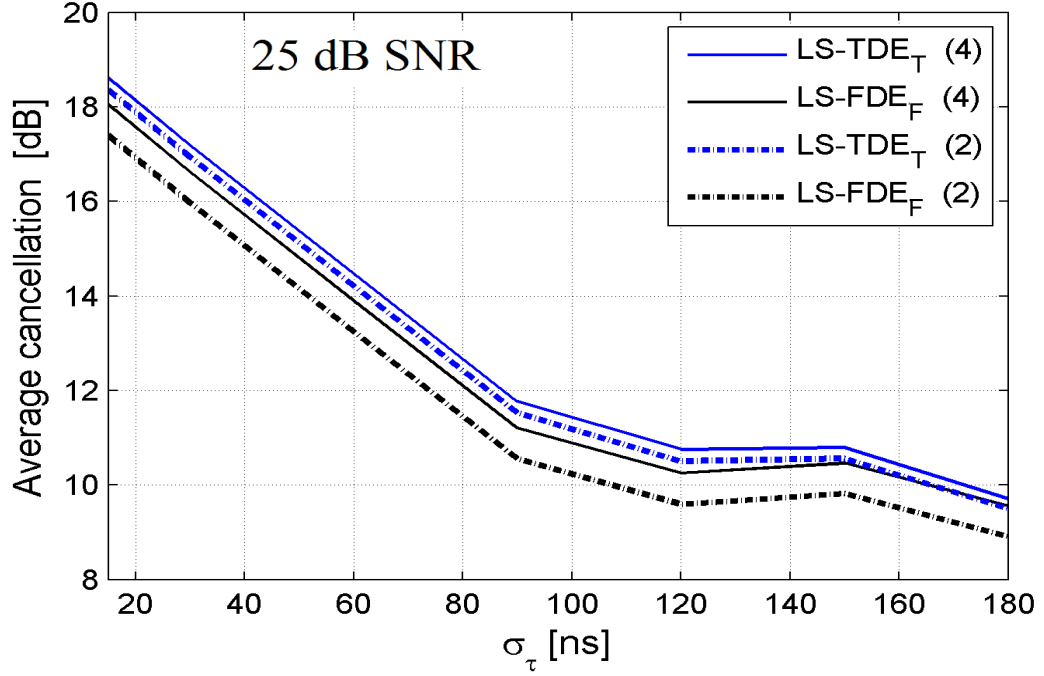
Figure 4.10: Performance of LS-TDE$_T$ [3, 9] and proposed LS-FDE$_F$ in channels with increasing delay spreads and 25 dB SNR.
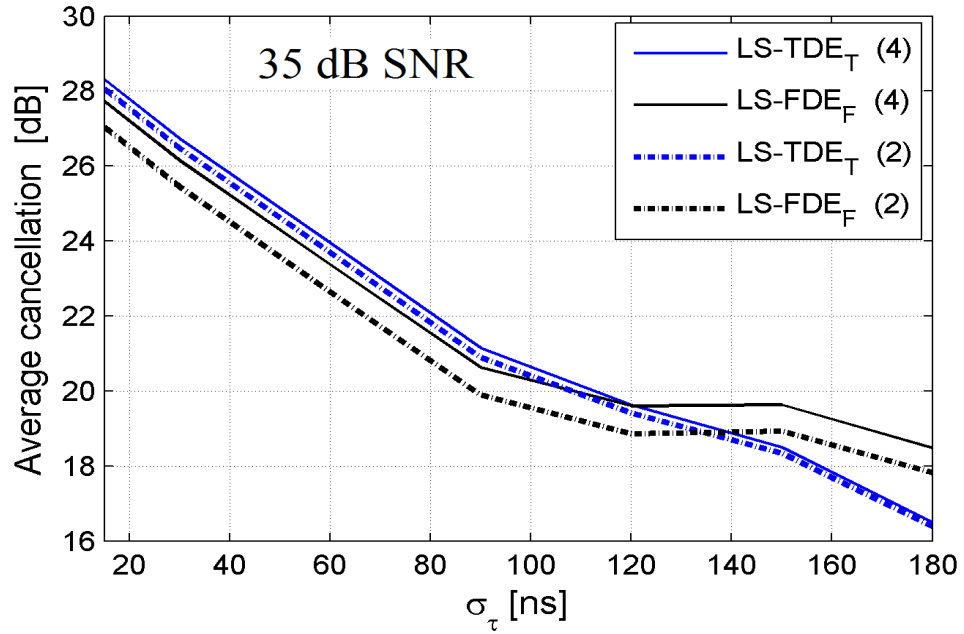
Figure 4.11: Performance of LS-TDE$_T$ [3, 9] and proposed LS-FDE$_F$ in channels with increasing delay spreads and 35 dB SNR.

symbols. In case of medium SNR (25 dB) LS-TDE$_T$ is leading with best digital cancellation results. However, for high SNR (35 dB) and large delay spread, there is a sharp drop in the performance of LS-TDE$_T$ compared to LS-FDE$_F$, certainly because of the prolonged channel impulse response that the CP cannot handle, leading to estimation error, thus a poor overall performance. Notice that in this simulation setup, the performance of the two estimation techniques, each with a different SI signal reconstruction is approximately similar, following what we have observe in the previous setup.

4.2.3 Performance Comparison of the Reconstruction Approaches

In the final simulation setup, we purely analyzed the digital cancellation performance of the two outstanding estimation techniques, i.e. LS-TDE and LS-FDE, as can be observed from Figure 4.6 and Figure 4.8, with both reconstruction approaches for each estimation technique. Figure 4.12 and Figure 4.13 presents the comparison results of the two reconstruction approaches, it can be seen that the LS-TDE technique with both time and frequency domain reconstruction approaches, and LS-FDE technique with frequency domain reconstruction, all three of them are roughly demonstrating the same amount of digital cancellation, under the two different delay spreads. However, the cancellation performance of LS-FDE technique with time domain reconstruction [10] poorer as compared to frequency domain reconstruction counterpart under same channel conditions. In case of frequency domain reconstruction approach under AWGN, and with 10 ns and 30 ns delay spreads, there is roughly 5 dB more cancellation with an SNR between $25 - 30$ dB, and even higher cancellation for SNR above 30 dB as compared to the time domain reconstruction approach. The main reason for this poor performance of time domain reconstruction approach with LS-FDE is that the LS-FDE techniques performs per carrier estimation, and taking the IFFT of the estimate distributes the concentrated channel taps power to all the k points of IFFT. Thus, the signal reconstructed using this distributed channel impulse response eventually performs poorer.
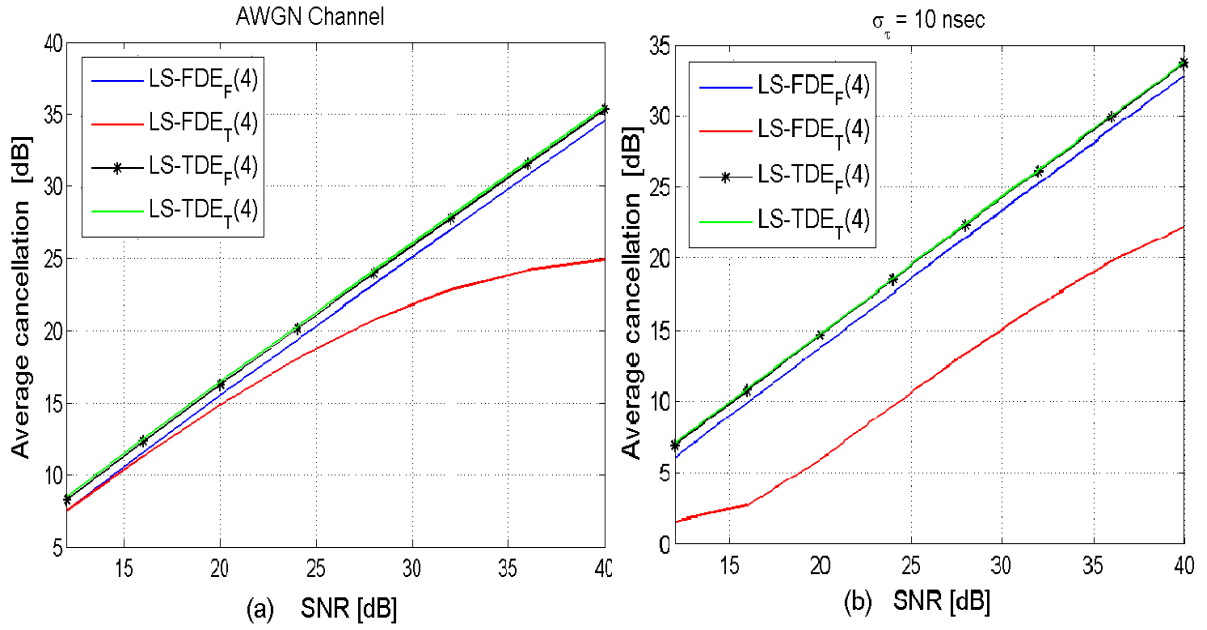
Figure 4.12: Performance of LS-FDE and LS-TDE techniques, with both time [3, 9, 10] and frequency domain reconstruction approaches.
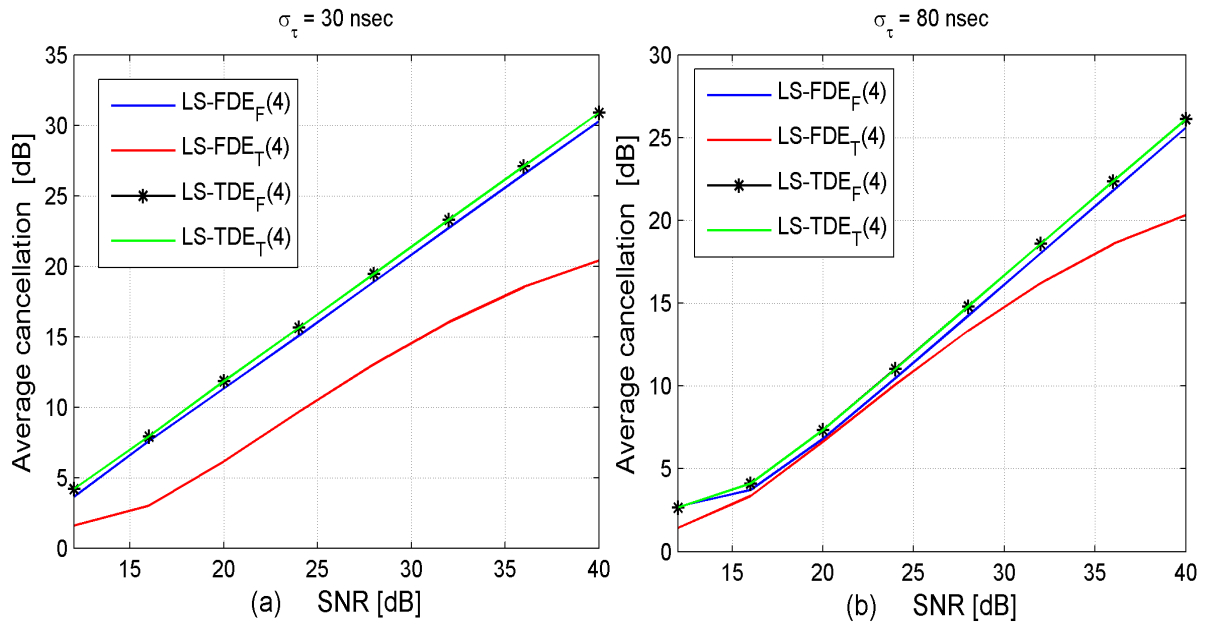
Figure 4.13: Performance of LS-FDE and LS-TDE techniques, with both time [3, 9, 10] and frequency domain reconstruction approaches.

4.3 Computational Complexity

Computational complexity basically presents the number of floating point operations (flops) required to compute an instance or input of a given size of a particular algorithm. It basically determines the efficiency of an algorithm, and usually used to compare the expensiveness of different algorithms in terms of resource requirement and feasibility, while performing the implementation on the processor.

From the simulation results, we confirmed that the proposed frequency domain approach offer similar digital cancellation results, for both LS-TDE and LS-FDE techniques but the reverse is not true. We have seen the poor performance of the time domain reconstruction used in [10] with LS-FDE. The purpose of presenting computational complexities of the estimation and reconstruction techniques is to analyze and compare their implementation requirements and complexities, as we have seen that digital cancellation performance of the two approaches is roughly similar. Therefore, with computational evaluation, we will be able to decide which estimation and reconstruction approach is efficient and less expensive for implementation perspective.

4.3.1 Estimation Complexity

The computational requirement of all the SI channel estimation schemes discussed in chapter 3 varies with their implementation structure.

The LS-FDE only requires a single FFT processing to compute the channel estimate as elaborated in section 3.3.1. A single k points *Radix-2 FFT* processing requires $(k/2).log_2(k)$ complex multiplications and $(k).log_2(k)$ complex additions as given in [31], where each complex multiplication requires four real multiplication and two real addition as explained in [32, 33]. Thus, to compute a single k points radix-2 FFT a total of $2k.log_2(k) - 7k + 12$ real multiplications and $3k.log_2(k) - 3k + 4$ real additions are required as given in [31]. Similarly, a different implementation structure, for example *split Radix FFT* processing requires a total of $4k.log_2(k) - 6k + 8$ real addition and multiplications as presented in [34], where k is required to be greater than 1.

On the other, LS-TDE is done prior to FFT processing and requires $(k.L)$ complex

multiplication and $(k \cdot L)$ complex additions to compute the estimate. Here k represents the length of the averaged receive preamble $y_{l,n}$ and L represents the length of channel impulse response as explained in section 3.3.2. Thus, a total of $4(k \cdot L)$ real multiplications and $4(k \cdot L)$ additions (computed using [32]) are needed to compute the estimate for implementation on a hardware. Also, if the acquired time domain estimate is required to be transformed into frequency domain, then an additional FFT processing is need as well.

Likewise, the FFT based estimates uses an additional IFFT and FFT processing on top of the processing required for computing LS-FDE, therefore straightaway making the estimate three times more expensive. The LMMSE-FDE is the most computationally expensive and complex estimator, besides the strict requirement of knowing the channel statistics and noise variance, it also demands the LS-FDE, computation of inverse of channel covariance matrix and the multiplication of k by k matrices. All of these strict needs make LMMSE undesirable and complexity wise difficult to be implemented on real-time systems. Table 4.1 presents the summary of the flops requirements for different estimation techniques, where k is FFT size with Radix-2 based processing, L represents channel taps and n represents number of samples.

Table 4.1: Estimation complexity summary

Estimation	Evaluation	Flops	
		Multiplication	addition
LS-TDE	$\hat{h} = \mathbf{X}^{\dagger} y_{l,n}$	$4(n \cdot L)$	$4(n \cdot L)$
LS-TDE with FFT transform	$\hat{H}_{\text{LS-T}} = \text{FFT}_k \left\{ \hat{h} \right\}$	$4(n \cdot L) + 2k.log_2(k) - 7k + 12$	$4(n \cdot L) + 3k.log_2(k) - 3k + 4$
LS-FDE	$\hat{H} = \text{FFT}_k \left\{ y_{l,n} \right\}$	$2k.log_2(k) - 7k + 12$	$3k.log_2(k) - 3k + 4$
LS-FDE with IFFT transform	$\hat{h}_{\text{LS-F}} = \text{IFFT}_k \left\{ \hat{H} \right\}$	$4k.log_2(k) - 14k + 24$	$6k.log_2(k) - 6k + 8$
FFT-FDE	$\hat{H}_{\text{FFT}} = \text{FFT}_k \left\{ \hat{h}' \right\}$	$6k.log_2(k) - 21k + 36$	$9k.log_2(k) - 9k + 12$

We have computed the computational requirements of the implementable estimation techniques, based on the specification of our system model that basically follows

IEEE 802.11a/g standard. We have kept the FFT size (k) of 64, with 64 symbols per subcarrier in each LTS making an OFDM symbol, and the maximum channel length (L) is defined by the cyclic prefix, i.e. L = 16. Table 4.2 presents the computational

Table 4.2: Computational Requirements of Different Estimation Schemes with Radix-2 FFT processing.

Sr no.	Estimation Technique	Real Multiplications	Real Additions	Total Flops
1	LS-FDE	332	964	1296
2	LS-TDE	4096	4096	8192
3	LS-TDE with FFT	4428	5060	8464
4	FFT-FDE	996	2892	3888
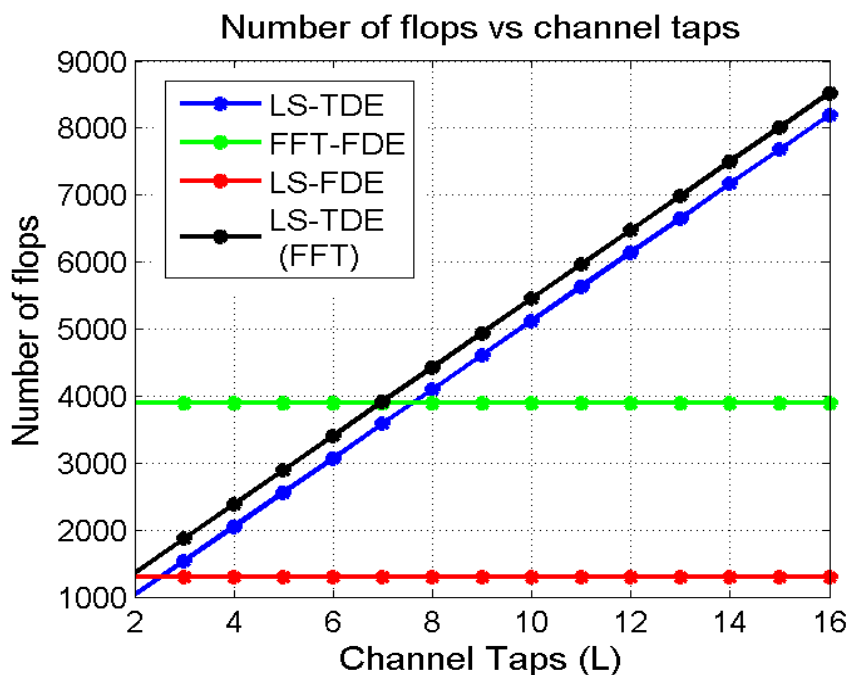
Figure 4.14: Number of flops required with increasing channel taps

figures. As can be seen that the LS-FDE technique is the least expensive, whereas the LS-TDE is most expensive and requires roughly six times more flops compared to

LS-FDE. Notice that these are the additional operations that are required every time the estimation is performed besides the usual RX processing. The other noticeable thing here, is that the number of flops presented in the Table 3.1 for LS-TDE is for the case, when L, the estimated channel impulse response is considered fixed with 16 taps. Figure 4.14 illustrate the effect of channel taps on the number of operation required to compute the channel estimate. For the cases of LS-FDE and FFT-FDE the number of flops remains the same, as these estimators do not depend on the channel taps, infact the frequency domain channel estimators, performs estimation for each subcarrier, regardless of channel taps. The order of computational complexity is as follows

$$\text{LS-FDE} \; < \; \text{FFT-FDE} \; < \; \text{LS-TDE} \; < \; \text{LS-TDE with FFT processing}$$

4.3.2 Reconstruction Complexity

The implementation structures of the two reconstruction approaches discussed in section 3.3 are quite different, as can be seen in Figure 3.4 and 3.5. The time domain reconstruction approach requires convolution operation, which can grow computationally expensive with transmitted packet size. On the other hand the frequency domain approach requires simple multiplication operation to equalize the transmitted symbols with channel characteristics. However, the apparent simple multiplication operation becomes computationally costly because of the IFFT processing, required to convert the frequency domain equalized symbols into time domain reconstructed samples.

The convolution operation required in time domain reconstruction approach can be achieved in two ways:

1) Direct convolution (DC)

2) Circular Convolution (CC)

The direction convolution simply applies the multiply and add (MAC) operation. To reconstruct one OFDM symbol containing "k" samples using "L" channel coefficients, $k.L$ complex additions and $k.L$ complex multiplications are required, where each complex addition requires two real additions and each complex multiplication requires four real multiplication and two real addition as given in [31], making a total of $4k.L$ real

multiplication and $4k.L$ real addition. To avoid the expensive MAC operation utilized by direct convolution the circular convolution is usually used, which utilizes the FFT processing to lower the computational requirements. The circular convolution algorithm, first takes the k point FFT of both OFDM symbols and the channel coefficients (where k represents the number of samples in one OFDM symbol), multiplies them in frequency domain, and convert the equalized result back into time domain via IFFT process. Thus, a total of three k point FFT's and a k point complex multiplication are needed, where each FFT processing requires $2k.log_2(k) - 7k + 12$ real multiplications and $3k.log_2(k) - 3k + 4$ real additions (as presented in subsection 4.3.1 for *Radix-2 FFT*), making a total of $6k.log_2(k) - 17k + 36$ real multiplications and $9k.log_2(k) - 7k + 12$ real addition operations to obtain the reconstructed signal.

On the other hand, frequency domain reconstruction approach takes the known transmitted symbols that are already in frequency domain, equalizes them with the acquired frequency domain channel estimate via multiplication operation, and convert the equalized output into time domain through IFFT process. Therefore, to reconstruct one OFDM symbol containing "k" data symbols using a "k" point channel estimate for each data subcarrier, requires to compute a "k" point complex multiplication first, and then an IFFT processing on the equalized data symbols which requires $2k.log_2(k) - 7k + 12$ real multiplications and $3k.log_2(k) - 3k + 4$ real additions, thus making a total of $2k.log_2(k) - 3k + 12$ real multiplications and $3k.log_2(k) - k + 4$ real additions operations to obtain the time domain reconstructed SI signal.

The flop count presented in Table 4.3 is for the IEEE 802.11a/g standard, with FFT size $k = 64$ and channel impulse response length $L = 16$, defined by the CP in the standard. Clearly, the TD-R with direct convolution is the most expensive approach and requires more than twice more flops as compared to TD-R with circular convolution, and between five to six times more flops compared to FD-R with Radix-2 FFT implementation. Note that these flops are required to reconstruct one OFDM symbol and for a fixed $L = 16$. Figure 4.15 illustrates the effect of channel taps on computational count.

Table 4.3: Computational requirements of different reconstruction approaches for IEEE 802.11a/g based OFDM standards with Radix-2 FFT processing.

Reconstruct-ion Approach	Flops				
	Multiplication		Addition		Flop Count
TD-R using DC (MAC)	$4n \cdot L$	5120	$4n \cdot L$	5120	10240
TD-R using CC (IFFT)	$6k.log_2(k) - 17k + 36$	1252	$9k.log_2(k) - 7k + 12$	3020	4272
FD-R using Radix-2 FFT	$2k.log_2(k) - 3k + 12$	588	$3k.log_2(k) - k + 4$	1092	1680
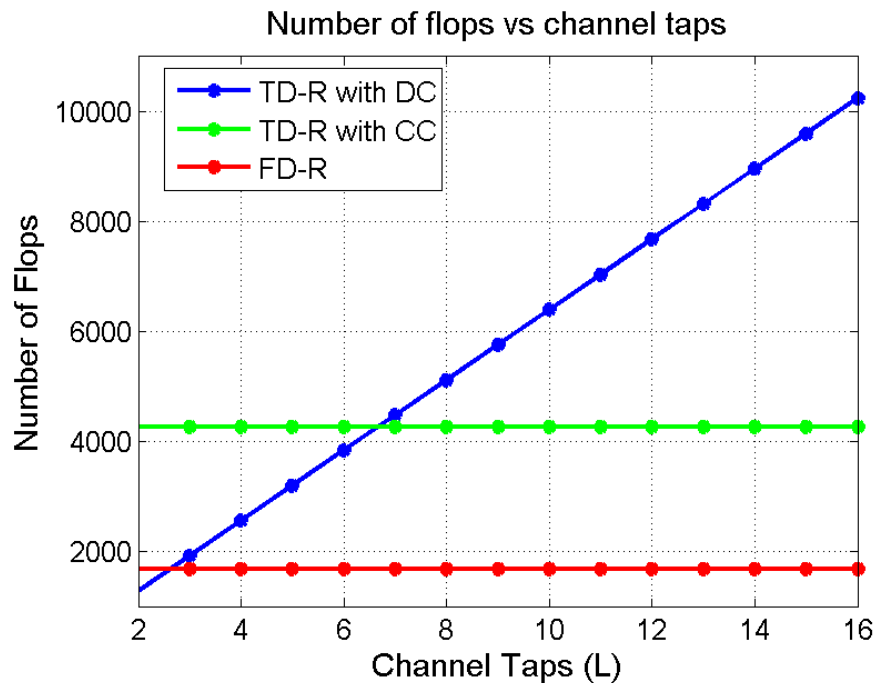
Figure 4.15: Number of flops required with increasing channel taps

4.3.3   Preamble Complexity

We know that the standard IEEE 802.11a/g preamble contain two LTS symbols, and their average is used to compute the channel estimate. The average of two LTS

Table 4.4: Computational requirements of different preamble lengths for IEEE 802.11a/g based OFDM standards.

Sr no.	Preamble Length (l)	Real Multiplications	Real Additions	Total Flops
1	2	128	128	256
2	4	128	384	512
3	6	128	640	768
3	8	128	896	1024

symbols requires k complex additions and k real multiplication, making a total of $2k$ real additions and k real multiplications. Therefore, adding more LTS symbols in the preamble structure requires more operations to compute the average of the received preamble. To compute an average of l transmitted LTS symbols, requires $2(l-1)k$ real additions and k real multiplications, thus requiring a total of $2lk - k$ floating point operations. Table 4.4 presents the total number of flops required to compute the average of the different lengths LTS symbols that has been used in this thesis, for the investigation of its effect on digital cancellation.

4.4 Performance vs Complexity Analysis

Table 4.5 presents a performance vs computational complexity comparison of the various estimation and reconstruction approaches with a preamble containing four LTS symbols under fading channel with $\sigma_\tau = 30$ ns. It can be clearly seen that the proposed frequency domain reconstruction approach offers high performance at the cost of least computational requirements with both least square time and frequency domain estimation techniques as compared to the time domain reconstruction approach used in [3, 9, 10]. These combine results of both simulations and computational requirements demonstrate the superiority of the proposed frequency domain approach, which is more than four times computationally efficient and offers similar high digital cancellation under any type of channel.

Table 4.5: Computational requirements vs performance of different digital cancellation approaches for preamble with 4 LTS symbols.

Digital Cancellation Technique	Estimation Complexity	Reconstruction Complexity	Preamble Complexity	Total Flops	Digital Cancellation Range (Minimum - Maximum) for Received SNR (12 dB - 40 dB)							
					AWGN		$\sigma_\tau = 10$ ns		$\sigma_\tau = 30$ ns		$\sigma_\tau = 80$ ns	
					Min dB	Max dB	Min dB	Max dB	Min dB	Max dB	Min dB	Max dB
LS-TDE$_T$ [3, 9]	8192	4272	512	12976	8.5	36	7	34	4	31	3	26
LS-TDE$_F$	8464	1680	512	10656	8.5	36	7	34	4	31	3	26
LS-FDE$_T$ [10]	2592	4272	512	7376	7.5	25	2	22	2	21	1.5	21
LS-FDE$_F$	1296	1680	512	3488	7.5	35	6.5	33	4	30	3	25.5
FFT-FDE$_F$	3888	1680	512	6080	8	24	6.5	23	4.5	22	2	20

Chapter 5

Performance Tests on a Software Defined Radio Setup

This chapter presents the further verification of the digital cancellation results, of the proposed frequency domain reconstruction approach, via testing on software defined radios. The chapter begins with a brief introduction of SDR used for the testing, after that we present the digital cancellation results measured using the SDR, then the performance of the digital cancellation techniques are tested with a channel emulator, and finally, we present the results of reception under FD transmission.

5.1 WARP SDR

WARP [21] is a short form of wireless open access research platform. It is among the largely used SDR for rapid prototyping of wireless system. WARP combines open-source repository of reference designs with high-performance programmable hardware and support materials. It is an extensible and scalable programmable wireless platform, built to prototype advanced wireless networks, beginning from physical to application layer. The architecture of the radio's processor is based on Xilinx FPGA, besides it is quite cheap compared to other high quality SDR like from Rod and Schwartz.

5.1.1   WARP v3 Mango Boards

WARP v3 is the latest generation of WARP hardware, integrating two flexible RF interfaces, with a capacity to add two more RF chains, making a total of four RF chain on signal board. It incorporates a high performance FPGA and multiple peripherals to facilitate rapid prototyping of custom wireless designs. WARP provides open source reference designs which serves as an excellent starting points for research projects on WARP v3.

Within WARP, there is a WARPLab reference design, which enables rapid physical layer prototyping using WARP hardware for Tx/Rx waveforms and MATLAB signal processing. While the reference design uses MATLAB to control nodes and perform signal processing, it also allows applications with strict latency requirements to move time critical processing in to the FPGA. In this work, we have used WARPLab reference design to first, test the digital cancellation, and then, reception under full duplex transmission. We first implemented our baseband FD OFDM system, and within that system model we have implemented both time and frequency domain reconstruction approaches along with the different channel estimation schemes, all within WARPLab reference design environment. We used the two RF chains in the WARP board for the transmission and reception of the SI and the desired signal.

5.2   Performance with WARP SDR and Gain Characterization

To validate the digital cancellation results presented in chapter 4 and to test FD transmission, we used the three highly performing estimation and reconstruction techniques namely: LS-TDE$_T$, LS-TDE$_F$ and LS-FDE$_F$ with WARP SDR, via WARPLab framework interface, that provides direct prototyping of physical layer through MATLAB. To investigate the performance of these techniques at maximum capacity, we first performed gain characterization of the RF and baseband amplifiers within WARP radios. In order to prevent the saturation of the ADC because of high power SI sig-

nal, while FD transmission, we have used three different interfaces to provide analog cancellation, i.e. direct cables with RF attenuators, two antennas with separation to provide RF isolation, also used in [11] and with a patch antenna that uses orthogonal polarization for analog isolation. The parameters setting in the experimental setups are mostly similar to the ones we used for simulations purposes in chapter 4. The OFDM symbols parameter settings are same as the ones given in Table 3.1. One transmitted OFDM burst carries 100 OFDM symbols and a preamble structure that can carry up to 18 symbols, in which the first 10 symbols are used for receiver synchronization and packet detection, and the remaining contribute towards estimation. The number of LTS symbols in the preamble structure is varied between two and eight symbols, like we did in simulations.

The WARP radio settings are as followed: we have used the channel one of 2.4 GHz band provided in the radio. The center frequency of this channel is 2.412 GHz with a 20 MHz bandwidth. We used RF chain A for transmission and chain B for reception. For gain characterization, we kept the RF gains fixed, while increasing the baseband amplifiers gains in steps, with each step providing an averaged digital cancellation of 100 OFDM burst transmissions, where each burst carries 100 OFDM data symbols. However, for the cases when the analog domain suppression is too high, the transmit gain is increased between 0 dBm to 5 dBm. In all the figures, in the legend, the channel estimation technique is specified with the subscript representing the reconstruction approach used for SI cancellation (F for frequency and T for time), the numeric enclosed within the brackets represents the number of LTS symbols in the preamble.

5.2.1   Tests with a Direct Cable Connection

In this test setup, illustrated in Figure 5.1, we used the direct cables with RF attenuators to provide RF isolation. The tests are conducted with three different RF attenuators, i.e. 32 dB, 40 dB and 50 dB. Figure 5.2a and b, and 5.4a and b presents the digital cancellation results of three SI suppression techniques, for the case when RF gain is 15 dB and the RF isolations are 32 dB and 40 dB respectively.   It can be notice
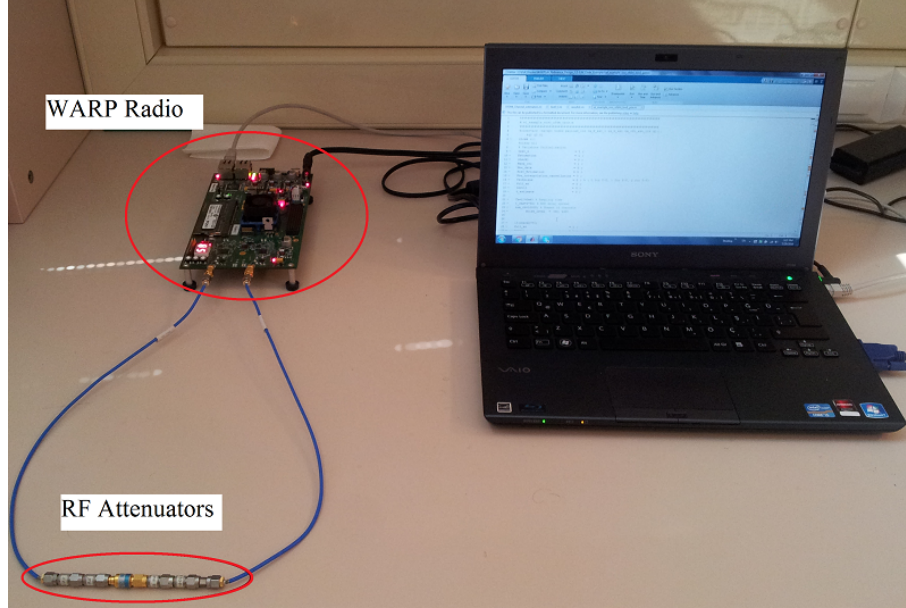
Figure 5.1: Experimental setup with RF attenuators providing analog isolation.
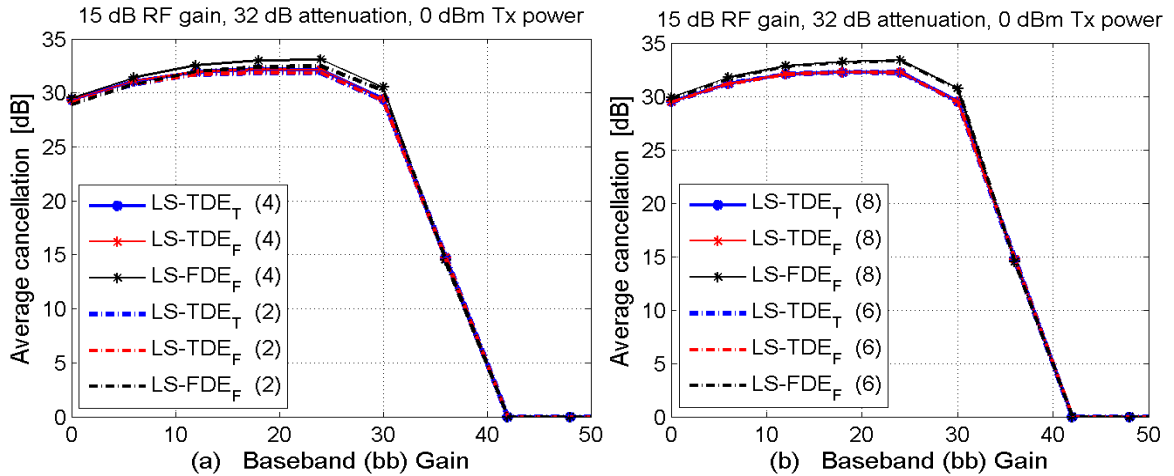
Figure 5.2: Performance of LS-TDE$_T$ [3, 9] and proposed algorithms with 32 dB analog attenuation and 15 dB RF gain.

that averaged cancellation achieved using proposed frequency domain reconstruction approach i.e. LS-FDE$_F$, is roughly 1 dB more than the other two techniques in which LS-TDE$_T$ has been used in previous works [3, 9], and both of these techniques are nearly four to five times more computationally expensive than LS-FDE$_F$. Preamble with more LTS symbols is still showing its effectiveness over standard two symbol LTS preamble, like we observed in simulations given in chapter 4. Here, it can be observe that there is
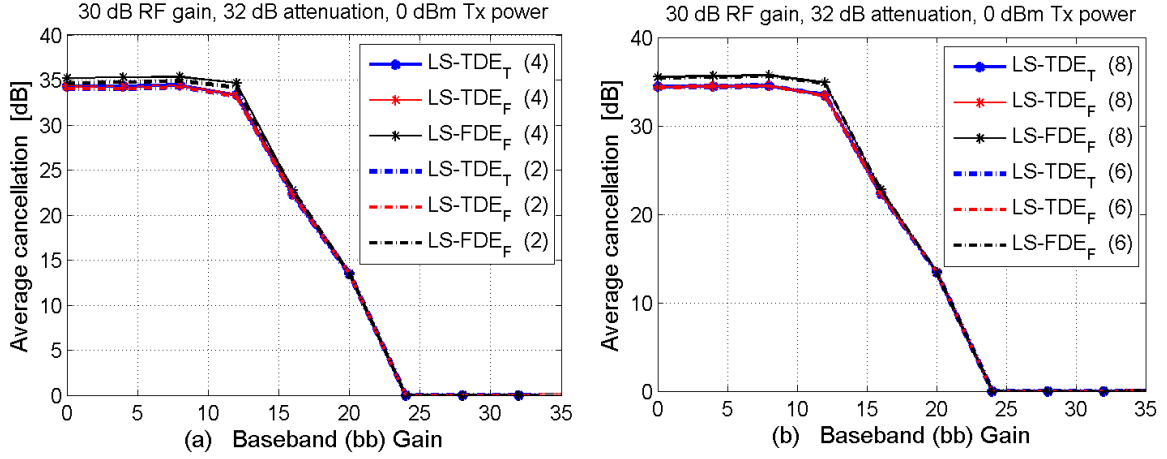
Figure 5.3: Performance of LS-TDE$_T$ [3, 9] and proposed algorithms with 32 dB analog attenuation and 30 dB RF gain.
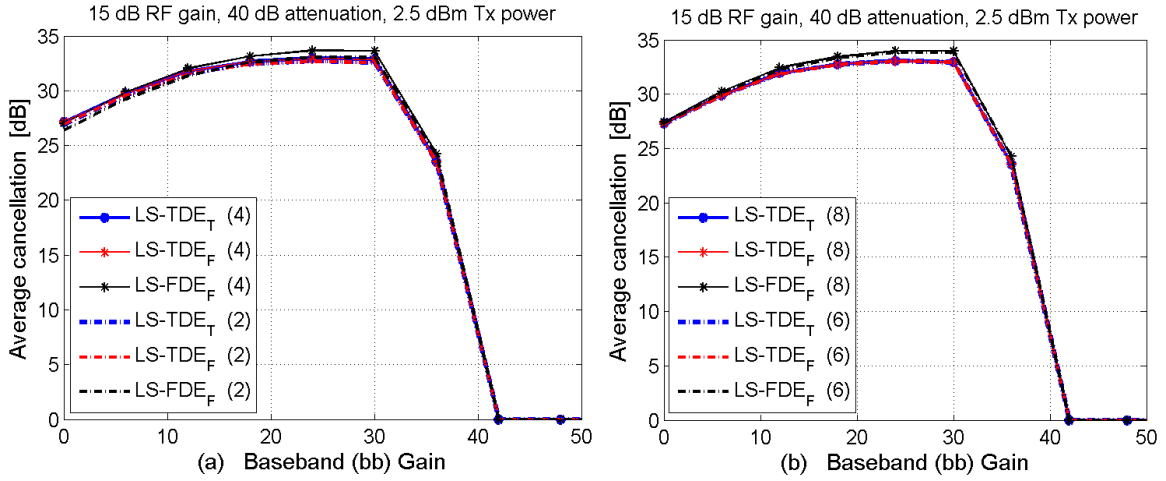
Figure 5.4: Performance of LS-TDE$_T$ [3, 9] and proposed algorithms with 40 dB analog attenuation and 15 dB RF gain.

no noticeable improvement with six and eight LTS symbols, besides an extra overhead. One more thing that can be observed in these figures is that the averaged cancellation, first increases with increasing baseband gains, reaches the maximum, and then starts to fall. This tells us that, there is a certain combine range of both RF and BB gains in which we can achieve maximum cancellation, and a gain more than this ranges amplifies the received signal to such a level that ADC gets saturated, leading to poor digital cancellation.
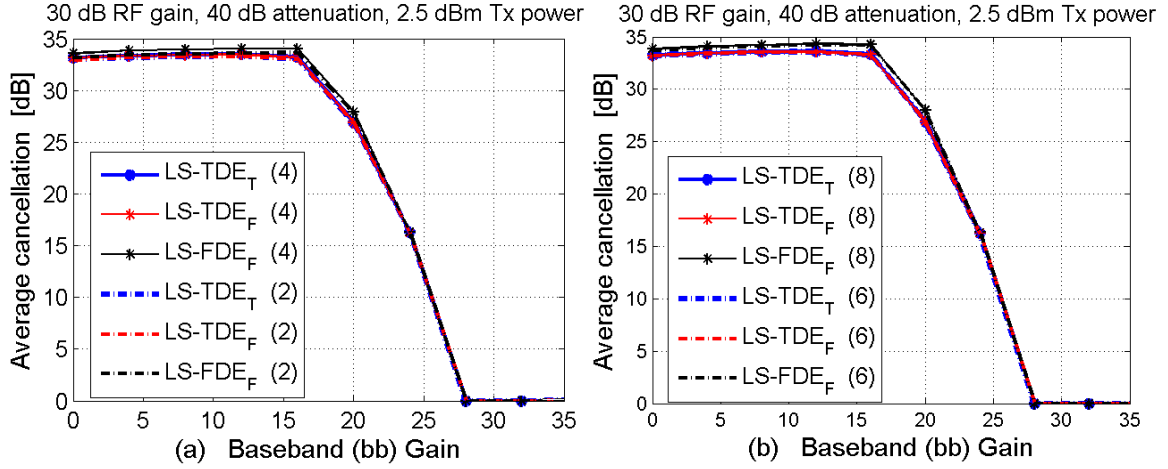
Figure 5.5: Performance of LS-TDE$_T$ [3, 9] and proposed algorithms with 40 dB analog attenuation and 30 dB RF gain.
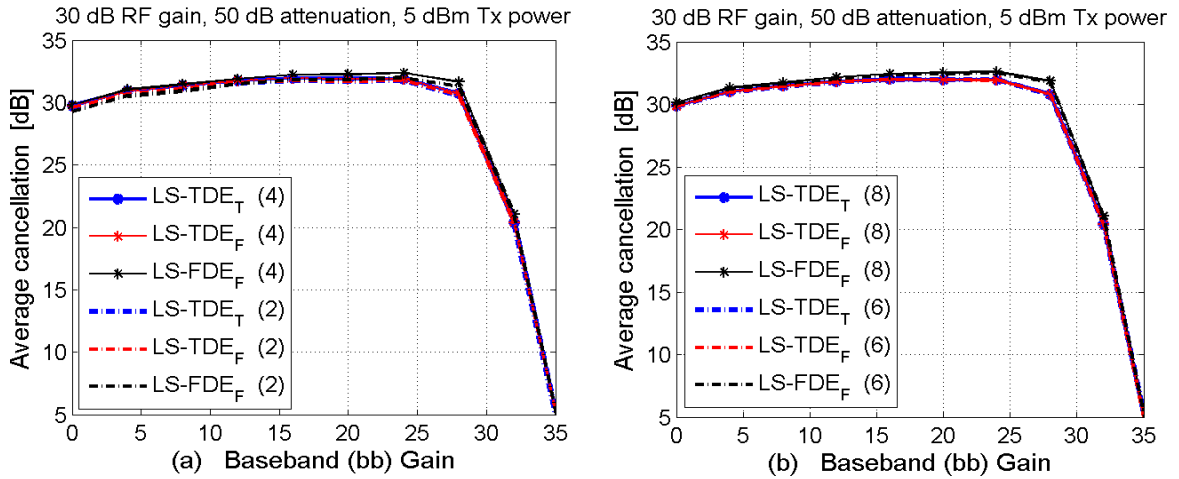
Figure 5.6: Performance of LS-TDE$_T$ [3, 9] and proposed algorithms with 50 dB analog attenuation and 30 dB RF gain.

Similarly, the analysis of the results presented by Figures 5.3, 5.5 and 5.6 for 30 dB RF gain, projects some similar findings as that were seen with 15 dB RF gain. The averaged cancellation decreases with increasing RF isolation e.g. for the case of 32 dB isolation the maximum cancellation is above 35 dB with LS-FDE$_F$, however, it drops down to 32 dB for an isolation of 50 dB, although the Tx power is 5 dBm in this case. We can see the saturation effect after a certain level of baseband gain, but this range varies with RF isolation, e.g. for 32 dB isolation, the saturation point is 12

dB baseband gain, whereas, for 50 dB isolation the saturation point of the baseband gain is 28 dB. One important result to observe here is that with more RF gain more digital cancellation is observed, for example, in case of LS-FDE$_F$ with 32 dB isolation, maximum digital cancellation observed with 15 dB RF gain is 33 dB, whereas, with 30 dB RF gain the cancellation is above 35 dB. This more digital cancellation with high RF gain is due to the fact that the noise figures of RF amplifiers are low compared to the noise figures of baseband amplifiers. Therefore, more RF gain mean less gain is required in baseband, thus reserving better SNR.

Finally, the most important conclusion that can be drawn from these characterization tests results with the direct cables is that the digital cancellation decreases with increase in analog suppression. This is due to the reason that with more analog suppression of SI signal in analog domain decreases its SNR, which results in poor SI channel estimation, leading to poor reconstruction and thus a lower digital cancellation.

5.2.2 Tests with Two Antennas

In this experimental setup for FD implementation, we performed the digital cancellation test measurement and gain characterization with two antennas separated by a distance, to provide analog suppression of SI signal as illustrated in Figure 5.7. This
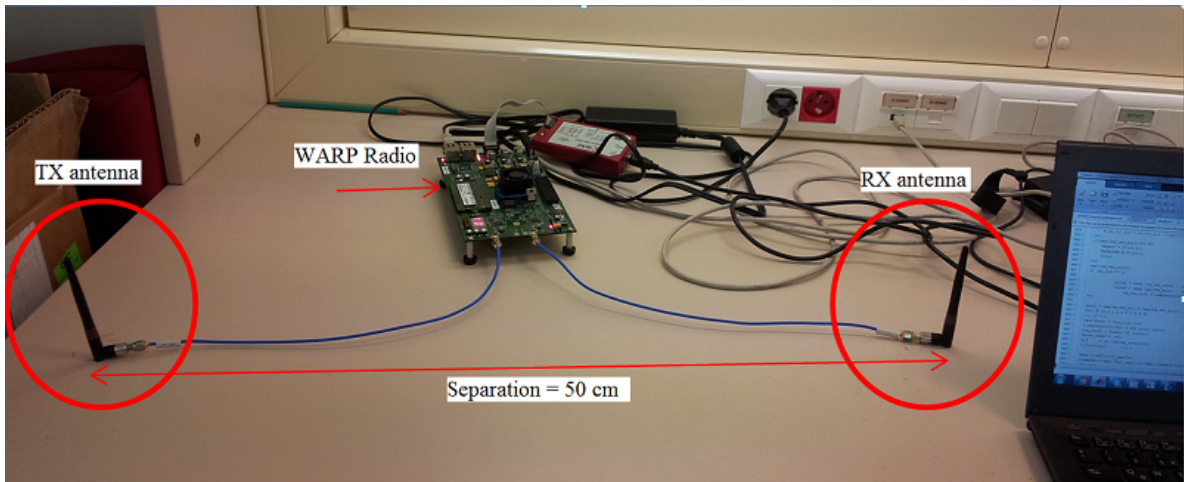
Figure 5.7: Experimental setup with two antennas providing analog isolation.

approach of analog separation is also used in [11]. In both antenna placements the

antenna direction is kept parallel, while digital cancellation is observed for 15 dB and 30 dB RF gains, with a transmit power of 2.5 dBm.
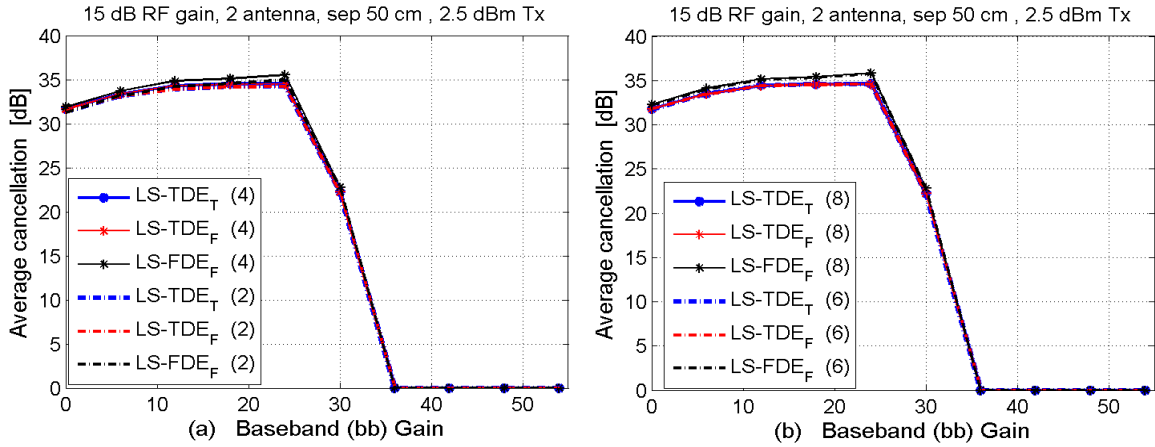
Figure 5.8: Performance of LS-TDE$_T$ [3, 9] and proposed algorithms with two antennas with 50 cm separation and 15 dB RF gain.
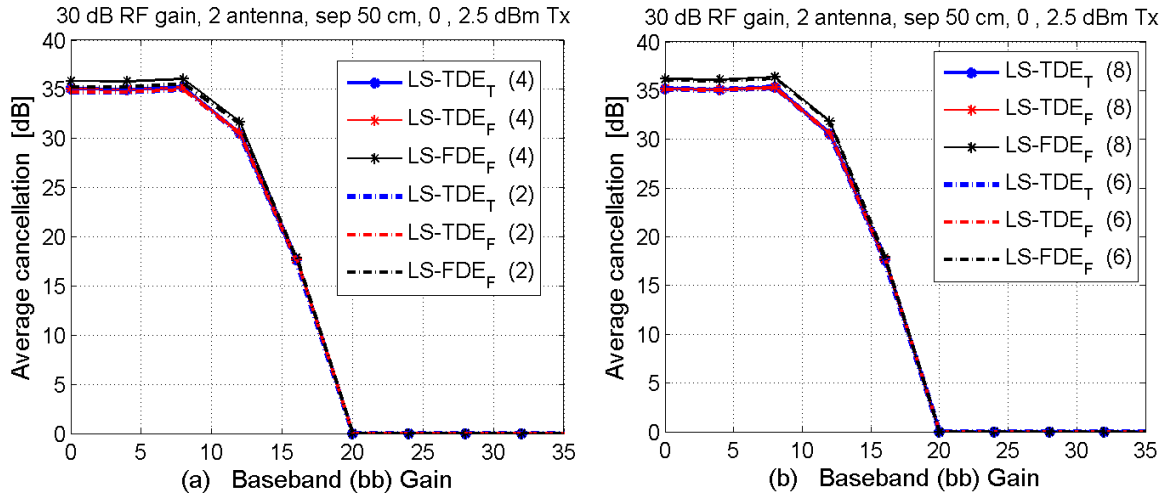
Figure 5.9: Performance of LS-TDE$_T$ [3, 9] and proposed algorithms with two antennas with 50 cm separation and 30 dB RF gain.

Figures 5.8 and 5.9 presents the digital cancellation results for 50 cm antenna separation providing 38 dB of RF isolation, with 15 dB and 30 dB RF gains respectively. Whereas, Figures 5.10 and 5.11 depicts the cancellation results obtained with an antenna spacing of 75 cm, giving an RF suppression of 52 dB, again with 15 dB and
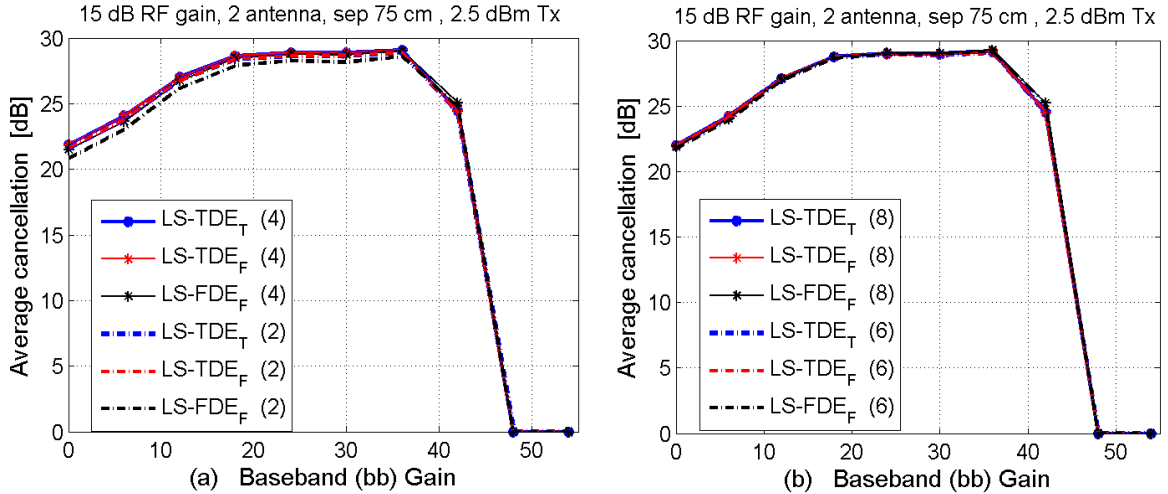
Figure 5.10: Performance of LS-TDE$_T$ [3, 9] and proposed algorithms with two antennas with 75 cm separation and 15 dB RF gain.
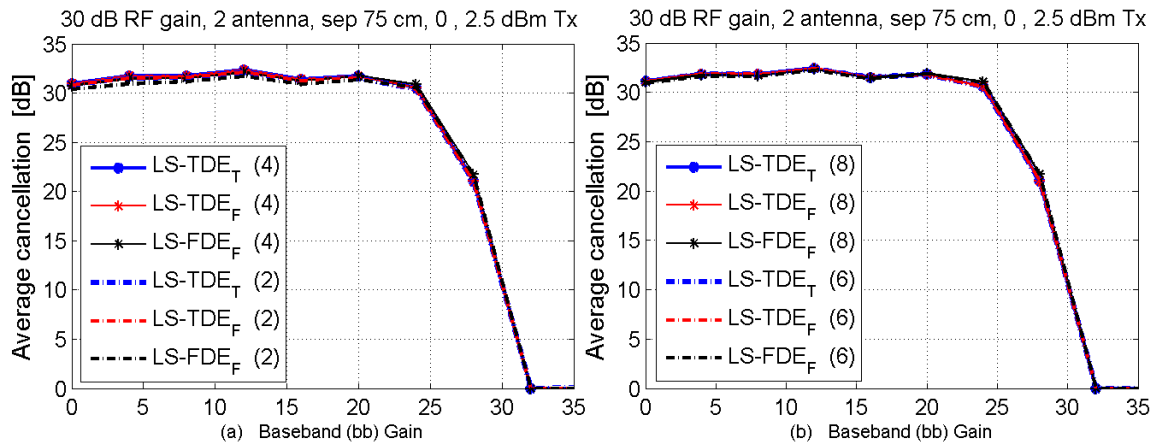
Figure 5.11: Performance of LS-TDE$_T$ [3, 9] and proposed algorithms with two antennas with 75 cm separation and 30 dB RF gain.

30 dB RF gains, respectively. First, we can see that due to more RF suppression in cases of Figure 5.10 and 5.11, we have less digital cancellation because of low SNR compared to the other antenna setting. Secondly, the gain saturation points of the two spacing are different, like we have seen with previous setup, and there is more digital cancellation with 30 dB RF gain, especially with antenna separation providing large isolation. An interesting result that can be observed here, is that the tests with cables, and the ones with two separates antenna with air as a medium for transmission, is

roughly demonstrating the same digital cancellation. These results clearly support the practical performance of digital cancellation techniques in wireless FD transmission.

5.2.3 Tests with a Patch Antenna

In this final experimental setup, for the gain characterization of the WARP RF chain amplifiers, while testing digital cancellation, we used a patch antenna as an interface between the two RF chains, to provide analog suppression of the SI signal as shown in Figure 5.12. Figure 5.13 presents the simulated and measured s-parameters of the
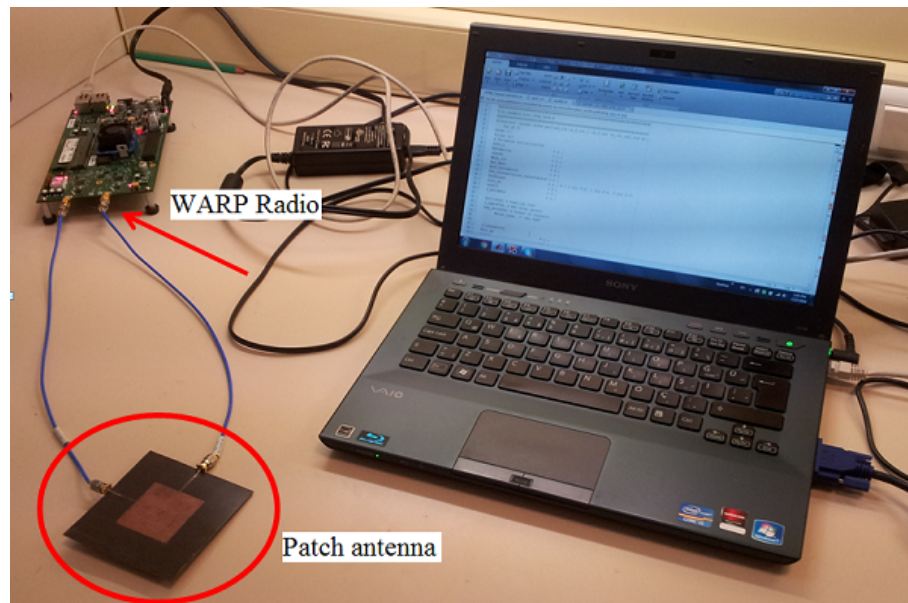
Figure 5.12: Experimental setup with patch antenna providing analog isolation.

patch antenna used in this setup. It can be seen that this patch antenna can provide an analog isolation of 46 dB in our band of transmission and reception, which is a little lower than the maximum isolation. Figures 5.14 and 5.15 present the amount of digital cancellation achieved using the three cancellation techniques, with 15 dB RF gain and 30 dB RF gain, respectively.
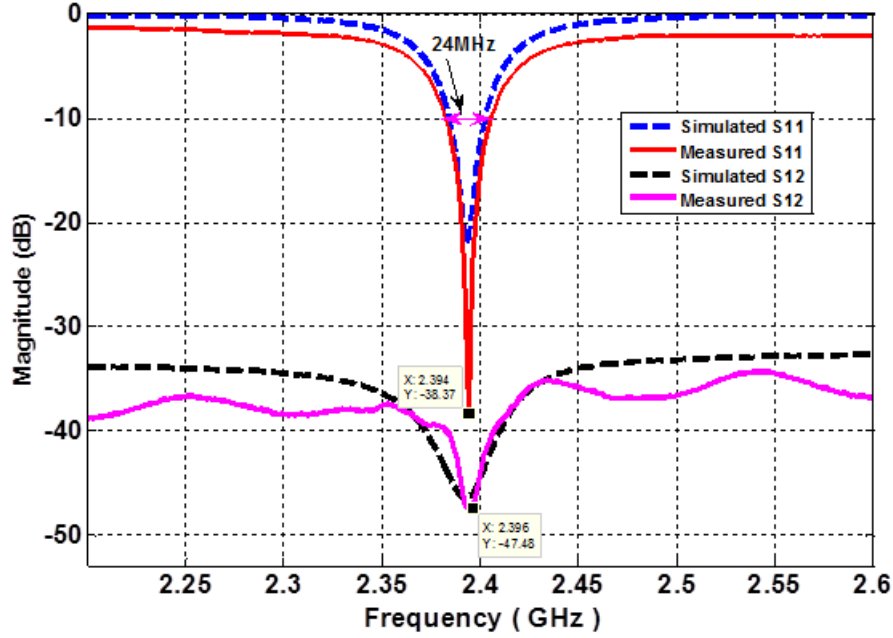
Figure 5.13: S-parameters of the patch antenna that can provide 48 dB of isolation between the Tx/Rx port.
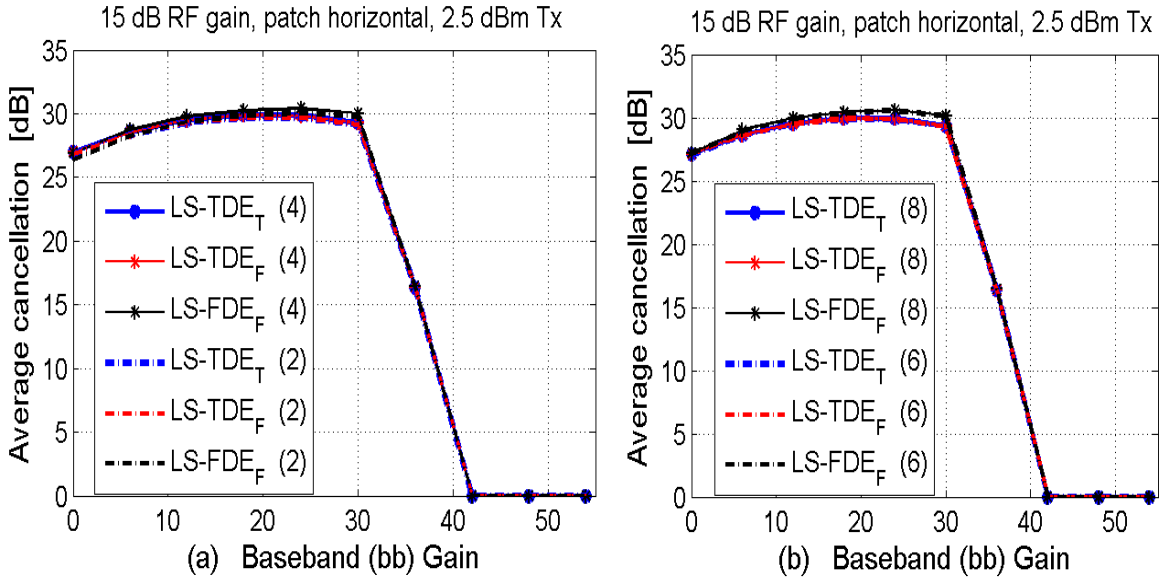
Figure 5.14: Performance of LS-TDE$_T$ [3, 9] and proposed algorithms using patch antenna with horizontal setting and 15 dB RF gain.

Similar results of digital cancellation with a certain gain saturation point can observed, like the ones we have seen in previous experimental setups, but with different
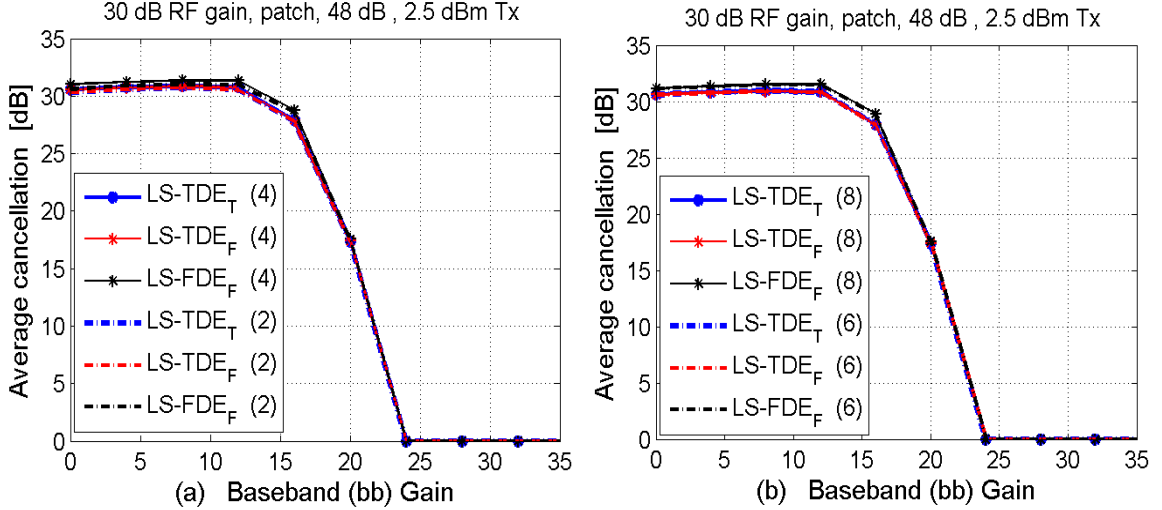
Figure 5.15: Performance of LS-TDE$_T$ [3, 9] and proposed algorithms using patch antenna with horizontal setting and 30 dB RF gain.

RF interfaces. The cancellation amount with proposed frequency domain reconstruction approach is still providing the maximum cancellation, a difference of $\sim$1 dB.

5.3 Performance Tests with WARP SDR and Channel Emulator

In the previous section, we performed extensive tests with WARP SDR for the validation of the digital cancellation techniques that we simulated in MATLAB environment, as presented in chapter 4. These tests were performed in a LAB with a controlled environment (to some extent). To further validate these test results under multi path fading conditions, we employed a channel emulator on top of the received signal, which we obtained via two different RF interfaces, i.e. two antennas and single patch antenna. The channel emulator that we used is based on the same IEEE 802.11 indoor channel model that we simulated for the performance analysis of the digital cancellation techniques in the previous chapter.

In the following tests, we passed the samples received, from the two mentioned RF interfaces, through the channels with increasing delay spreads, and the resultant samples

with self-induced channel effects are then processed to observe the digital cancellation performance. We have used the gain characterization results, to find the best baseband gain, providing maximum digital cancellation with 30 dB RF gain.

5.3.1 Performance with Two Antennas

Figures 5.16 and 5.17 presents the digital cancellation performance results of the three cancellation techniques under increasing channel severity, with two antennas as RF interface that are 50 cm apart. For the baseband gain selection, we have used the digital cancellation results presented in the previous section of the gain characterization with two antennas that are 50 cm apart. In those curves, it can be seen that the maximum digital cancellation is achieved with 30 dB RF and 6-8 dB of baseband gain, and any further gain leads into the saturation region.

It can be seen that averaged digital cancellation is less than what we observed without the channel emulator. This is understandable, because we have imposed an additional source of signal degradation on the received samples in the form of channel emulator. The other important thing that can be noticed here, is that after a certain RMS delay spread (in this case after 75 ns), the total digital cancellation achieved using the three cancellation techniques starts decreasing. However, it can be seen that the proposed LS-FDE$_F$ in such channel degradations, outperformed the other two cancellation techniques, which are based on time domain least square estimates and are computationally expensive as well. The main reason of their poor performance, is the limited length of the cyclic prefix, because while performing LS-TDE the duration of the channel impulse response is assumed to be less than the duration of the CP, which is 800 ns with 16 samples, that's why, the number of channel taps (L) are kept same as CP, i.e. L = 16. Therefore, if the channel impulse response exceeds 800 ns, (e.g. in our channel emulator settings, that is the case when the RMS delay spread σ_τ is greater than 80 ns) then, the time domain estimation process lacks the capacity to fully estimates this channels, which results in poor estimate, that leads to poor SI signal reconstruction and eventually lower digital cancellation. This limited channel taps problem does not affect frequency domain channel estimates, because LS-FDE
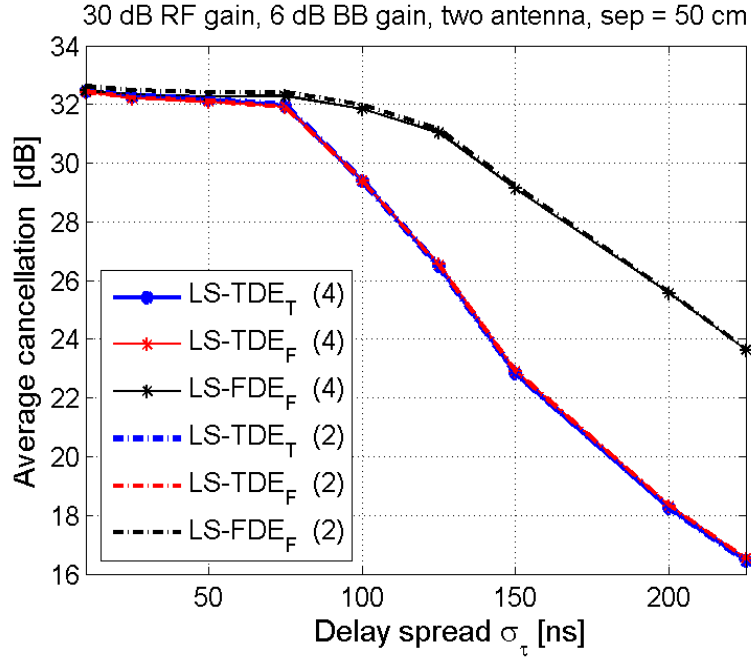
Figure 5.16: Performance of LS-TDE$_T$ [3, 9] and proposed algorithms using two antennas with 50 cm separation and time dispersive channel effects.
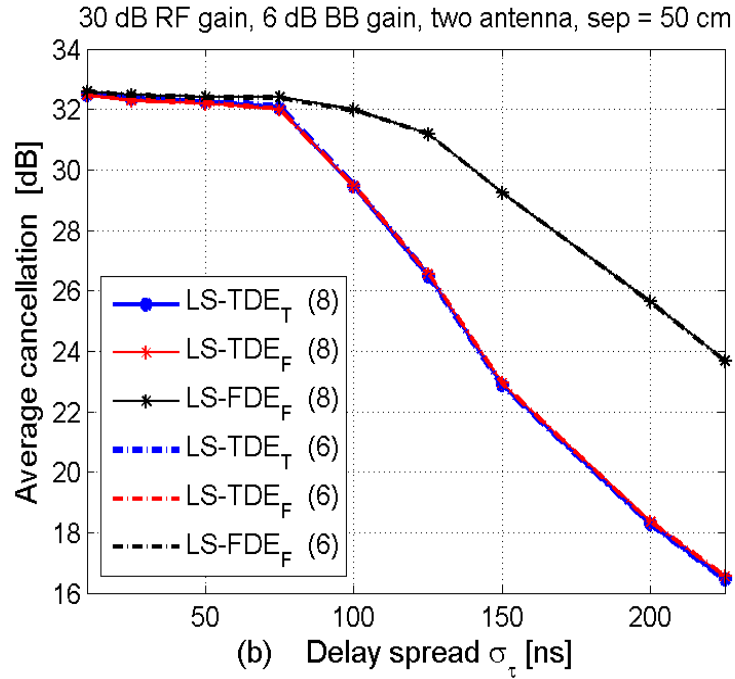
Figure 5.17: Performance of LS-TDE$_T$ [3, 9] and proposed algorithms using two antennas with 50 cm separation and time dispersive channel effects.

performs estimation of all the subcarriers at the same time, that's why in the figures, it can be seen that the digital cancellation with LS-FDE$_F$ does not follow the sharp drop showed by the other two time domain estimation based cancellation techniques. The drop in its performance is only due to the increasing selective nature of the fading channel.

5.3.2 Performance with a Patch Antenna

The digital cancellation performance results presented with Figures 5.18 and 5.19, are for the case, when we used a patch antenna with $\sim$47 dB isolation, to provide analog suppression. For the baseband gain selection in this case, we again used the digital cancellation results presented in section 5.2.3 of gain characterization, but now for the results with patch antenna. In those curves for the patch antenna, it can be seen that the maximum digital cancellation is achieved with 30 dB RF and 10-12 dB of baseband gain, and any exceeding gain leads to the saturation of the ADC.
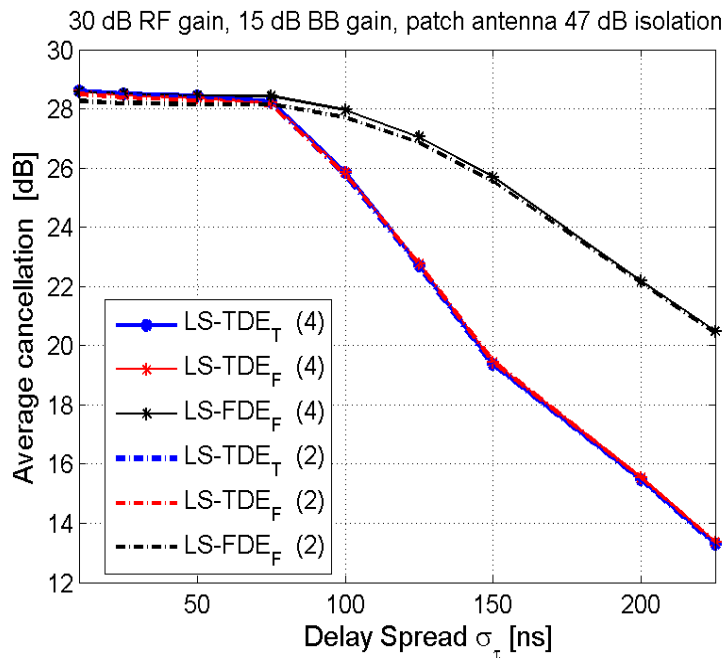
Figure 5.18: Performance of LS-TDE$_T$ [3, 9] and proposed algorithms using a patch antenna with 47 dB isolation and time dispersive channel effects.

30 dB RF gain, 15 dB BB gain, patch antenna 47 dB isolation
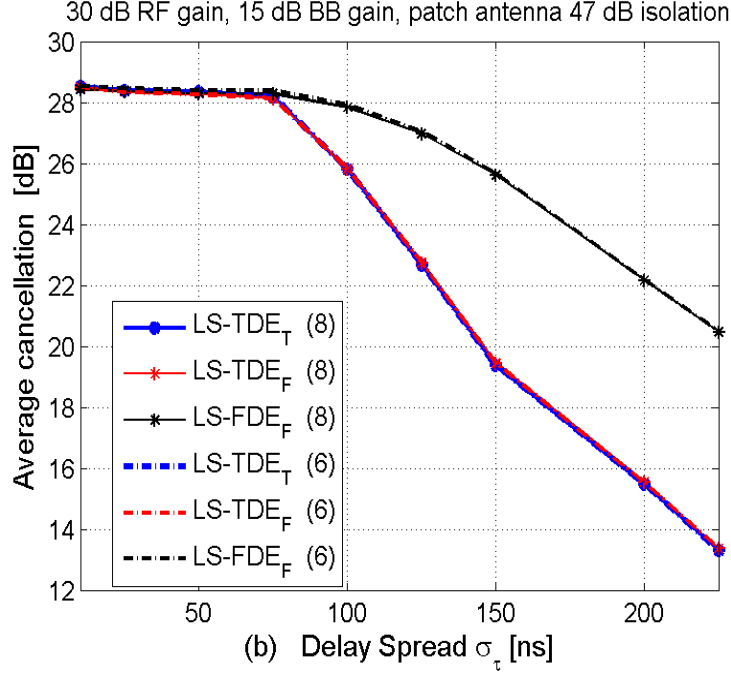
Figure 5.19: Performance of LS-TDE$_T$ [3, 9] and proposed algorithms using a patch antenna with 47 dB isolation and time dispersive channel effects.

In these results with patch antenna, it can be seen that we have a lesser digital cancellation for all the techniques, which is certainly due to the reason that, with patch antenna we have more analog suppression, and we know the fact that with high analog suppression, we have less digital cancellation, due to low SNR of SI signal. Besides that, we observed similar results, e.g. a sharp drop in the amount of digital cancellation achieved with LS-TDE$_T$ and LS-TDE$_F$ cancellation techniques after σ_τ is greater than 80 ns, because of the same reasons explained in the previous section.

5.3.3   Digital Cancellation Tests Results Summary

The Table 5.1 and Table 5.2 presents the digital cancellation tests result summary without channel effects and with channel emulator, respectively. The better performance of the proposed digital cancellation technique $LS-FDE_F$, especially in severe fading conditions, is evident in these tables, suggesting its suitability for long range transmissions.

Table 5.1: Maximum cancellation test results for different digital SI cancellation techniques with channel effects

Digital SI Cancellation Techniques	Flop Count	Maximum cancellation (dB) with 30 dB RF gain					
		RF Attenuator (dB)			Antenna Separation (cm)		Patch Antenna (dB)
		32	40	50	50	75	48
LS-TDE$_T$ [3, 9]	12976	34.5	33	32	35	33	31
LS-TDE$_F$	10656	34.5	33	32	35	33	31
LS-FDE$_F$	3488	35.5	34	32.5	36	33	32

Table 5.2: Maximum cancellation test results for different digital SI cancellation techniques under fading channel conditions

Digital SI Cancellation Techniques	Flop Count	Maximum cancellation (dB) with increasing RMS delay Spread σ_τ (ns)									
		Antenna Separation 50 cm					Patch Antenna 48 dB				
		10	80	100	150	200	10	80	100	150	200
LS-TDE$_T$ [3, 9]	12976	32.5	32	29.5	23	18	29	28	26	19.5	15.5
LS-TDE$_F$	10656	32.5	32	29.5	23	18	29	28	26	19.5	15.5
LS-FDE$_F$	3488	32.5	32.5	32	29	26	29	28.5	28	26	22

5.4 Reception Tests Under SI: FD Communication

In this section, we will present the successful FD transmission demonstration results, which we obtained with WARP SDR, here Figure 5.20 illustrates the experiment setup. The FD transmission results for both *least square time domain estimation with*
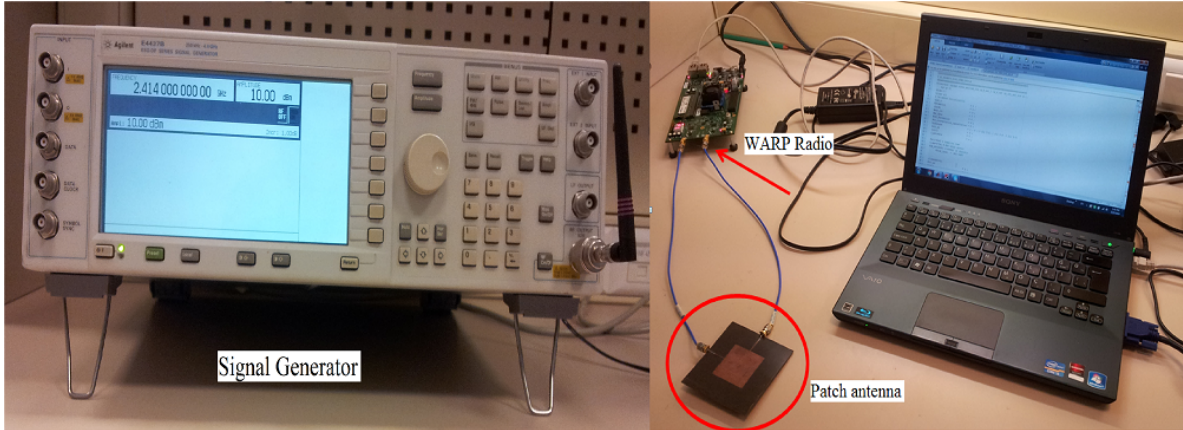
Figure 5.20: FD reception experimental setup.

time domain reconstruction used in [3, 9] and *least square frequency domain estimation* with proposed *frequency domain reconstruction* approach are presented here. For this demonstration, the basic OFDM symbol and packet parameters are the same as that we used in the previous tests. We have used the patch antenna that can provide an analog isolation of 47 dB at the RF carrier frequency of 2.412 GHz, which have been used for transmission and reception. The RF and baseband gains are 30 dB and 8 dB, respectively.

To analyze the spectrum and received power with WARP radio, we transmitted a tone at 2.414 GHz using a signal generator with 10 dBm power under half duplex mode. One thing to mention here is that there is no LOS link between the antennas of the two transmitters, and the separation between the two transmitters is roughly 3-4 meters. Figure 5.21 depicts the results under HD mode. In the figure, both frequency domain response of the received tone centered at 2.414 GHz with no considerable non-linear components, and the time domain I and Q samples can be seen.
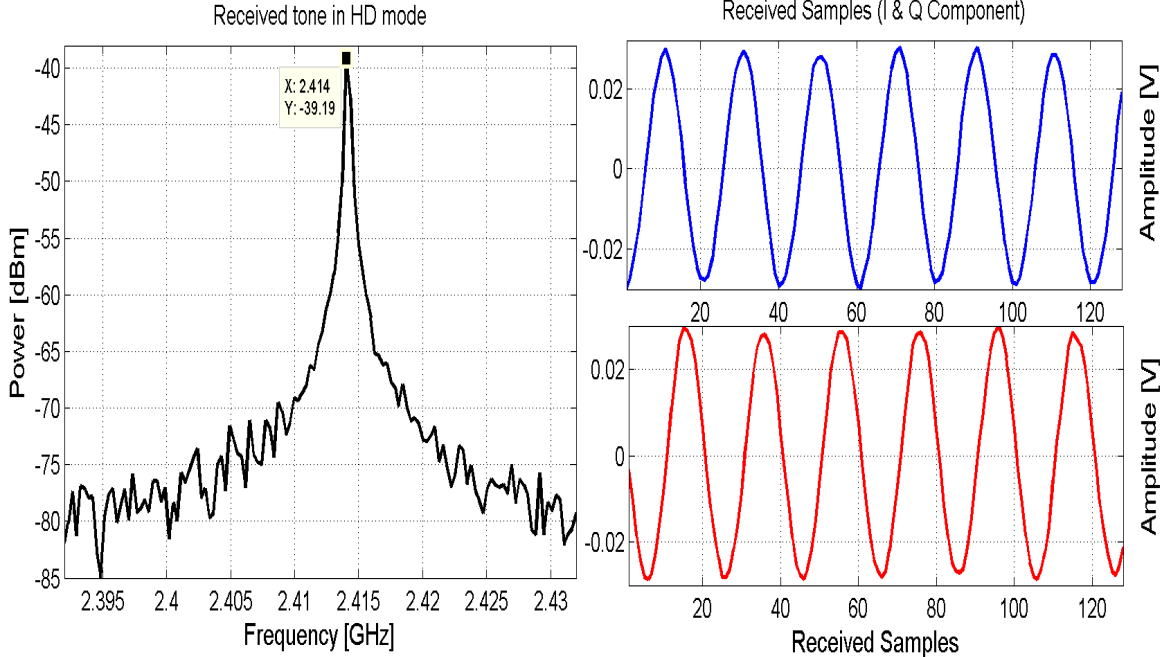
Figure 5.21: Frequency and time domain representation of a 2.414 GHz tone received in half duplex mode.

5.4.1 Reception Test Under FD with LS-TDE$_T$ Technique

In this section, we presents the FD transmission results, that we obtained by employing the digital cancellation technique used in [3, 9, 10]. The test is performed in the following manners: first before turning on the signal generator, we performed one transmission on the WARP radio to get the SI channel estimate. Once we got the SI channel estimate, we turned on the signal generator transmitting a tone at 2.414 GHz, and at the same time, started the transmission of the OFDM packet through the WARP radio. Now, while simultaneously transmitting an OFDM packet and receiving that same packet plus the desired tone, we used the channel estimate that we acquired in the absence of the tone, to reconstruct the self-interfering OFDM packet.

The Figures 5.22 and 5.23 illustrate the FD transmission results in frequency and time domain for one OFDM symbol, respectively. Figure: 5.22a presents the frequency domain representation of the transmitted OFDM symbol, 5.22b represent the received self-interfering OFDM symbol and the desired signal, where the distortion effect in the
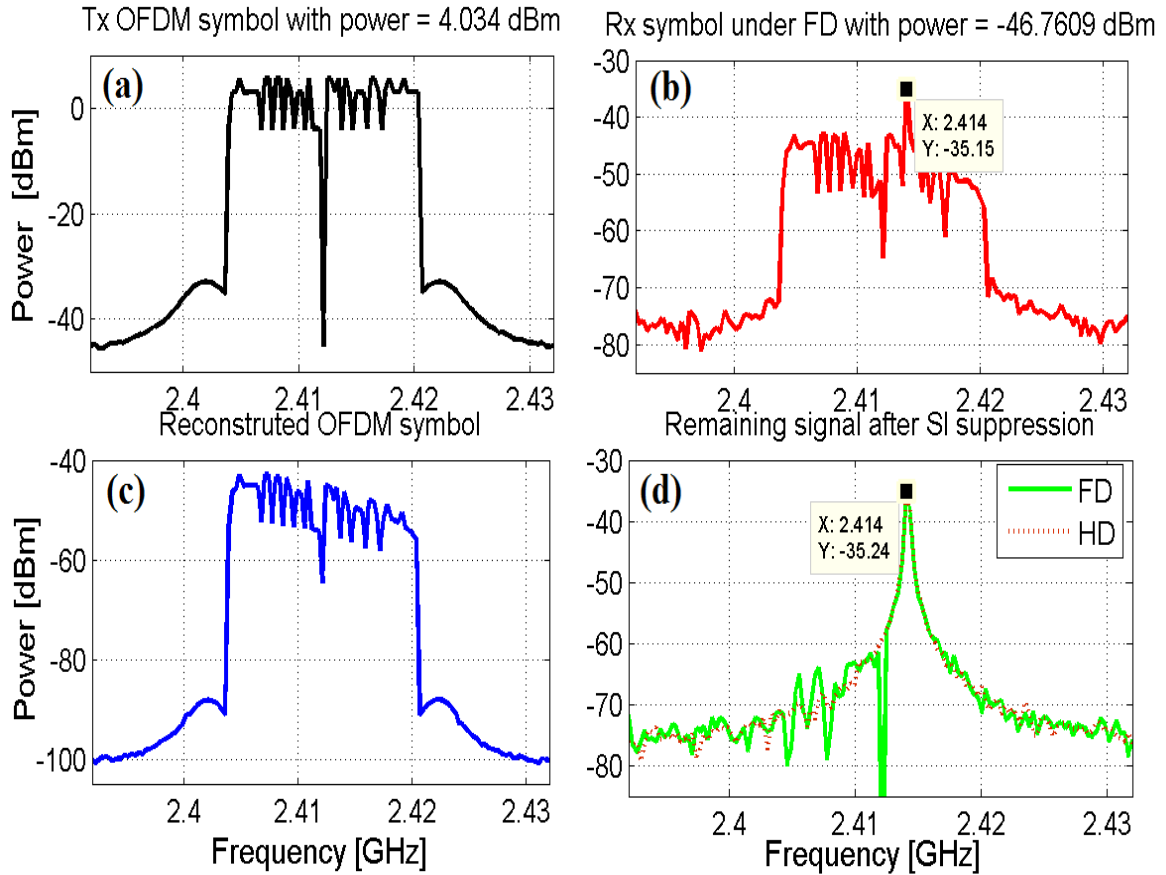
Figure 5.22: Frequency domain representation of a simultaneous transmission and reception of an OFDM symbol and a 2.414 GHz tone in full duplex mode, with LS-TDE$_T$ technique [3, 9].

received symbol can be seen clearly. 5.22c presents the reconstructed ODFM symbol carrying only channel effects, and 5.22d presents the final result after the suppression of the self-interfering OFDM symbol. The two spectrums shown in 5.22d are for the tone received in both HD and FD transmission. Besides, the few very low power nonlinear components, the spectrum of the received tone under FD mode is quite similar to that under HD mode with a received SNR of 40 dB. Also, it can be seen that the self-interfering OFDM packet is suppressed to noise floor of the WARP, while the desired tone at 2.414 GHz is their with clean spectrum. Similarly, the Figure 5.23d depicts the time domain representation of the tone received in both FD and HD mode and the clarity of the received tone under FD is no-doubt obvious, thus, validating FD
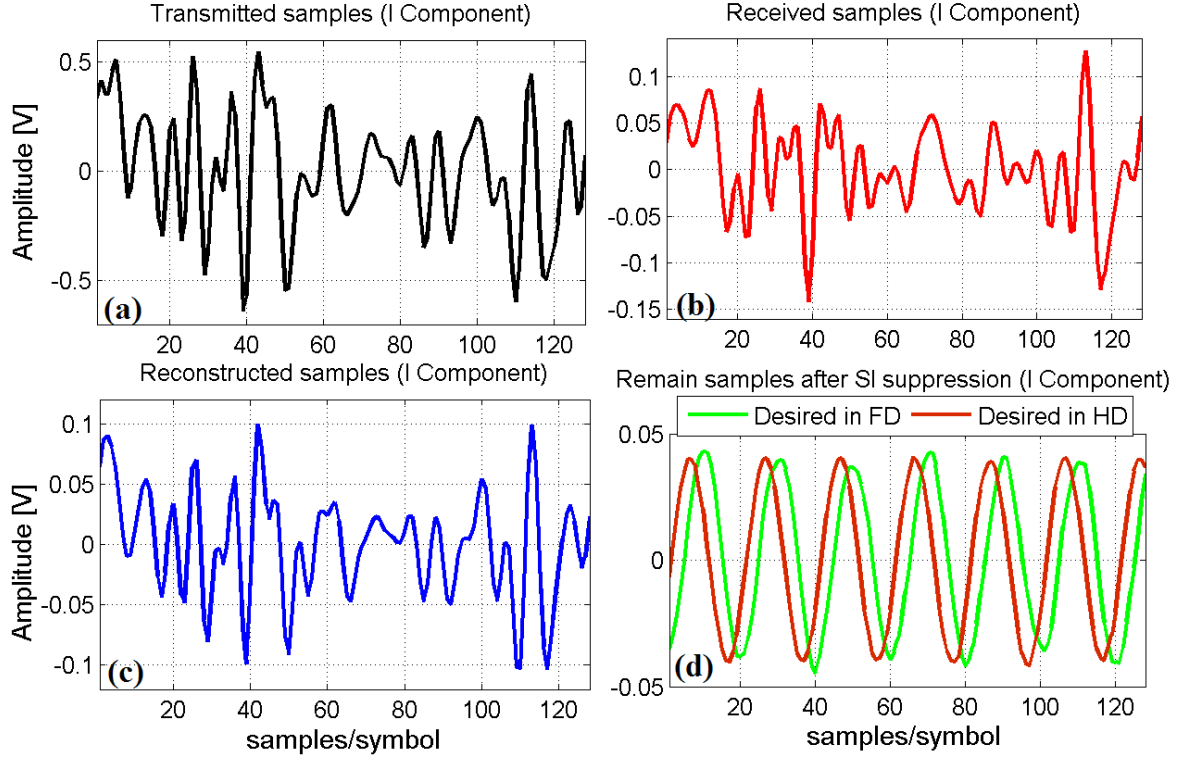
Figure 5.23: Time domain representation of a simultaneous transmission and reception of an OFDM symbol and a 2.414 GHz tone in full duplex mode, with LS-TDE$_T$ technique [3, 9].

transmission.

5.4.2   Reception Test Under FD with LS-FDE$_F$ Technique

After testing the previously used approach [3, 9, 10] of digital SI cancellation, in this section, we presents the FD transmission results that we obtained by incorporating the LS-FDE technique with the proposed frequency domain reconstruction approach for achieving digital cancellation. This FD transmission test is conducted in the same manners as that the previous one with LS-TDE$_T$ technique.

Figures 5.24 and 5.25 presents the FD transmission results in frequency and time domain, respectively. Similar, performance results can be observed in these results, demonstrating the capacity of the proposed approach to transmit and receive in a single band, i.e. FD wireless transmission, with very less computational requirements
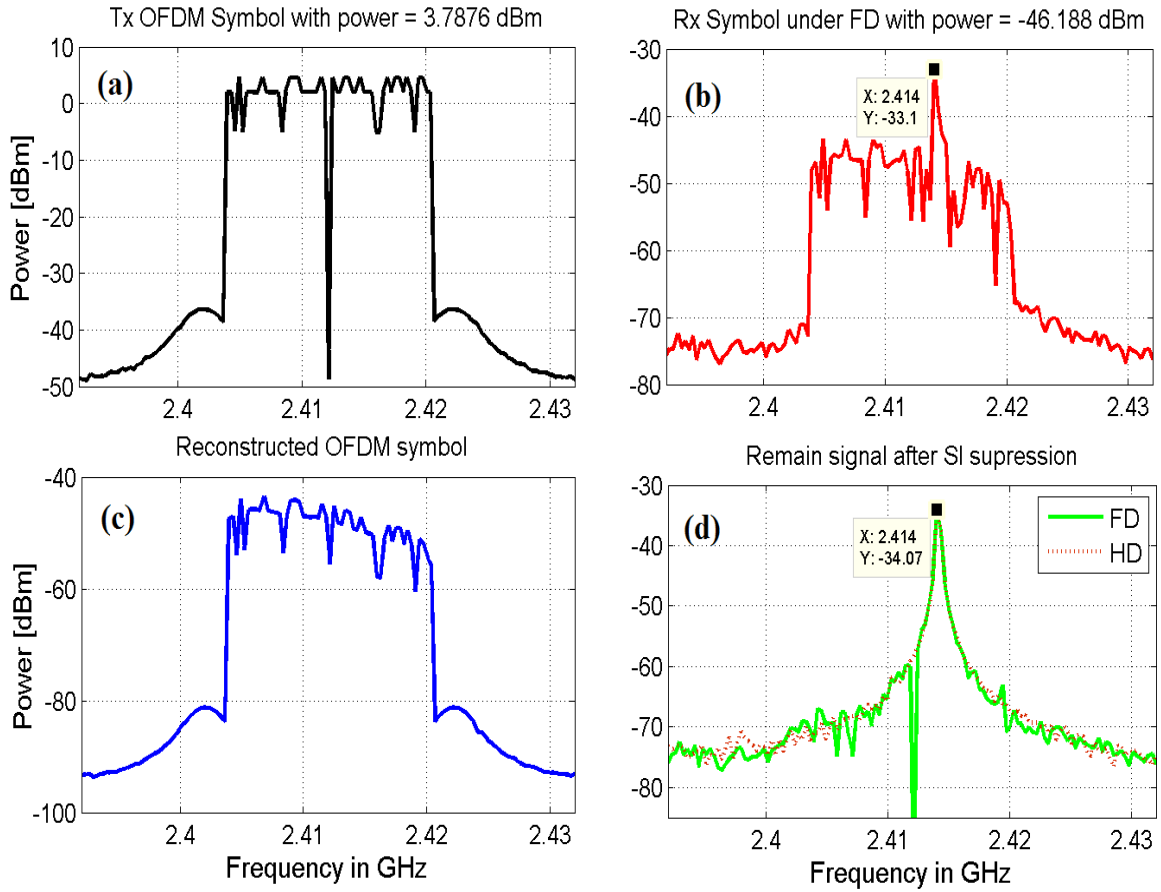
Figure 5.24: Frequency domain representation of a simultaneous transmission and reception of an OFDM symbol and a 2.414 GHz tone in full duplex mode, with proposed LS-FDE$_F$ technique.

compared to the existing time domain reconstruction approach. Again, the spectral clarity of the desired tone after SI suppression, can be seen in Figure 5.24d, with a received SNR of 39 dB.
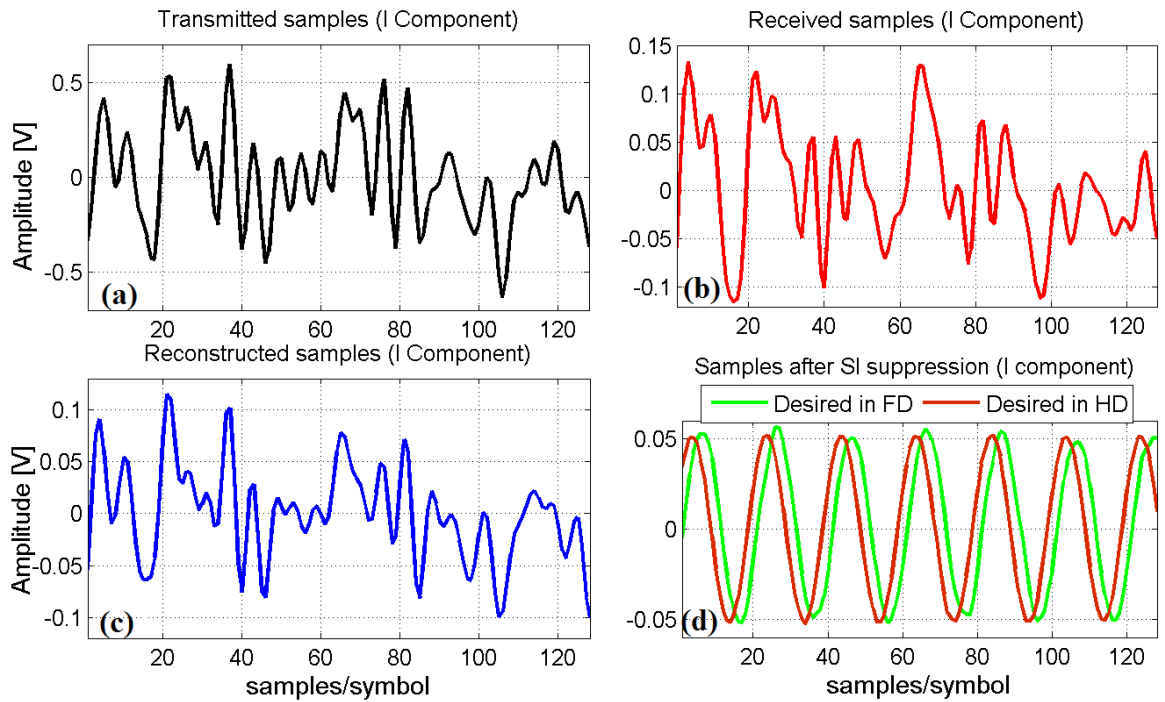
Figure 5.25: Time domain representation of a simultaneous transmission and reception of an OFDM symbol and a 2.414 GHz tone in full duplex mode, with proposed LS-FDE$_F$ technique.

Chapter 6

Conclusions

Full-duplex is certainly a promising communication mode for wireless connectivity, due to the potential to significantly improve the spectral efficiency and throughput of a wireless network. In this thesis, we have presented a novel frequency domain approach to reconstruct the self-interference signal in digital domain. Unlike the time domain based SI signal reconstruction approach that requires convolution operation, the proposed frequency domain approach is simple, involving only multiplication and following that an FFT processing to reconstruct SI signal.

We have conducted a detailed performance and computational complexity analysis of the various SI signal estimation and reconstruction techniques employed to achieve digital self-interference cancellation in FD radios, while considering OFDM based FD baseband model, and multi path fading channel conditions. Firstly, it is observed that the amount of digital cancellation increases with increasing SNR of SI signal, and a maximum digital cancellation of ∼36 dB is achieved in AWGN channel with SNR of 40 dB, however, the performance of the digital cancellation gets significantly worse in fading channels having large RMS delay spread, i.e. high frequency selectivity. These results propose that with more analog suppression of SI signal, i.e. less SNR of received baseband SI signal, lower digital cancellation will be obtained. Also, poor digital cancellation performance in highly selective channels point out the performance limitations for enabling FD systems particularly for long range transmission with large delay spreads and weak desired signal. Nevertheless, frequency domain estimates being

resilient towards large delay spreads perform relatively well in poor channel conditions as compared to time domain estimates, which are more susceptible to frequency selectivity. Secondly, the performance comparison of the two reconstruction approaches, via simulations suggest that, for frequency domain channel estimates, which perform significantly well in highly selective channel conditions, the proposed frequency domain approach is a more suitable reconstruction technique, as it offers 10 - 15 dB more digital cancellation as compared to the time domain reconstruction approach. Finally, it has been shown that the most efficient implementation structure of the existing time domain reconstruction approach requires 4272 flops to reconstruct a single OFDM symbol, whereas the proposed approach reduces this number to 1680 flops, i.e. a complexity reduction of nearly three times is offered by the proposed method.

Our extensive tests of digital cancellation with WARP radio, have further validated the performance of the proposed reconstruction approach, as it has demonstrated the similar high performance, even with the non-linearities introduced by the RF chains of the radio. Furthermore, we have observed degradation in the digital cancellation performance with high analog isolation, which we also concluded from the simulation results with low SNR of the SI signal. The simulations on MATLAB and the test with WARP radio both have confirmed that the preamble with increased LTS length, i.e. with four or more symbols, is more effective, as it provides approximately 1 dB of additional digital cancellation compared to the preamble with standard IEEE 802.11a/g LTS length of two symbols; however, diminishing returns were observed as the LTS was further increased to six, eight symbols.

Lastly, our FD communication test has demonstrated the clean reception of a tone at 2.414 GHz, in the presence of a self-interfering OFDM packet, which has proved the capacity of our proposed reconstruction approach to successfully perform the task of digital cancellation for enabling full-duplex communication. Our reception under FD tests with proposed approach demonstrates a received SNR (after SI suppression) of 40 dB. As a future work, the proposed frequency domain based SI signal reconstruction technique can be implemented on FPGA to test and compare its performance in real-time with different additional analog SI suppression techniques.

Bibliography

[1] E. Everett, A. Sahai, and A. Sabharwal, "Passive self-interference suppression for full-duplex infrastructure nodes," *IEEE Transactions on Wireless Communications*, vol. 13, no. 2, pp. 680–694, 2014.

[2] A. Sabharwal, P. Schniter, D. Guo, D. W. Bliss, S. Rangarajan, and R. Wichman, "In-band full-duplex wireless: Challenges and opportunities," *IEEE Journal on Selected Areas in Communications*, vol. 32, no. 9, pp. 1637–1652, 2014.

[3] D. Bharadia, E. McMilin, and S. Katti, "Full duplex radios," *ACM SIGCOMM Computer Communication Review*, vol. 43, no. 4, pp. 375–386, 2013.

[4] "Ieee 802.11a/g, vocal technologies, voice and data communications," 2012.

[5] Y. S. Cho, J. Kim, W. Y. Yang, and C. G. Kang, *MIMO-OFDM wireless communications with MATLAB*. John Wiley & Sons, 2010.

[6] N. Instruments, "The "perfect simulation" for wireless receiver test, national instruments," *White paper*, May, 2014.

[7] T. S. Rappaport *et al.*, *Wireless communications: principles and practice*, vol. 2. Prentice Hall PTR New Jersey, 1996.

[8] GaussianWaves, "Power delay profile, gaussianwaves," 2014.

[9] D. Bharadia and S. Katti, "Full duplex mimo radios," in *11th USENIX Symposium on Networked Systems Design and Implementation (NSDI 14)*, pp. 359–372, 2014.

[10] M. Jain, J. I. Choi, T. Kim, D. Bharadia, S. Seth, K. Srinivasan, P. Levis, S. Katti, and P. Sinha, "Practical, real-time, full duplex wireless," in *Proceedings of the 17th annual international conference on Mobile computing and networking*, pp. 301–312, ACM, 2011.

[11] M. Duarte and A. Sabharwal, "Full-duplex wireless communications using off-the-shelf radios: Feasibility and first results," in *2010 Conference Record of the Forty Fourth Asilomar Conference on Signals, Systems and Computers*, pp. 1558–1562, IEEE, 2010.

[12] E. Ahmed, A. M. Eltawil, and A. Sabharwal, "Self-interference cancellation with nonlinear distortion suppression for full-duplex systems," in *2013 Asilomar Conference on Signals, Systems and Computers*, pp. 1199–1203, IEEE, 2013.

[13] M. E. Knox, "Single antenna full duplex communications using a common carrier," in *Wireless and Microwave Technology Conference (WAMICON), 2012 IEEE 13th Annual*, pp. 1–6, IEEE, 2012.

[14] J. I. Choi, M. Jain, K. Srinivasan, P. Levis, and S. Katti, "Achieving single channel, full duplex wireless communication," in *Proceedings of the sixteenth annual international conference on Mobile computing and networking*, pp. 1–12, ACM, 2010.

[15] E. Ahmed, A. M. Eltawil, and A. Sabharwal, "Self-interference cancellation with phase noise induced ici suppression for full-duplex systems," in *2013 IEEE Global Communications Conference (GLOBECOM)*, pp. 3384–3388, IEEE, 2013.

[16] B. Radunovic, D. Gunawardena, P. Key, A. Proutiere, N. Singh, V. Balan, and G. Dejean, "Rethinking indoor wireless mesh design: Low power, low frequency, full-duplex," in *Wireless Mesh Networks (WIMESH 2010), 2010 Fifth IEEE Workshop on*, pp. 1–6, IEEE, 2010.

[17] E. Ahmed and A. M. Eltawil, "All-digital self-interference cancellation technique

for full-duplex systems," *IEEE Transactions on Wireless Communications*, vol. 14, no. 7, pp. 3519–3532, 2015.

[18] M. Duarte, C. Dick, and A. Sabharwal, "Experiment-driven characterization of full-duplex wireless systems," *IEEE Transactions on Wireless Communications*, vol. 11, no. 12, pp. 4296–4307, 2012.

[19] E. Ahmed, A. Eltawil, and A. Sabharwal, "Simultaneous transmit and sense for cognitive radios using full-duplex: A first study," in *Proceedings of the 2012 IEEE International Symposium on Antennas and Propagation*, pp. 1–2, IEEE, 2012.

[20] N. Chayat, "Ieee 802.11-97/96," September, 2014.

[21] "Warplab reference design, warp sdr, mango board, http://warpproject.org/trac/wiki/warplab,"

[22] A. Sahai, G. Patel, and A. Sabharwal, "Pushing the limits of full-duplex: Design and real-time implementation," *arXiv preprint arXiv:1107.0607*, 2011.

[23] J. Terry and J. Heiskala, *OFDM wireless LANs : a theoretical and practical guide*. Indianapolis, Ind. Sams, 2002. OFDM : Orthogonal Frequency Division Multiplexing.

[24] S. Bernard, "Digital communications fundamentals and applications," *Prentice Hall, USA*, 2001.

[25] I. Recommendation, "1225, guidelines for evaluation of radio transmission technologies for imt-2000," *International Telecommunication Union*, 1997.

[26] R. Clarke, "A statistical theory of mobile-radio reception," *Bell system technical journal*, vol. 47, no. 6, pp. 957–1000, 1968.

[27] Y. Kang, K. Kim, and H. Park, "Efficient dft-based channel estimation for ofdm systems on multipath channels," *IET communications*, vol. 1, no. 2, pp. 197–202, 2007.

[28] J. Ma, H. Yu, and S. Liu, "The mmse channel estimation based on dft for ofdm system," in *2009 5th International Conference on Wireless Communications, Networking and Mobile Computing*, pp. 1–4, IEEE, 2009.

[29] O. Edfors, M. Sandell, J.-J. Van de Beek, S. K. Wilson, and P. O. Borjesson, "Ofdm channel estimation by singular value decomposition," *IEEE Transactions on communications*, vol. 46, no. 7, pp. 931–939, 1998.

[30] J.-J. Van de Beek, O. Edfors, M. Sandell, S. K. Wilson, and P. O. Borjesson, "On channel estimation in ofdm systems," in *Vehicular Technology Conference, 1995 IEEE 45th*, vol. 2, pp. 815–819, IEEE, 1995.

[31] D. L. Jones, "Decimation-in-time (dit) radix-2 fft," *Connexions, September*, vol. 15, p. 2006, 2006.

[32] R. E. Greene and S. G. Krantz, *Function theory of one complex variable*, vol. 40. American Mathematical Soc., 2006.

[33] S. G. Johnson and M. Frigo, "A modified split-radix fft with fewer arithmetic operations," *IEEE Transactions on Signal Processing*, vol. 55, no. 1, pp. 111–119, 2007.

[34] R. Yavne, "An economical method for calculating the discrete fourier transform," in *Proceedings of the December 9-11, 1968, fall joint computer conference, part I*, pp. 115–125, ACM, 1968.